Transfer Across the Air-Sea Interface

2

Christoph S. Garbe, Anna Rutgersson, Jacqueline Boutin, Gerrit de Leeuw, Bruno Delille, Christopher W. Fairall, Nicolas Gruber, Jeffrey Hare, David T. Ho, Martin T. Johnson, Philip D. Nightingale, Heidi Pettersson, Jacek Piskozub, Erik Sahlée, Wu-ting Tsai, Brian Ward, David K. Woolf, and Christopher J. Zappa

Abstract

The efficiency of transfer of gases and particles across the air-sea interface is controlled by several physical, biological and chemical processes in the atmosphere and water which are described here (including waves, large- and small-scale turbulence, bubbles, sea spray, rain and surface films). For a deeper understanding of relevant transport mechanisms, several models have been developed, ranging from conceptual models to numerical models. Most frequently the transfer is described by various functional dependencies of the wind speed, but more detailed descriptions need additional information. The study of gas transfer mechanisms uses a variety of experimental methods ranging from laboratory studies to carbon budgets, mass balance methods, micrometeorological techniques and thermographic techniques. Different methods resolve the transfer at different scales of time and space; this is important to take into account when comparing different results. Air-sea transfer is relevant in a wide range of applications, for example, local and regional fluxes, global models, remote sensing and computations of global inventories. The sensitivity of global models to the description of transfer velocity is limited; it is however likely that the formulations are more important when the resolution increases and other processes in models are improved. For global flux estimates using inventories or remote sensing products the accuracy of the transfer formulation as well as the accuracy of the wind field is crucial.

2.1 Introduction

The transfer of gases and particles across the air-sea interface depends not only on the concentration difference between the water and the air, but also on the efficiency of the transfer process. The efficiency of the transfer is controlled by complex interaction of a variety of processes in the air and in the water near the interface. Here we treat both gases and particles since the transfer, to some extent, is governed by similar mechanisms.

Studies of transfer across the air-sea interface include a variety of methods and techniques ranging from laboratory studies, modeling and large-scale field studies. Various methods reach somewhat different conclusions, due to representation of different

C.S. Garbe (✉)
e-mail: christoph.garbe@iwr.uni-heidelberg.de

A. Rutgersson (✉)
e-mail: anna.rutgersson@met.uu.se

P.S. Liss and M.T. Johnson (eds.), *Ocean-Atmosphere Interactions of Gases and Particles*,
Springer Earth System Sciences, DOI 10.1007/978-3-642-25643-1_2,

mechanisms, but also because of uncertainties in the different methodologies.

Much of the interest in air-sea gas and particle transfer relates to global or regional phenomena, by using models or remote sensing products to determine oceanic sinks and sources of gases and particles. Upscaling of transfer involves relating the transfer to the environmental factors that influence the exchange. Figure 2.1 summarises factors most likely to be of great importance. Most commonly the transfer is described by a wind speed dependent function. There is, however, increasing understanding that a variety of processes influence gases of varying properties (like solubility) and particles differently.

The transport of a quantity is characterised by the *transfer velocity*, k. The transfer velocity is given by the flux F of the transported quantity divided by the "concentration difference" of the quantity between surface (C_0) and the bulk (C_{bulk}):

$$k = \frac{F}{C_0 - C_{\text{bulk}}}. \tag{2.1}$$

For the transport of CO_2, the water-sided transfer velocity k_w is often related to the partial pressure difference ΔpCO_2 between air and water by $k_w = F/(\alpha \Delta pCO_2)$. The transfer velocity k will then depend both on the Schmidt number (Sc) and the dimensionless solubility α. It is related to the friction velocity u_* and the Schmidt number $Sc = \nu/D$ given by

$$k = u_* \beta(s) Sc^{n(s)}, \tag{2.2}$$

where both $\beta(s)$ and $n(s)$ depend on parameters describing the surface conditions and the related transport processes. If heat is the transported quantity of interest, then Sc is substituted by the Prandtl number $Pr = \nu/\varkappa$ in this equation. Here ν is the kinematic viscosity, D is the molecular mass diffusivity and $\varkappa$ is the thermal diffusivity.

There exist a number of previous books and reviews concerning air-sea gas and particle transfer (e.g. Fairall et al. 2000; Wanninkhof et al. 2009; Le Quéré and Saltzman 2009; de Leeuw et al. 2011). Here we summarise mechanisms of importance, measurement techniques frequently used to investigate the transfer, present state-of-the-art parameterisations and applications of the air-sea transfer description. The accuracy of the various methods and the importance of measurement uncertainty for global flux estimates are further discussed.

2.2 Processes

The major processes influencing the air-sea transfer velocity are described here. This includes processes important for a relatively insoluble gas like CO_2: micro scale wave breaking, small and large scale turbulence in the water, waves, bubbles, sea spray, rain and surface films (see Fig. 2.1). In addition biological and chemical enhancement is described having been recognised as important for a small number of gases (including O_3 and SO_2). Atmospheric processes are also briefly described due to the importance for turbulence generation at the surface as well as their direct importance for the transfer velocity of air-side controlled (soluble) gases.

2.2.1 Microscale Wave Breaking

Microscale wave breaking, or microbreaking (Banner and Phillips 1974), is the breaking of very short wind waves without air entrainment and begins at wind speeds well below the level at which whitecaps appear (Melville 1996). Laboratory and field observations show microbreaking waves are ~ 0.1–1 m in length and ~ 0.01–0.1 m in amplitude and have a bore-like crest with parasitic capillary waves riding on the forward face (Zappa et al. 2001).

Other defining characteristics exist between microbreaking and whitecapping. Oh et al. (2008) have shown that a single strong coherent structure develops beneath a large-scale whitecapping breaking crest. The coherent structure rotates in the same sense as the wave orbital motion. In contrast, a series of coherent structures whose rotation sense is not fixed are generated beneath microscale breakers. However, the overall characteristics of the spatio-temporal evolution of the coherent vortical structures are qualitatively the same between the two types of wave breaking. It is also significant that unlike energetic whitecapping breakers, no jet is formed at the crest of a microscale breaking wave, suggesting that surface

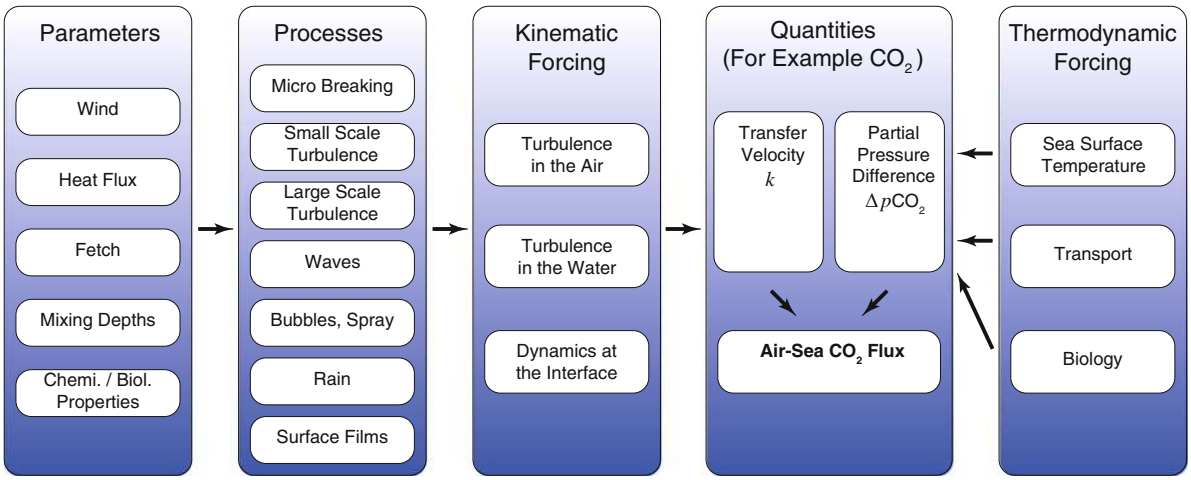

Fig. 2.1 Simplified schematic of factors influencing air-sea CO_2 fluxes. On the *right* are factors that affect the air-sea pCO_2 difference (thermodynamic forcing). On the *left* are environmental forcing factors that control the efficiency of the transfer (kinematic forcing)

tension has a significant impact on the breaking of waves shorter than 1 m (Tulin and Landrini 2001). Instead, the bore-like crest of the microbreaker can propagate for a considerable distance without significant change of shape. Microbreakers inherently lose a significant portion of their height and dissipate their energy during the breaking.

Laboratory experiments in wind-wave tunnels provide a growing body of evidence that turbulence generated by microscale wave breaking is the dominant mechanism for air-water gas transfer at low to moderate wind speeds. Laboratory measurements indicate that a wave-related mechanism regulates gas transfer because the transfer velocity correlates with the total mean-square wave slope, $\langle S^2 \rangle$ (Jähne et al. 1987). Wave slope characterises the stability of water waves (e.g. Longuet-Higgins et al. 1994) and certain limiting values of slope are typically used to detect and define wave breaking (e.g. Banner 1990). Therefore, Jähne et al. (1987) have argued that wave slope is representative of the near-surface turbulence produced by microscale wave breaking.

Microbreaking is widespread over the oceans, and Csanady (1990) has proposed that the specific manner by which it affects k_w is the thinning of the aqueous mass boundary layer (MBL) by the intense surface divergence generated during the breaking process. Infrared (IR) techniques have been successfully implemented in the laboratory to detect this visually ambiguous process and have been used to quantify regions of surface renewal of the MBL caused by microbreakers (Jessup et al. 1997a). Analogous to the MBL, Wells et al. (2009) suggest that an appreciable change in skin temperature of the thermal boundary layer requires a large strain rate, such as might be generated by high vorticity wavelets (Okuda 1982) or microbreaking waves. Skin layer straining may be important for large Péclet (Pe) number flows. The Péclet number is defined to be the ratio of the rate of advection to the rate of diffusion of a physical quantity. In the context of heat transport, the Péclet number is given by the product of the Reynolds number and the Prandtl number. In the context of mass diffusion, the Péclet number is the product of the Reynolds number and the Schmidt number. For example, Peirson and Banner (2003) and Turney et al. (2005) measured surface divergence of approximately 1–10 s^{-1} for microbreaking surface waves, yielding Pe ~ 10–100 for a 0.1 cm skin layer. In addition, flow separation can produce high vorticity wavelets with Pe ~ 200 (Csanady 1990). On the basis of the experimental data, the variation of the skin temperature for steady large Péclet number flows is reasonably well described by $\frac{Q}{\rho C_p}\sqrt{\frac{\pi}{2\kappa E}}$, where Q is the net heat flux, ρ is the density, C_p is the specific heat capacity at constant pressure, κ is the thermal diffusivity and E is the strain rate (Wells et al. 2009). The IR signature provides qualitative evidence of the turbulent wakes of

microbreakers that is consistent with Csanady (1990) idea for the effect of microbreaking on the MBL.

In the infrared imagery, the microbreaking process is observed to disrupt the aqueous thermal boundary layer, producing fine-scale surface thermal structures within the bore-like crest of the microbreaking wave and in its wake. In the slope imagery, microbreaking generates three-dimensional dimpled roughness features of the bore-like crest and in its wake. The spatial scales of the fine-scale thermal structures and the three-dimensional roughness features within the bore-like crests of microbreakers were observed to be ~ 10^{-2} m, the same as the length scale for the vortical eddy structures measured beneath wind-forced waves by Siddiqui et al. (2004). Furthermore, the dimpled roughness features of the bore-like crest correspond directly to the warmest fine-scale features of the skin-layer disrupted by microbreaking. The implication is that the fine-scale thermal structures and the dimpled roughness features are directly related to the near-surface turbulence generated at the bore-like crests. Because near-surface turbulence increases k_w, microbreakers are likely to be the mechanism that enhances both heat and mass transfer.

Understanding the nature and key features of the interfacial flows associated with small-scale waves is fundamental to explaining the prominent enhancement of air-water exchange that occurs in their presence. Within a few hundred microns of the surface of laboratory microscale breaking wind waves, the mean surface drift directly induced by the wind on the upwind faces and crests is $(0.23 \pm 0.02)u_{*a}$ in the trough increasing to $(0.33 \pm 0.07)u_{*a}$ at the crest, where u_{*a} is the wind friction velocity (Peirson and Banner 2003). Substantial variability in the instantaneous surface velocity exists up to approximately $\pm 0.17u_{*a}$ in the trough and $\pm 0.37u_{*a}$ at the crest. Peirson and Banner (2003) attribute this variability primarily to the modulation of the wave field, although additional contributions arise due to the influence of transient microscale breaking or from near-surface turbulence generated by shear in the drift layer or from fluctuations in wind forcing.

Microscale wind-wave breaking plays an important role in the direct transport of fluid from the surface to the turbulent domain below. The toe of a microscale breaker spilling region exhibits an intense and highly localized convergence of surface fluid, with convergence rates generally exceeding 100 s^{-1} (Peirson and Banner 2003). However, the variability in mean surface drift along the upwind (windward) faces of the waves produces mean surface divergences of between 0.2 and 1.3 s^{-1} with the occurrence of locally intense flow divergence observed to be only of order 10 s^{-1}. Therefore, the convergence zones at the toes of spilling regions are significantly more energetic and efficient than these windward divergence zones.

The phase-averaged characteristics of the turbulent velocity fields beneath steep short wind waves suggest, that under conditions of short fetches and moderate wind speeds, a wind-driven water surface can be divided into three regions based on the intensity of the turbulence (Siddiqui and Loewen 2010). The regions are the crests of microbreaking waves, the crests of non-breaking waves and the troughs of all waves. The turbulence is most intense beneath the crests of microbreaking waves. In the crest region of microbreaking waves, coherent structures are observed that are stronger and occur more frequently than beneath the crests of non-breaking waves. Beneath the crests of non-breaking waves the turbulence is a factor of 2–3 times weaker and beneath the wave troughs it is a factor of 6 weaker.

The mean velocity profiles in the wind drift layer formed beneath short wind waves have been shown to be logarithmic and the flow is hydrodynamically smooth at short fetch up to moderate wind speeds (Siddiqui and Loewen 2007). The turbulent kinetic energy dissipation rate for these conditions is significantly greater in magnitude than would occur in a comparable wall-layer. At a depth of 1 mm, the dissipation rate is 1.7–3.2 times greater beneath microbreaking waves compared to non-breaking waves. In the crest−trough region, 40–50 % of the dissipation is associated with microbreakers. These results demonstrate that the enhanced near-surface turbulence in the wind drift layer is the result of microscale wave breaking.

Terray et al. (1996) proposed that the turbulent kinetic energy dissipation rate due to wave breaking is a function of depth, friction velocity, wave height and phase speed. Vertical profiles of the rate of dissipation showed that beneath microscale breaking waves there were two distinct layers (Siddiqui and Loewen 2007). Immediately beneath the surface, the dissipation decayed as $\zeta^{-0.7}$ and below this in the second layer it decayed as ζ^{-2} where ζ is the vertical coordinate in the wave-following Eulerian system.

The enhanced turbulence associated with microscale wave breaking was found to extend to a depth of approximately one significant wave height. The only similarity between the flows in these wind drift layers and wall-layers is that in both cases the mean velocity profiles are logarithmic.

A comprehensive study was performed to show that microbreaking is the dominant mechanism governing k_w at low to moderate wind speeds (i.e. nominally up to 10 ms^{-1}) (Zappa et al. 2001, 2004). Simultaneous and collocated IR and wave slope imagery demonstrated that the IR signature of the disruption of the aqueous thermal boundary layer corresponds directly to the wakes of microbreakers (Zappa et al. 2001). Concurrently, simultaneous particle image velocimetry and IR imagery showed that vortices are generated behind the leading edge of microbreakers and that the vorticity correlated with k_w (Siddiqui et al. 2001). Furthermore, k_w was shown to be linearly correlated with the fraction of water surface covered by the wakes of microbreaking (A_B) and this correlation was invariant with the presence of surfactants (Zappa et al. 2001). This correlation is evidence for a causal link between microbreaking and gas transfer. Zappa et al. (2004) showed that the surface renewal in the wakes of microbreakers enhanced transfer by a factor of 3.4 over that in the background. Furthermore, microbreaking directly contributed up to 75 % of the transfer across the air-water interface under moderate wind speed conditions. Zappa et al. (2004) argued that these results show conclusively that microbreaking is an underlying mechanism that explains the observation of enhanced gas transfer in the presence of waves and may govern air-sea gas transfer at low to moderate wind speeds.

Microbreaking events directly enhance heat and gas transfer and produce surface roughness elements that contribute directly to $\langle S^2 \rangle$. Also, A_B was correlated with $\langle S^2 \rangle$. Since many capillary and non-breaking gravity waves may dominate $\langle S^2 \rangle$, these results suggest there is an indirect link between microbreaking and the correlation of transfer velocity with $\langle S^2 \rangle$. Furthermore, the modulation of capillary waves as microscale breaking waves evolve and the transient roughness features associated with microbreaking have shown promise in identifying individual microbreaking events. A comprehensive examination of the IR and wave slope imagery data should clarify the relationship between microbreaking and $\langle S^2 \rangle$.

The correlation of k_w with wave slope has shown results similar to the correlation of k_w with A_B. Jähne et al. (1987) observed a correlation of k_w with $\langle S^2 \rangle$ for both fetch-limited and unlimited fetch cases, and Frew (1997) and Bock et al. (1999) showed the correlation was independent of surfactant for the unlimited fetch case. Zappa et al. (2004) suggest that the reason k_w correlates with wave slope is that microbreaking is the wave-related mechanism controlling gas transfer and contributes to $\langle S^2 \rangle$.

The greatest contribution of microbreaking to $\langle S^2 \rangle$ occurs in areas not directly affected by active microbreaking. The density of capillary waves present during the microscale wave breaking process is less than for non-breaking waves. Specifically, the capillary waves on the forward face of the bore-like crest become extremely short during the most intense initiation of microscale breaking when steep slopes occupy the dimpled bore-like crest. The wave field slope characteristics are constantly evolving throughout the growth process of the wave packet from the moment capillary waves are formed to the moment that microscale wave breaking occurs. The wave evolution up to microbreaking incorporates contributions of slopes from waves of all scales. Microscale wave breaking is of short duration and merely one component of this wind-wave cycle. Dense packets of capillary-gravity waves ubiquitous in regions not affected by microbreaking dominate the contribution to the total mean-square wave slope.

Since the bore-like crest produces the signature of breaking detected as A_B in the infrared imagery, only the steep slopes associated with the front of the actively breaking crest and the wake of a microscale breaker influence $\langle S^2 \rangle$. Capillary waves have been shown to contribute significantly to $\langle S^2 \rangle$ (Bock et al. 1999) and are observed to be transient during the microscale breaking process. The fact that capillary waves are damped by surfactants, coupled with the fact that the smallest scale waves have been shown to correlate with the gas transfer velocity, suggests that capillary waves characterise the importance of the wave field to gas transfer. The potential for capillary waves as a direct mechanism for gas transfer has been demonstrated both experimentally (Saylor and Handler 1997) and theoretically (Coantic 1986; Szeri 1997; Witting 1971). However,

microbreaking clearly dominates over these capillary wave processes. The contribution of capillary waves to $\langle S^2 \rangle$ is symptomatic of a simultaneous increase in overall microbreaking and the densely structured capillary-gravity wave system that increases with wind forcing. The link between k_w and $\langle S^2 \rangle$ is more complicated than simply stating that microbreaking is the direct link. It is more likely that microbreaking controls k_w, the capillary-gravity wave system facilitates microbreaking, and the non-breaking capillary and gravity waves contribute significantly to $\langle S^2 \rangle$.

Breaking of small-scale waves can be affected by longer waves in a number of ways that provide insights into the hydrodynamics of formation, propagation and evolution of microbreaking waves. One of them is modulation of the train of the short waves riding the underlying large-scale waves (Babanin et al. 2009). The large-scale waves compress the short-wave lengths at their front face and extend those at the rear face. As a result, the front-face small waves become steeper and frequently break (Donelan 2001). Small-scale breaking is also affected by the breaking of large waves (Banner et al. 1989; Manasseh et al. 2006; Young and Babanin 2006). The growth of short waves is affected by the existence of energetic breaking waves, which not only modulate the microbreakers, but virtually eliminate them as the microbreakers are overcome by the energetic breakers. In principle, short waves can be dissipated without breaking, because of interaction with the turbulent wake of the large breaker (Banner et al. 1989). Regardless, microbreakers begin growing again from very short waves and their eventual length is determined by the effective fetch between energetic breakers.

2.2.2 Small Scale Turbulence

The kinematic viscosity and thermal diffusivity of water differ by an order of magnitude. Hence, the thermal sublayer is embedded within the viscous sublayer, its momentum analogue.

This points to the significance of small-scale processes, such as near-surface turbulence, for the transport of heat and gas though the interface (McKenna and McGillis 2004). Eddies close to the surface bring "fresh" bulk water to the surface from which gases can diffuse in or out of the water. Overall this leads to enhanced gas exchange.

Wind generates turbulence at the air-water interface directly through shear or indirectly through the wave field. Turbulence generated by wind-induced waves will be covered in Sect. 2.2.4. In this section, we are focusing on shear induced turbulence.

The turbulence generated at the air-water interface can be isotropic or, more importantly, coherent. Numerical simulations performed by Tsai et al. (2005) and experiments conducted by Rashidi and Banerjee (1990) have shown that shear stress alone without waves is sufficient for coherent turbulent structures to evolve. The structure of coherent shear induced turbulence has implications for turbulent kinetic energy dissipation (c.f. Sect. 2.6.4). The shear induced turbulence is of a similar scale to the shear layer thickness (Hunt et al. 2011). Infrared thermography will be introduced in Sect. 2.5.1.2. In infrared images of the water surface, the near surface turbulence becomes visible because areas of surface divergence consist of water parcels that have been in contact with the water surface for a longer time. In the presence of a net heat flux away from the interface, such water parcels cool down and evolve into cold streaks. The opposite holds true for upwelling regions. The temperature distribution of such coherent structures visualized with thermography can be seen in Fig. 2.2. Such patterns were termed fish-scales by Tsai et al. (2005) and Handler et al. (2001) and consist of narrow cold bands of high speed fluid.

The narrow dark streaks form the characteristic intersections when they encounter slow warm plumes that "burst" into the surface. Schnieders et al. (2013) performed a statistical analysis of the streak spacing. These spacings were extracted accurately using an image processing approach based on supervised learning.

The streaky pattern observed at the water surface is very similar to the pattern of low speed streaks near no-slip walls, as described by Nakagawa and Nezu (1981) and Smith and Paxson (1983). They found the spacing between these streaks to be lognormally distributed with a mean dimensionless streak spacing of $l^+ = lu_{*_w}/\nu = 100$, where the mean streak spacing is given by l, the friction velocity by u_{*_w} and the kinematic viscosity by ν. The factor u_{*_w}/ν which when divided by l is dimensionless is estimated to be the inverse of the thickness of the thermal boundary layer (Grassl 1976).

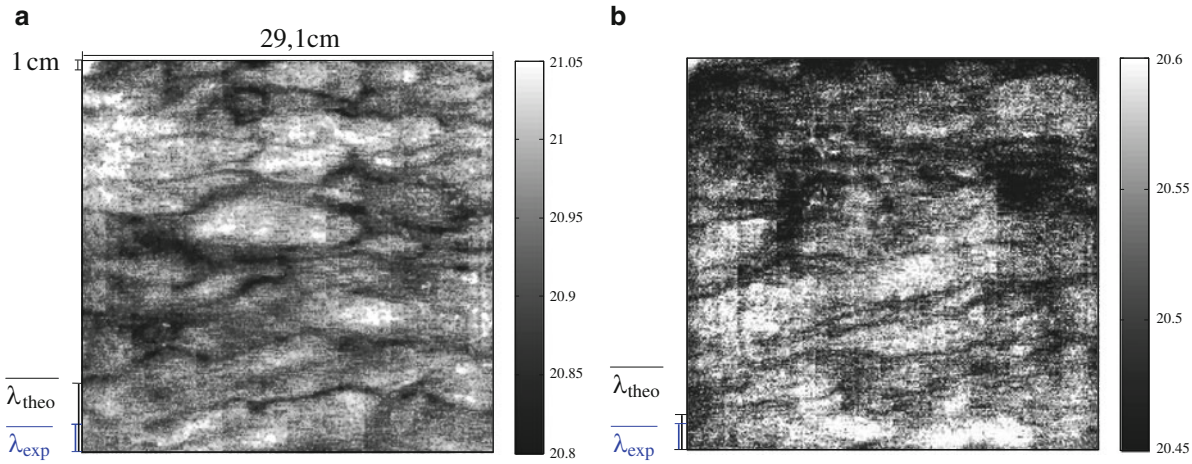

Fig. 2.2 Thermographic images of the water surface at two different wind conditions. $\overline{\lambda_{theo}} = 100u_{*w}/\nu$ describes the expected value of the mean dimensionless streak spacing in the case of low speed streaks near a no-slip wall, with the friction velocity given by u_{*w}, and the kinematic viscosity by ν. $\overline{\lambda_{exp}} = \overline{l_{exp}}u_{*w}/\nu$ describes the mean dimensionless streak spacing, where l is the determined mean streak spacing for each case (Images reproduced from Schnieders et al. (2013))

The generally agreed scaling of $l^+ = lu_{*w}/\nu = 100$ leads to the scaling of the streak spacing with the friction velocity in water u_{*w}. With increasing u_{*w} the spacing of the streaks is therefore supposed to decrease linearly in the regime of low wind speeds (Scott et al. 2008). Schnieders et al. (2013) performed a statistical analysis of the streak spacing in different laboratory facilites in different conditions. They found the spacing to plateau for higher wind speeds.

Although the fish-scale pattern seems to be universal and has been described by several authors, the process that causes these streaks has not been conclusively identified. It has been suggested (Tsai et al. 2005) that low speed streaks near no-slip walls and high speed streak near the water surface are caused by a similar process. Tsai et al. (2005) point out that one possible mechanism causing these streaks is that of horseshoe vortices that form in the turbulent shear layer by turning and stretching the spanwise vortices (see Kline et al. (1967)). These coherent turbulent structures move upward until their upper ends burst into the surface and subsequently lead to upwelling of warmer and slower water at the surface.

Chernyshenko and Baig (2005) suggest another mechanism for the formation of streaks. In their scheme, the lift-up of the mean profile in combination with shear stress and viscous diffusion lead to the formation of the streaky pattern. Currently, no conclusive measurements of these processes have been conducted.

2.2.3 Bubbles, Sea Spray

Transfer of matter across the air-sea interface may occur not only by molecular diffusion of volatiles across the sea surface but also through the mediation of bubbles and sea spray. Non-volatile material can only be ejected from the sea into the lower atmosphere within sea spray. Sea spray can be produced by "tearing" of the sea surface by the action of the wind ("spume drops"); which is most efficient near the crests of breaking waves and sharply crested waves. This tearing process is mostly effective at wind speeds greater than 10 ms^{-1} (Monahan et al. 1983), though it can be observed at the crest of breaking waves at moderate wind speeds. The spume droplets are generally large, ranging from tens of micrometres to a few millimetres. These large droplets will generally only be airborne for a short time (seconds to minutes) but are significant for their role in the transfer of moisture and latent heat (Andreas 1992). Smaller droplets that are more likely to evolve over hours or days in the marine atmosphere are almost entirely associated with the bursting of bubbles at the sea surface. A comprehensive review of sea salt aerosol production was

presented by Lewis and Schwartz (2004), the production of sub-micron sea spray aerosol particles was recently reviewed by de Leeuw et al. (2011). An overview of both production of sea spray aerosol and effects of aerosols produced over land on biogeochemical processes in the ocean is presented in Chap. 4 of this book (de Leeuw et al. 2013).

Bubble generation at the sea surface is associated with all types of precipitation falling on the sea surface and can result from supersaturation of air in the upper ocean, but is primarily associated with air entrainment within breaking waves. When these bubbles burst at the sea surface they produce two types of drops, jet drops and film drops (Blanchard 1963; Woolf et al. 1987). Jet drops are pinched off from the "Worthington jet" that projects from the open cavity of a bursting bubble and their initial radii are typically a tenth of the radius of the parent bubble. Jet drops are inferred to be the main source of the important subset of marine aerosol particles with radii between 1 and 25 μm radius (de Leeuw et al. 2011). Film drops were originally assumed to be formed from the shattering of the film cap of large bubbles, but a more complicated picture emerged from later investigations (Spiel 1998). Nevertheless the numerous small sea spray particles in the lower atmosphere (approximately 10 nm–1 μm) are associated with film drop production.

The study of small sea spray particles underpins our understanding of direct and indirect radiative effects of this aerosol (the latter through their role in cloud microphysics) and chemical reactions and pathways in the lower atmosphere involving both the sea spray particles and natural and anthropogenic volatiles. Models and quantitative estimates of these processes requires a "sea spray source function" (SSSF) and estimates of this function have recently been reviewed (de Leeuw et al. 2011). Several methods have been proposed for estimating SSSF including those based on a balance between production and deposition (wet or dry), micrometeorological methods and the whitecap method. Micrometeorological methods are showing considerable promise, but most estimates are based on the whitecap method. The whitecap method requires an assessment of aerosol production by a "standard whitecap", usually by measuring the aerosol production by a simulated whitecap in the laboratory, which is then scaled to the ocean using predictions of whitecapping. A serious problem remains since "order-of-magnitude variation remains in estimates of the size-dependent production flux per white area" (de Leeuw et al. 2011). An additional uncertainty arises from the challenge of parameterising whitecap coverage W (see below).

When bubbles are formed they will accumulate material on their surface that was previously on the sea surface. As they are mixed through the upper ocean, the bubbles may scavenge further material (primarily surface-active) from the water column. Some bubbles will dissolve leaving fragments (a "microbubble" enclosed in a shell of organics, or particles), but most surface and burst. Material carried to the surface on the bubble, or skimmed from the sea surface in the bursting process may be ejected on the sea spray. The cycling of organic material described above represents another role of bubbles in geochemical transport and air-sea transfer. It is recognised that the sea surface microlayer is highly dynamic when waves are breaking and constantly renewed by the action of bubbles (Liss et al. 1997). It follows that bubbles and spray have an indirect effect on interfacial transfer through their effect on the composition of the sea surface (see Sect. 2.2.7). The sea spray aerosol will be enriched in organic material and much of the current interest and progress in studying that aerosol focuses on the organic content and its effects (de Leeuw et al. 2011).

Air-sea transfer of volatiles is also dependent on bubbles and spray. In principle, sea spray should have some effect on the deposition or exchange of soluble gases across the atmospheric surface layer, but this pathway is usually not explicitly identified in parameterisations of air-side transfer velocity (Johnson 2010). Far more attention has been given to the role of bubbles in the air-sea exchange of poorly soluble gases. As already mentioned, bubbles may influence air-sea gas transfer through their influence on the composition of the sea surface. Both breaking waves and surfacing bubbles generate turbulence and this may enhance transfer at the sea surface. The greatest influence on poorly soluble gases appears to be through "bubble-mediated transfer", defined as the net transfer of gas across the surface of bubbles while they are submerged (Woolf and Thorpe 1991). Both laboratory experiments and numerical calculations suggest that bubble-mediated transfer is a highly effective mechanism for poorly soluble gases. The effect of bubbles on gas transfer can be seen in Fig. 2.3 where the transfer velocity k_w is shown for both CO_2 and dimethylsulfide (DMS). DMS has a much higher solubility coefficient

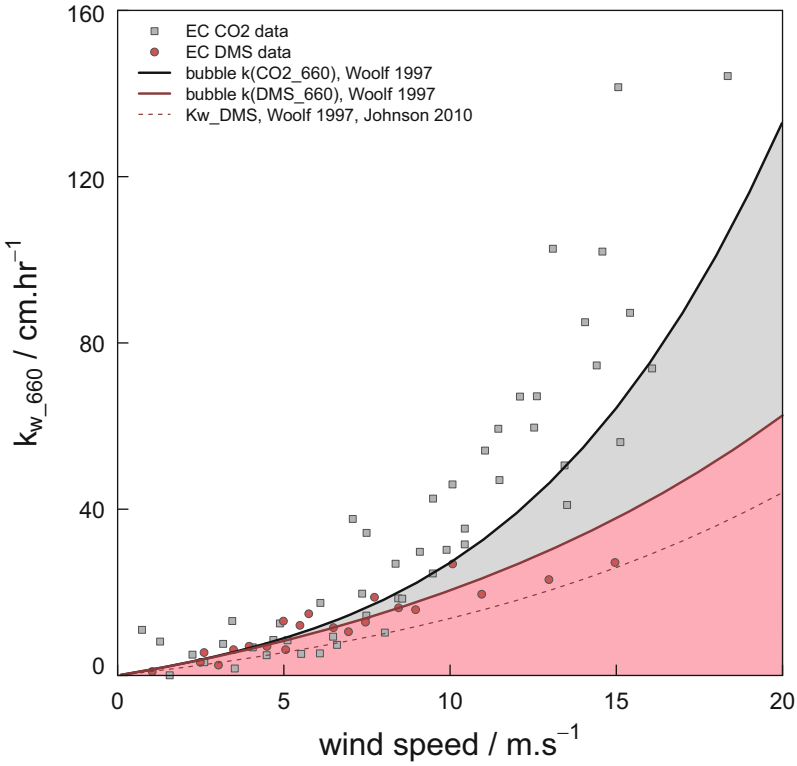

Fig. 2.3 The magnitude of the bubble effect on transfer velocity for the relatively soluble gas dimethylsulpide (*DMS*) compared to less soluble CO_2. *Pink dots* summarise eddy covariance estimates of DMS transfer velocity to date and *grey squares* those for CO_2 (detailed in Fig. 2.10). These are plotted over predicted k_{660}-normalized transfer velocities from the bubble model of Woolf (1997) for DMS (*dark pink solid line*) and CO_2 (*solid black line*), using solubility at 15 °C from Johnson (2010). For DMS, the bubble-mediated transfer is very small, so the *pink* shaded area effectively represents the diffusive transfer, which is approximately equal for both CO_2 and DMS (at the same Schmidt number), with the *grey* shaded area showing the additional bubble-mediated transfer for CO_2. Total transfer velocity, K_W, for DMS is also calculated using the scheme of Johnson (2010), applying the Woolf (1997) bubble parameterization for k_w and the Johnson (2010) k_a term (Figure by M.T. Johnson, shared under creative commons license at http://dx.doi.org/10.6084/m9.figshare.92419)

than CO_2. When the effect is scaled to the ocean by variants of the whitecap method, bubble-mediated gas transfer is calculated to contribute substantially to the transfer of poorly soluble gases (Keeling 1993; Woolf 1993, 1997; Asher et al. 1996). The inclusion of bubble-mediated transfer is crucial to the successful application of physically-based models such as NOAA-COARE (see Sect. 2.6.3) to the air-sea transfer of carbon dioxide and other poorly soluble gases (Fairall et al. 2011).

Bubble-mediated gas transfer is distinct in several respects from direct transfer of gas across the sea surface. Firstly, since bubbles may dissolve and are always subject to additional pressure, bubble-mediated transfer is asymmetric with a bias to invasion of gas (Woolf and Thorpe 1991). Secondly, through the change in composition of a bubble while it is submerged, the contribution of bubble-mediated transfer to the water-side transfer velocity of a gas is dependent on solubility and has a complicated dependence on Schmidt number. This feature complicates the interpretation of dual tracer experiments (Sect. 2.5.3; Asher and Wanninkhof 1998) and affects the applicability of gas transfer parameterisations across gases and the range of water temperature (see Sect. 2.6.5). Some estimates of the sensitivity of transfer velocity to whitecap coverage are depicted in Fig. 2.4, emphasising particularly the theoretical sensitivity to solubility and structural uncertainty relating to the specific model.

The precise dependences of bubble-mediated transfer on the environment and the molecular properties of

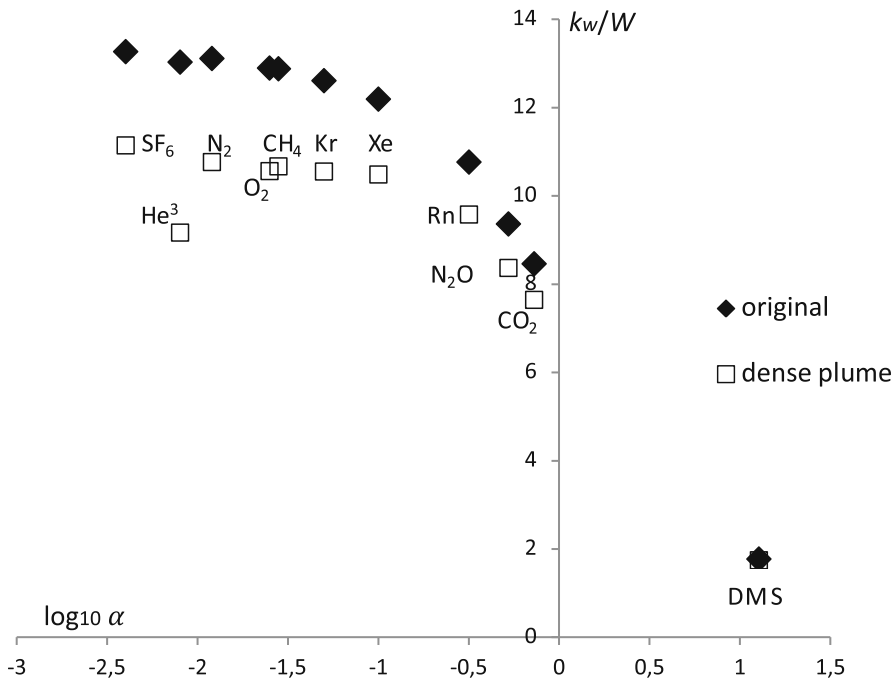

Fig. 2.4 Sensitivity of gas transfer velocity to whitecap coverage (k_w/W in cm(h %)$^{-1}$) plotted against logarithm of Ostwald solubility ($\log_{10} \alpha$). Based on the original "independent bubble model" (*filled diamonds*) and "dense plume model" (*open squares*) of Woolf et al. (2007). Dense plume model calculated for a plume void fraction of 20 %. All transfer velocities calculated for seawater at 20 °C using gas constants suggested by Wanninkhof et al. (2009) and normalised to a Schmidt number of 660

the dissolved gas require further investigation (Woolf et al. 2007). A third important feature of bubble-mediated gas transfer is that since it is dependent on wave breaking, whitecapping and the dispersion by mixing processes in the upper ocean (see Sect. 2.2.5), its environmental dependence (on wind speed, sea state, water temperature . . .) is a function of the environmental dependence of these processes. In particular, in common with the sea spray source function, the environmental dependence of whitecap coverage is critical for quantification of bubble-mediated gas transfer.

Whitecap coverage W is a practical but enigmatic measure of the whitening of the sea surface associated with wave breaking, air entrainment, bubble plumes and surface foam. Its indefinite nature and practical obstacles to its systematic measurement make applying field measurements and parameterisations of whitecapping within the whitecap method difficult (de Leeuw et al. 2011). Nevertheless, studies of historical data sets (Bortkovskii and Novak 1993; Zhao and Toba 2001) have elucidated the environmental dependence of whitecapping. There have also been significant advances in its systematic measurement (Callaghan and White 2009) that enable more detailed analysis of environmental dependence (Goddijn-Murphy et al. 2011). Wind speed is the main driver of whitecapping and wind-speed-only parameterisations are useful (Monahan and O'Muircheartaigh 1980; Goddijn-Murphy et al. 2011), but their accuracy for instantaneous whitecap coverage is poor. Recent measurements all indicate that the whitecap fraction is lower than that predicted by Monahan and O'Muircheartaigh (1980) which is most frequently used in models (de Leeuw et al. 2011). It may be inferred that the sea spray source function and gas transfer velocities are also likely to vary greatly at a given wind speed. Water temperature and sea state appear to be major additional factors in determining whitecap coverage, and by implication aerosol production and gas transfer. Long et al. (2011) suggests scaling particle production by wave-breaking energy.

2.2.4 Wind-Generated Waves

Wind-generated waves affect processes at the air-sea interface in several ways. In the form of variable roughness elements and group speeds, they interact with and modify the wind field above the sea surface (c.f. Sects. 2.2.9 and 2.4.1). The Stoke's drift caused by the waves is involved in the generation of the Langmuir circulation which, in turn, is one of the mixing processes of the surface layer of the ocean (Sect. 2.2.5) and affects the distribution of surfactants (Sect. 2.2.7). Breaking waves inject bubbles (Sect. 2.2.3) and cause turbulence in the surface waters contributing to the surface processes and to the mixing of the surface layer. Another source of turbulence is the microscale breaking of short waves (Sect. 2.2.1).

The properties of the irregular wave field cannot be parameterised by wind speed alone. For example, wave breaking depends on the wave steepness and not on the wind speed. In addition to the wind speed, the development of waves depends also on wind duration, fetch, the shape of the basin, water depth and atmospheric stratification. Typically, the wave field consists of one or several wave systems, e.g. locally generated waves and a swell originating from a distant storm. Their influence on the interaction with the atmosphere varies with state of development, the relative dominance of the wave systems and the difference of their directions (e.g. Donelan et al. 1997; Drennan et al. 1999; Veron et al. 2008). The properties of the wave field can be quite different in the oceans to that in marginal seas. While in the oceans the waves more often reach full development, in areas closer to the shore waves are typically strongly forced due to the limited fetch and are thus steeper. Depending on the fetch geometry, the direction of the waves can differ from the wind direction (Pettersson et al. 2010). If the sea is shallow enough for the waves to 'feel' the bottom, there will be further changes in the steepness of the waves and changes in wave directions leading to areas of wave energy convergence and divergence. In high latitudes the seasonal ice cover forms a changing fetch and fetch geometry affecting the properties of the wave field adjacent to the ice edge.

For transfer across the air-sea interface the turbulence in the subsurface layer is one of the key factors. When present, the breaking waves contribute strongly to the subsurface turbulence. Babanin (2006) has suggested that the orbital motion of the waves causes turbulence also in the absence of the breaking waves.

In view of the importance of the water-side turbulence for the processes at the interface and the surface layer of the ocean, studies have been undertaken on the dissipation of the turbulent kinetic energy in the upper layer. The experimental data needed in these studies are not easy to obtain (see Terray et al. (1996) and Soloviev et al. (2007) for a review), but the limited data shows that in the presence of breaking waves the dissipation values are higher than given by the shear-driven wall layer approach (e.g. Agrawal et al. 1992; Osborne et al. 1992; Anis and Moum 1995; Drennan et al. 1996; Terray et al. 1996; Phillips et al. 2001; Zappa et al. 2007). Anis and Moum (1995) measured high dissipation rates at depths greater than the height of the breaking waves and suggested that the orbital motions of swell could be one possible mechanism that transports the wave induced turbulence to deeper depths. On the other hand, Terray et al. (1996) found that the dissipation has a constant value to a certain depth below which the wall-layer behaviour is found. Their premise was that the dissipation is balanced with the wind input and the depth of the constant dissipation layer is of the order of the significant wave height. Based on his similarity analysis, Kitaigorodskii (1984, 2011) proposed the existence of a constant dissipation rate under breaking waves. He concluded that the dissipation is dependent on the water-side friction velocity and the turbulent viscosity constant in the layer of constant dissipation. In both approaches (Terray et al. 1996; Kitaigorodskii 1984, 2011), the dissipation is dependent on the state of development of the waves. Sutherland et al. (2013) compared measured dissipation rates in the surface ocean boundary layer to various scalings (e.g. Terray et al. (1996) and Huang and Qiao (2010)). They found that the depth dependence was consistent with that expected for a purely shear-driven wall layer. Many dissipation profiles scaled with a Stokes drift-generated shear, suggesting there may be occasions where the shear in the mixed layer are dominated by wave-induced currents.

So far there have been only a few experimental studies on the dependence of gas exchange on the dissipation caused by the breaking waves. Zappa et al. (2007) demonstrated the dependence of gas transfer velocity on the subsurface dissipation rate.

Presently there are on-going field campaigns aiming to study this question (e.g. Pettersson et al. (2011) and using the ASIP profiler see Sect. 2.6.4). Kitaigorodskii (2011) proposed a wave-age-dependent transfer velocity based on his considerations of the dissipation rate and previously published data. Soloviev et al. (2007) have proposed a gas exchange parameterisation based on present knowledge of the different processes in the exchange. Their model includes three sources of turbulence, the convective, shear and wave-induced turbulence. The model predicted that at wind speeds of up to $10\,\mathrm{ms}^{-1}$ the exchange is not dependent on the wave age due to factors that cancel each other. At higher wind speeds, the bubble-mediated transfer is dominating. Due to the lack of coincident observations, this behaviour could not be confirmed and also hindered a detailed analysis of the relative importance of different sources of the turbulence.

2.2.5 Large-Scale Turbulence

Upper ocean dynamics is dominated by shear-generated eddies (small-scale turbulence) that coexist with buoyant plumes and wave-generated coherent structures (large-scale turbulence). The buoyant large eddies are generated by cooling at the surface resulting in convection extending to the bottom of the mixed layer, at which depth stability suppresses turbulence (Csanady 1997).

The surface cooling (net heat flux and evaporation) increases density of the surface water, thereby enhancing buoyancy. The buoyancy flux is defined according to e.g. Jeffery et al. (2007) as:

$$B = \frac{gaQ_{net}}{c_{pw}\rho_w} + \frac{g\beta_{sal}Q_{lat}}{\lambda\rho_w} \tag{2.3}$$

where a is the thermal expansion coefficient, g acceleration due to gravity, Q_{net} is the net surface heat flux (i.e. sensible and latent heat flux plus net long-wave radiation), c_{pw} is the specific heat of water, ρ_w is the density of water, β_{sal} is the saline expansion coefficient, Q_{lat} is the latent heat flux, and λ is the latent heat of vaporisation. Following convective scaling in the atmosphere (see Eq. 2.11), the characteristic velocity scale of the turbulence generated by convection (the water-side convective velocity scale) is defined as follows (MacIntyre et al. 2002):

$$w_* = (Bz_{ml})^{1/3} \tag{2.4}$$

where z_{ml} is the depth of the mixed layer. According to Eq. 2.4, a stronger buoyancy flux (a larger value of B) and a deeper mixed layer (a larger value of z_{ml}) produce enhanced convective mixing in the water. The convective velocity scale exhibits diurnal as well as seasonal cycles depending on variations in surface heating and variations of mixed layer depth. Rutgersson et al. (2011) suggested relating the convective velocity scale to the friction velocity of the water (u_{*w}) as u_{*w}/w_*. This parallels the description of atmospheric flow by combined convective and shear-generated turbulence, and characterises the comparative energetic roles of surface shear and buoyancy forces (Zilitinkevich 1994). This scaling can be used to express the additional parallel resistance to transfer initiated by the water-side convection. When wind is in the low to intermediate speed regime, convection is important for mixing, and it has in several studies been shown to enhance surface gas transfer (MacIntyre et al. 2002; Eugster et al. 2003; McGillis et al. 2004b; Rutgersson and Smedman 2010; Rutgersson et al. 2011). Water-side convection is expected to dominate in situations with cooling at the water surface (during the night, or during advection of cold air masses) and deepening of the mixed layer.

The interaction between the mean particle drift of surface waves (Stokes drift) and wind-driven surface shear current generates Langmuir circulation consisting of counter-rotating vortices roughly parallel to the wind direction (Langmuir 1938). The Langmuir circulation can be seen at the surface by the collection of surface foam in meandering lines in the along-wind direction or by sub-surface observations, following bubbles trapped in downwelling regions between vortices and current profiles (Smith 1998; Thorpe 2004; Gargett and Wells 2007). McWilliams et al. (1997) defined a turbulent Langmuir number describing the relative influence of directly wind-driven shear and Stokes drift:

$$La = \left(\frac{u_{*a}}{u_S}\right)^{1/2} \tag{2.5}$$

where u_{*a} is the atmospheric friction velocity and u_s is the surface Stokes velocity. Sullivan and McWilliams (2010) summarise several studies focusing on the Langmuir mechanism and it is clear that Langmuir circulation (or Langmuir turbulence) greatly enhances

turbulent vertical fluxes of momentum and heat at the surface.

A regime diagram for classifying turbulent large eddies in the upper ocean was suggested by Li et al. (2005) using the Hoennecker number (Li and Garrett 1995) as a dimensionless number comparing the unstable buoyancy force driving thermal convection with the wave forcing driving the Langmuir circulation. According to Li et al. (2005), the wind driven upper ocean is dominated by Langmuir turbulence under typical sea state conditions. Transition from Langmuir to convective turbulence occurs with strong thermal convection, relatively low winds and small surface velocity. An alternative descrition of the relative role of Langmuir and convectively generated turbulence is given by Belcher et al. (2012) as z_{ml}/L_L, where L_L is a convective-Langmuir number stability length as an analogue to Obukhov length for convective-shear turbulence.

Large scale turbulence disrupts the molecular sublayer and initiates a more efficient gas transfer at the surface. The large scale turbulence is dominated by Langmuir circulation or buoyancy depending on environmental conditions.

2.2.6 Rain

Because rain events in nature are episodic and rain rates are variable, only a few field studies have been conducted. These experiments, using natural rain and geochemical mass balances of O_2 invasion and SF_6 evasion in small plastic pools (Belanger and Korzun 1990, 1991; Ho et al. 1997), demonstrated that rain could significantly enhance $k_w(660)$, although the exact relationship between rain and $k_w(660)$ was not established in these studies.

Most systematic studies on the effect of rain on air-water gas exchange have been conducted in the laboratory using a rain simulator and a receiving tank. These studies began in the 1960s, where initial laboratory studies using O_2 invasion employed a rain simulators that had only 8–12 nozzles so only produced a few raindrops at a time, and only investigated a range of rain rates up to 17 mm h^{-1} (Department of Scientific and Industrial Research 1964; Banks and Herrera 1977; Banks et al. 1984). In the last two decades, systematic laboratory studies examining the full range of rain rates encountered in nature have quantified the effect of rain on gas exchange (Ho et al. 1997; Takagaki and Komori 2007), the interaction between rain and wind (Ho et al. 2007), the mechanism behind the enhancement (Ho et al. 2000), the effect in saltwater Ho et al. (2004); Zappa et al. (2009). Furthermore, some modeling studies have been conducted to examine the potential effect of rain on air-sea CO_2 exchange (Komori et al. 2007; Turk et al. 2010).

In laboratory experiments using evasion of He, N_2O, and SF_6 or invasion of CO_2, rain has been shown to enhance the rate of gas exchange significantly, and the relationship between $k_w(660)$ and rain can easily be related to either the kinetic energy flux or momentum flux of rain, both of which encompass variability in rain rate and drop size (Ho et al. 1997; Takagaki and Komori 2007). Enhancement in $k_w(660)$ is due mostly to increased near surface turbulence, whereas bubbles play a minor role (Ho et al. 2000). Experiments in saltwater demonstrate that the relationship between rain and $k_w(660)$ is the same as in freshwater, but density stratification could inhibit vertical mixing and decrease the overall gas flux (Ho et al. 2004; Zappa et al. 2009).

Some SF_6 evasion experiments have been conducted to examine the combined effects of rain and wind on gas exchange. Initial results indicated that the effect of rain and wind might be linearly additive (Ho et al. 2007), but further experiments have shown that the enhancement effects of rain fades with increasing wind speeds (Harrison et al. 2012), and wind speeds in the initial experiments were not high enough to exhibit that effect. While the exact mechanistic interaction between wind and rain has not been determined, it has been shown that when Kinetic Energy Flux (KEF) from wind (calculated from u_*) is greater than KEF from rain, the enhancement effects of rain is diminished (Harrison et al. 2012).

Modeling studies using relationships derived in the laboratory shows that the effect of rain on air-sea CO_2 exchange is insignificant on a global scale, but could be important on regional scales (Komori et al. 2007; Turk et al. 2010). However, those studies made simple assumptions that remain to be tested, including those about the dynamics of rain falling on the ocean, and about how rain and wind interact.

Future experiments should examine the effect of temperature change caused by rainfall on gas

exchange, the interaction of rain with surfactants, and detail the mechanism behind the interaction of rain and wind and how they affect gas exchange. Field experiments should also be conducted in areas likely to be impacted by rain.

2.2.7 Surface Films

Surfactants can influence air-sea gas transfer rates via several mechanisms. Firstly, the presence of concentrated insoluble surfactant films (slicks) can act as a barrier to gas exchange, either by forming a condensed monolayer on the sea surface (Springer and Pigford 1970) or by providing an additional liquid phase that provides a resistance to mass transfer (Liss and Martinelli 1978). However, in the field, this effect is believed to be important only at low wind speeds, as slicks are easily dispersed by wind and waves (Liss 1983). The main effect of surface-active material is believed to be due to the occurrence of soluble surfactants that alter the hydrodynamic properties of the sea surface and hence turbulent energy transfer. Their presence reduces the roughness of the sea surface and hence the rate of micro-scale wave breaking (see Sect. 2.2.1), lowers sub-surface turbulence (see Sect. 2.2.2) and impacts on rates of surface renewal (see Sect. 2.3.1).

Early experiments in wind/wave tanks showed that artificial surfactants could cause reductions in k_w of up to 60 % for a given wind speed (Broecker et al. 1978). Indeed, contamination of the air-water interface by surface films was a common problem, particularly in circular tanks where there was no "beach" at the end of the tunnel for the film to collect (Jähne et al. 1987). Later experiments found that the presence of surfactants influenced the point at which small scale waves were observed at the water surface, co-incident with a rapid increase in k_w (Frew 1997). Even more interesting were observations that k_w could vary with biological activity (Goldman et al. 1988) due to the exudation of soluble surface-active material (including carbohydrates, lipids and proteins) by phytoplankton (Frew et al. 1990).

Supporting evidence came from laboratory experiments using seawater collected on a transect from the United States of America to Bermuda (Frew 1997) indicating that the decrease in k_w correlated inversely with bulk-water chlorophyll, dissolved organic carbon (DOC) and coloured dissolved organic matter (CDOM), see Fig. 2.5. The relationship of k_w with CDOM is important because this parameter can be determined remotely by satellite.

Although the importance of surfactants in determining air-sea gas transfer rates has long been recognised, it has proven exceedingly difficult to demonstrate that they exert a measurable effect in the field. Perhaps the first direct evidence came from a study of air-sea gas transfer rates using the heat flux technique (see Sect. 2.5.1) off the coast of New England in fairly light winds (Frew et al. 2004). The transfer of heat was measured inside and outside of a naturally occurring CDOM-rich slick and was found to be substantially inhibited by the presence of the slick (from 4.1 to 1.3 cm hr^{-1}). Due to the patchy nature of the slick and changeable wind speed the exact magnitude of the inhibition due to the slick is unclear.

It is commonly thought that surfactants may only be important in retarding gas transfer at very low winds. However, a big unknown is whether exchange rates might be reduced at higher winds when, despite wave breaking, surfactants are predicted to be brought back to the sea surface via bubble scavenging (Liss 1975). Support for this hypothesis came from Asher et al. (1996) who demonstrated, in a series of laboratory experiments, that soluble surfactants inhibited gas transfer even under wave-breaking conditions. Very recently, Salter et al. (2011) reported on a deliberate large scale release of an artificial surfactant (oleyl alcohol), in the north-east Atlantic Ocean. Gas transfer rates were measured by both the dual tracer technique (see Sect. 2.5.3) and direct covariance measurements of the DMS flux (see Sect. 2.5.2). Air-sea gas transfer rates were reduced by about 50 % at 7 ms^{-1} and were still impacted by the presence of the surfactant at high wind speeds; k_w was lowered by 25 % at 11 ms^{-1}.

Whilst the Salter et al. (2011) study has proven that surfactants can significantly impinge on gas transfer in the world's oceans, it is not yet clear that they do so at ambient levels. A recent study (Wurl et al. 2011) found many of the world's oceans (subtropical, temperate and polar) are covered to a significant extent by surfactants. Enrichments in the sea surface microlayer compared to bulk seawater were observed to persist at wind speeds of up to 10 ms^{-1}

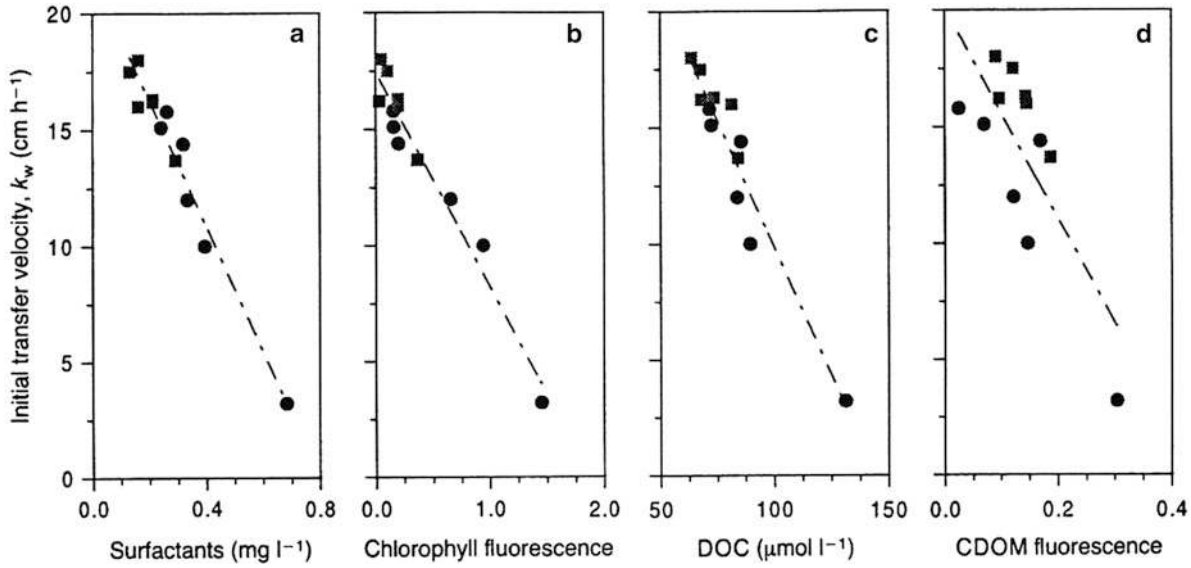

Fig. 2.5 Correlations of k_w with (**a**) surfactant concentration, (**b**) in situ fluorescence, (**c**) dissolved organic carbon (DOC) and (**d**) coloured dissolved organic matter (CDOM) fluorescence at 450 nm (Figure reproduced from Frew (1997))

consistent with the observations of the Salter et al. (2011) study. Clearly, this is an area worthy of further effort.

How important might surfactants be on a global basis? Asher (1997) predicted a global decrease of 20 % in the net sea to air flux of carbon dioxide based on the reasonable assumption that surfactant concentrations would scale with primary productivity. Tsai and Liu (2003) estimated that the net uptake of CO_2 could be reduced by between 20 % and 50 %; the range reflecting the uncertainty in measurements of surfactants and their impact on gas transfer. However, a simple relationship between chlorophyll and a reduction in k_w may be unrealistic as sea surface surfactant enrichments have been found to be greatest in oligotrophic (i.e. low productivity) waters rather than, as might have been expected, in highly productivity waters (Wurl et al. 2011); presumably due to the greater occurrence of bacterial degradation in the latter waters. Nightingale et al. (2000a) found no decline of gas transfer rates during the development of a large algal bloom in the equatorial Pacific. The implication of these studies of surfactants and air-sea gas transfer is that wind speed may not be the best parameter with which to parameterise k_w in the oceans, particularly in biologically productive regions.

A reasonable correlation with the total mean square wave slope for both filmed and film-free surfaces, particularly of shorter wind waves, suggested that this parameter, although difficult to measure at sea, might be a more useful predictor of k_w (Jähne et al. (1987) – see Sect. 2.6.2). This has been shown experimentally in the field by Frew et al. (2004) who found that k_w was better correlated to the mean square wave slope than to wind speed, specifically when winds were below 6 ms^{-1} and when CDOM levels were enhanced in the microlayer.

2.2.8 Biological and Chemical Enhancement

The enhancement of gas transfer by chemical reaction within the mass boundary layer(s) has been recognised as important for a small number of gases including O_3 (Fairall et al. 2007) and SO_2 (Liss 1971), and potentially important for CO_2 (Hoover and Berkshire 1969; Wanninkhof and Knox 1996; Boutin and Etcheto 1995). Suitably rapid reactions serve to 'steepen' the concentration gradient of the gas and thus reduce the effective depth of the mass boundary layer, thus leading to an enhancement in the transfer velocity (Johnson et al. 2011).

Note that whilst reversible reactions such as the hydration of CO_2 will act to buffer a reaction in either direction and thus lead to enhancement of fluxes into and out of the ocean (albeit assymetrically where forward and reverse reactions occur at different rates), irreversible reactions have the capacity to inhibit fluxes by a similar mechanism (i.e. to decrease the steepness of the concentration gradient where either a production reaction acts against a flux into the ocean or a breakdown reaction acts against a flux out) (Johnson et al. 2011). Here we will refer only to enhancement, but the reader should be aware that enhancement factors can be negative in some situations.

The enhancement of CO_2 exchange by hydration to carbonic acid and subsequent acid dissociation has been estimated to account for between 0 % and 20 % of the global CO_2 flux estimated from the ^{14}C technique (Keller 1994). Unlike the near-instantaneous hydration of SO_2 (Liss 1971), the hydration of CO_2 is relatively slow and its enhancement is thought to be important only when turbulent forcing is weak (and thus the timescale of transport across the mass boundary layer is relatively large). The effect on global CO_2 fluxes is rather complex. Boutin and Etcheto (1995) estimate that the net global atmosphere-to-ocean CO_2 flux is reduced by approximately 5 % due to the bias introduced by outgassing areas being generally associated with low average winds. On a local scale, CO_2 hydration must enhance the flux at low or zero wind speeds. The magnitude of this effect is represented in the hybrid parameterisation of Wanninkhof et al. (2009) as a constant component of k_w of 2.3 cm h^{-1}. Interactions between different compounds and reactions might lead to more complex behaviour than simple first-order enhancement. For instance, air-water mass transfer of CO_2 can be inhibited or enhanced by the mass transfer of NH_3 due to the reversible and pH dependent formation of ammonium carbamate (Budzianowski and Koziol 2005), although this phenomena has not been studied in the natural environment.

Just as physico-chemical processes may enhance mass transfer by modifying the concentration gradient in the mass boundary layers, biological activity might achieve the same, at least on the water side of the interface. Microbial communities at the ocean surface tend to be different from bulk water communities, often with considerably enhanced population densities (Cunliffe et al. 2009), which would lead to potentially rapid processing of bio-active compounds. There is some circumstantial evidence for the asymmetrical biologically-mediated transfer of methane (Upstill-Goddard et al. 2003), and O_2/CO_2 (Garabetian 1991; Matthews 1999), but these processes are not well studied.

2.2.9 Atmospheric Processes

Within a few millimetres of the water surface there is a thin sublayer dominated by molecular diffusion. Above the molecular diffusion layer is the atmospheric surface layer where the vertical transport is dominated by turbulent eddies; it extends upwards from the molecular layer to a rather poorly defined distance (ranging from approximately 10–100 m). Further away from the surface (in the Ekman layer) the Coriolis effect gradually changes the flow. These layers make up the Atmospheric Boundary Layer (ABL), in which the presence of the surface has a profound effect on the flow. Traditionally the atmospheric surface layer is described by the Monin-Obukhov Similarity Theory (MOST), it assumes stationary and homogeneous conditions and a solid surface (Panofsky and Dutton 1984). The fluxes are approximated to be constant with height (within 10 %) and it is thus enough to describe the flux at just one height. Using MOST the turbulent surface fluxes are often expressed using the bulk aerodynamic formula. Stress (τ), heat and scalar fluxes can be written as:

$$\tau = \rho_a u_{*a}^2 = \rho_a C_D (U_z - U_0)^2 \tag{2.6}$$

$$H = \rho_a c_p \overline{w'\theta'} = \rho_a c_p C_H U_z (T_z - T_0) \tag{2.7}$$

$$C = \rho_a c_p \overline{w'c'} = D_C U_z (C_z - C_0) \tag{2.8}$$

where ρ_a is the air density, u_{*a} the friction velocity on the air-side, C_D, C_H and D_C are the transfer coefficients for momentum heat and scalars at the specific height z. Transfer coefficients for scalars (Dalton number) can be related to transfer velocity by $D_C = k/U_z$. Wind speed, temperature and scalar values at height z are U_z, T_z and C_z, corresponding parameters at the surface are U_0, T_0 and C_0.

In the atmosphere, gradients of wind, temperature, and scalars are dependent on the atmospheric stratification, which also influences the transfer coefficients. Neutral stratification (giving logarithmic profiles, assuming MOST) is used as the reference state and

flux coefficients are then normalised using the actual stratification. Stratification can be expressed in terms of the Monin-Obukhov length ($L = -\frac{u_{*a}^3 T}{\kappa g \overline{w'\theta'_v}}$, where $\overline{w'\theta'_v}$ is the surface virtual potential temperature flux). For unstable atmospheric stratification $L < 0$ and for stable atmspheric stratification $L > 0$. Turbulence in the atmosphere (and thus the vertical gradients) is stability dependent and the non-dimensional gradients of wind, temperature and scalars are expressed as:

$$\phi_\alpha = \frac{d\chi}{dz}\frac{\kappa z}{\chi_*} \tag{2.9}$$

where $\alpha =$ m, h, c and $\chi =$ U, θ and C. The ϕ -functions are expressed by empirical expressions for wind (ϕ_m) and temperature (ϕ_h); see Högström (1996) for a review of expressions for momentum and heat, and in Edson et al. (2004) functions for humidity are given. McGillis et al. (2004a) suggest the same expressions for CO_2 as for humidity. For stable stratification, expressions from Holtslag and De Bruin (1988) are frequently used.

Over the sea in the presence of surface gravity waves the wave boundary layer (WBL) is the atmospheric layer that is directly influenced by surface waves. For a growing sea the WBL is of the order of 1 m (Janssen 2004) and for swell waves it is significantly larger, it can even extend throughout the ABL (Smedman et al. 1994).

The neutral transfer coefficients are related to the roughness length defined as the intersect of the logarithmic profiles with the surface value. Roughness length for momentum (z_0) is crudely related to the roughness of the surface. Charnock (1955) expressed z_0 over the ocean as:

$$z_0 = \alpha \frac{u_{*a}^2}{g} \tag{2.10}$$

where the Charnock coefficient, α, is a constant or described as a function of the state of the waves, where younger waves are expected to give a rougher surface (Fairall et al. 2003; Drennan et al. 2003; Carlsson et al. 2009). For temperature and scalars it is more complicated (Garratt 1992). The scalar roughness lengths can basically be expressed by the velocity roughness length, friction velocity and Schmidt number (see Fairall et al. (2000) for a discussion of different approaches). When the flow is aerodynamically smooth, a thin viscous sublayer exists adjacent to the surface.

Stability is a dominating parameter in the atmosphere since it determines the scale of the turbulence and thus the efficiency of eddy transport. For stable stratification, turbulence is suppressed, being dominated by intermittent turbulent events and atmospheric gravity waves and with a low boundary layer height. For unstable stratification, the convection at the surface enhances turbulence initiating convective eddies. The mean wind can be close to zero, but there is a non-zero wind component due to the gustiness. Godfrey and Beljaars (1991) suggested adding a gustiness wind component proportional to the convective scaling velocity (Deardorff 1970):

$$w_{*a} = \left(\frac{g}{T} z_i \overline{w'\theta'_v}\right)^{1/3} \tag{2.11}$$

where z_i is the height of the ABL. For specific conditions (during free convective conditions, swell or low boundary layer height) the wind gradients are altered (Beljaars 1995; Fairall et al. 2003; Guo et al. 2004; Högström et al. 2008). For gradients of temperature and scalars, free convection is important, but less is known about swell and boundary layer height.

Over land, stratification is mainly determined by the diurnal cycle due to effective radiative heating and cooling of land surfaces. Over sea, the diurnal cycle is not as dominating due to the larger heat capacity of water. Then stronger atmospheric stratification occurs during advection of air masses with a different temperature to the water surface. Strongly stratified conditions thus occur in areas close to coasts or with great horizontal temperature gradients.

For momentum, heat, and gases with high solubility (like water vapour) the atmosphere induces the major resistance to transfer. For gases with low solubility, processes in the water contribute the main resistance to transfer. Taking atmospheric stability into account when determining transfer coefficients makes a significant difference when calculating fluxes of momentum, heat and humidity. For CO_2 the effect is relatively minor, up to about 20 % for low wind speeds (Rutgersson and Smedman 2010).

2.3 Process Models

To gain a deeper understanding of relevant transport mechanisms, several models have been developed. These range from conceptual models to numerical models based on first principles. Conceptual models are major simplifications of the actual processes and frequently address one dominant process taking place. Nevertheless, they are appealing as they can be used for deriving certain properties of the transport, such as gradients, fluxes or Schmidt number exponents. Such models will be discussed in Sect. 2.3.1. These simplistic models cannot describe interfacial properties, such as temperature distributions or the wave field. Numerical simulations based on first principles may be used for addressing such problems. The current state-of-the-art of such models is presented in Sect. 2.3.2.

2.3.1 Interfacial Models

The ocean–atmosphere exchange of insoluble gases and sparingly soluble chemical species such as CO_2, as well as other properties such as heat and momentum, is controlled by the mass boundary layer occupying the upper 10–100 μm of the ocean surface. Within this boundary layer, molecular diffusive transport tends to dominate over turbulent transport, with increased turbulent forcing leading to an increase in the rate of exchange by a reduction of the thickness of the diffusion-dominated domain. Various models have been proposed to represent such diffusion-mediated transport across the air-sea interface, and these lead to different dependency of exchange kinetics (i.e. the transfer velocity) on the diffusivity of the tracer (due to differences in the balance between the diffusive and turbulent processes controlling exchange). These models are described below, along with brief consideration of analogous models for the transport on the air-side of the interface for soluble gases.

2.3.1.1 Thin (Stagnant) Film Model

The simple thin film model (Whitman 1923) applied to the air-sea interface by Liss and Slater (1974), represents the sea-surface as a flat, solid boundary, with stagnant mass boundary layers on either side, through which diffusion is the sole transport processes. The diffusive flux through the water side stagnant film can be written as

$$F = -D\frac{dC}{dz} \tag{2.12}$$

where D is the diffusivity of the gas in the medium, C is concentration of the gas of interest and z is the vertical depth of the mass boundary layer. The thickness of the stagnant film must also be a function of the properties of the medium, notably the viscosity. We can rewrite the equation in terms of a transfer velocity of the water side, k_w as follows:

$$F = -k_w \Delta C \tag{2.13}$$

where

$$k_w = \frac{D}{\delta_c} \tag{2.14}$$

It can be seen from this approach that the transfer velocity is a function of both the gas properties (D) and the thickness of the thin film (δ_c), and has units of velocity ($m^2 s^{-1}\ m^{-1} = ms^{-1}$). This transfer velocity (also known as piston velocity) represents the rate of vertical equilibration between water column and atmosphere. Equation 2.14 is directly proportional to the diffusivity of the gas. The effect of (e.g. wind-driven) turbulence is to reduce the effective depth of the mass boundary layer and thus reduce the resistance to transfer.

Where the stagnant film models describe discrete layers where turbulent and diffusive mixing dominate transfer, the rigid boundary or solid wall models (e.g. Deacon 1977; Hasse and Liss 1980) apply a velocity profile at either side of the interface to describe a smooth transition between molecular and turbulent transport regimes. Such models predict that the transfer velocity is proportional to $D^{2/3}$, demonstrating that as turbulence plays a (modest) role in determining the rate of transfer in such a model, the diffusivity of the tracer becomes somewhat less important in determining the rate of exchange than for the stagnant film model. This diffusivity dependency has been demonstrated rather conclusively for a smooth (laminar flow) water surface by tank and wind tunnel heat and gas exchange experiments (see e.g. Liss and Merlivat 1986, for a summary).

2.3.1.2 Surface Renewal Model

A second class of models has historically been applied to interfacial exchange problems, where the diffusion-limited surface water layer is episodically and instantaneously replaced by bulk water from below (e.g. Higbie 1935; Danckwerts 1951). This episodic replacement leads to an increased role for turbulence in bringing water to the surface to exchange with the atmosphere. The details of the various surface renewal models differ; for example Higbie (1935) assumes a single turbulence-dependent renewal rate, whereas Dankwerts describes a statistical distribution of possible renewal timescales which is modulated by turbulent forcing. However, they all demonstrate the same dependence of the transfer velocity on $D^{1/2}$ which results from the description of an average flux resulting from episodic replacement of the surface with water of maximum disequilibrium and subsequent reduction in flux as this disequilibrium is reduced prior to the next renewal event. The general form of the surface renewal model transfer velocity term is

$$k_w \propto \left(\frac{D}{\tau}\right)^{\frac{1}{2}} \tag{2.15}$$

where τ is the renewal timescale. Surface renewal models have been widely used in studies of heat fluxes from water surfaces, including in the ocean, with generally good agreement at moderate to high winds (e.g. Garbe et al. 2004). This is strong validation of the dependency of the transfer velocity on the square root of the diffusivity for non-smooth water surfaces.

2.3.1.3 Eddy Renewal Model

The surface renewal model describes periodic 'disturbances' of the surface by discrete events, which are not physically described. Fortescue and Pearson (1967) and Lamont and Scott (1970) developed the surface renewal approach by explicitly modelling the physical processes at the interface assuming eddy turbulence to be the dominating process in transporting bulk water to the interface. This treatment models the eddy turbulence as a series of stationary cells of rotating fluid in long 'rollers' in the along-wind direction, alternatively converging and diverging, leading to regions of upwelling and downwelling to and from the surface. The transfer velocity in this model is related to ε, the energy dissipation rate, (along with molecular diffusivity) and can be generalised as

$$k_w = D/\delta_c \quad \text{with} \quad \delta_c = (D/\nu)^{1/2}\delta_\nu = (D/\nu)^{1/2}(\nu^3/\varepsilon)^{1/4} \tag{2.16}$$

$$\Rightarrow k_w = bS_c^{-1/2}(\varepsilon\nu)^{1/4} \tag{2.17}$$

where $f(\varepsilon\nu)$ is some function of ε and the kinematic viscosity of water, ν. As with instantaneous surface renewal models, the predicted transfer velocity is found to vary with $D^{\frac{1}{2}}$. Recently, eddy renewal models have been used with considerable success in predicting not only observed heat fluxes from environmental and laboratory water surfaces but also patterns of heat distribution – parallel streaks of warmer and colder water on the surface (e.g. Hara et al. 2007; Veron et al. 2011). The parallel development of eddy renewal models and surface infrared imaging has the potential to directly relate surface turbulence measurements, mean surface renewal timescales and transfer velocities leading to alternative parameterisations of transfer velocities.

2.3.1.4 Surface Penetration

Whilst good agreement has been found between surface and eddy renewal models and heat fluxes and distributions at water surfaces, it has been found that these do not scale well to gas transfer velocities via the diffusivity dependency (e.g. Atmane et al. 2004). This led to the application of the surface penetration model of Harriott (1962) to detailed heat and mass flux data by Asher et al. (2004). The surface penetration model differs from renewal models as it considers incomplete replacement of the surface by eddy transport from the bulk. This means that as well as eddy lifetime, the transfer velocity is a function of the 'approach distance'. The implication of this is that the diffusivity dependence of transfer is not constant with turbulent forcing. This is demonstrated by Asher et al. (2004) by using a special case of the model of Harriott (1962) for constant eddy approach distance and lifetime:

$$\frac{1}{k_w} = \frac{h}{D} + \frac{1}{1.13}\left(\frac{t}{D}\right)^{\frac{1}{2}} \tag{2.18}$$

where h is the eddy approach distance and t is the renewal timescale. The application of the surface penetration model is found by Asher et al. (2004) to

explain the apparent discrepancy between transfer velocities of heat and mass through the surface water layer from surface/eddy renewal models.

The diffusivity dependence of the transfer velocity as predicted by surface penetration theory is not constant with turbulent forcing. This implies that as well as step changes in the diffusivity transfer velocity relationship (from $k_w \propto D^{2/3}$ to $k_w \propto D^{1/2}$ at the transition between smooth and rough surface regimes) there is a continuous change in the exponent with changing turbulent forcing.

2.3.1.5 Air-Side Transfer

A similar array of physical models of the transfer velocity on the air-side of the interface exist (e.g. Fairall et al. 2003; Jeffery et al. 2010), which are principally concerned with the flux of water vapour from water surfaces. Such models are also applicable to other soluble gases or those whose transfer is significantly chemically enhanced in the water phase (and thus under gas-phase control) and also to the dry deposition of particles to the water surface. Generally these models show that, as in the water phase, the diffusivity dependence on transfer is between $D^{0.5}$ and $D^{0.7}$ (e.g. Fairall et al. 2003; Johnson 2010).

2.3.2 Direct Numerical Simulations (DNS) and Large Eddy Simulations (LES)

High-resolution numerical simulation of the turbulent flow and heat/gas transport in the vicinity of an air-water interface is an alternative approach for studying interfacial transfer processes. The computational approach, which is also called direct numerical simulation (DNS), solves the posed initial-boundary-value problem and resolves the flow fields down to that of dissipation and diffusion scales, and examines the detailed dynamics and transfer processes. The boundary-value problem consists of conservation equations of mass and momentum, and advection–diffusion equations of temperature and gas in the bulk fluids, subject to stress/flux balance and kinematic constraint at the air-water interface. The interfacial boundary conditions also govern the dynamics of surface waves ranging from capillary wavelets to gravity waves. Imposing the nonlinear conditions accurately on the interface, which is also an unknown to be solved, is the most challenging part in solving such a "fully-nonlinear" free-surface problem. Owing to the limit in previous computing capacity, DNS of three-dimensional turbulent flow underneath a free-moving water surface was not feasible until recently. The numerical model of Fulgosi et al. (2003) (also Lakehal et al. 2003) is among the first attempts to consider the dynamical effect of a deformable interface in numerical simulation of interfacial turbulence and transfer processes. The simulation, however, is confined to very small surface deformation and the maximum wave steepness ak_{wave} (a is the amplitude and k_{wave} the wavenumber) never exceeds 0.01.

A more recent development by Tsai and Hung (2007) successfully simulates the turbulent boundary layer bounded by wind-generated surface waves and the accompanying transfer processes up to immediate surface steepness (maximum $ak_{\text{wave}} \approx 0.25$). The simulation resolves all modes of the turbulent flow, including the coherent vortical structures (the renewal eddies), the laminar sublayer immediately next to the interface, and the Kolmogoroff scale turbulence, as well as the interfacial motions, including the gravity-dominant waves and the parasitic capillary ripples. A representative three-dimensional surface profile from the simulation is shown in Fig. 2.6 with the corresponding distributions of temperature and surface gas-flux density, streamwise vorticity is shown on a vertical plane. The result clearly reveals high correlation between the surface temperature and the gas-flux density. Two distinct signatures appear in these distributions: elongated streaks and random localised spots, indicative of different "surface renewal" processes in the underlying aqueous flow. The computed distribution of surface temperature resembles the measured thermal imagery of a wind-driven water surface (e.g. Garbe et al. 2004; Smith et al. 2007). Parasitic capillary wavelets form on the forward face of the carrier gravity wave, as commonly observed in wind-generated waves (e.g. Jähne and Riemer 1990). The impact of these capillary wavelets on cross-interface transfer, however, is not as significant as expected previously (e.g. Jähne et al. 1979). Note that the initial condition in posing the numerical simulation consists of a pure gravity wave and random velocity fluctuations without any prescribed vortical structures and surface capillaries. The appearance of these coherent eddies and parasitic ripples all arise from the nonlinear dynamics of the surface waves and the underlying turbulent boundary layer.

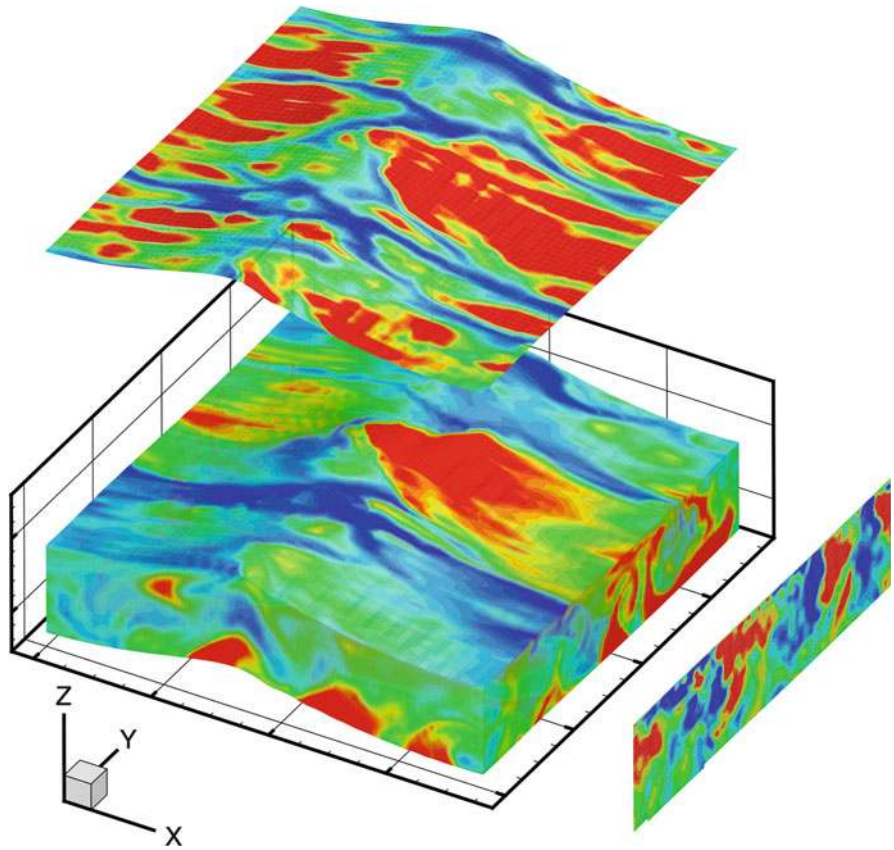

Fig. 2.6 Representative surface profile of a simulated wind-driven surface flow at the time instance of ten linear wave periods from the start of the computation. The wave propagates in the x direction. The wavelength of the carrier gravity wave is 7.5 cm. The contours superimposed on the surface, the front and side planes depict the temperature distributions. The corresponding distribution of gas-flux density is shown on an additional surface above the air-water interface. The contours of streamwise vorticity in the flow is also depicted on a cross-stream vertical plane

Despite the success of the high-resolution numerical model in simulating realistic transfer processes of wind-generated waves, DNS of interfacial turbulent boundary-layer flow is still limited to low Reynolds number (Re of the order of 10^3). The wavelength of the simulated gravity wave is also restricted to centimetres scale, and the wind speeds are limited to low to immediate regime. This is due to the fact that in DNS of the turbulent boundary layer the computation grid must be fine enough to resolve all spatial scales of the velocity, temperature and dissolved gas fields. For isotropic turbulence, the number of spatial modes increases as Reynolds number to the power 3/4, meaning the number of computation grids increases as $Re^{9/4}$. The minimum spatial scale of dissolved gas field is even smaller than that of velocity fluctuation (e.g., the diffusivities of dissolved CO_2 and O_2 are $\sim 10^{-3}$ of the viscosity of water). If all of these modes must be computed accurately, the required computer capacity becomes overwhelming. As such, the current DNS model is mainly applied to qualitative study of transfer process (e.g. Tsai et al. 2013) or testing of hypotheses in parameterization development (e.g. Hung et al. 2011).

The new advances in computer hardware and the use of parallel computing can certainly increase the size of the physical domain and speed up the computation. An alternative approach will be to adopt the method of large-eddy simulation (LES) in combination with new large-wave simulation (LWS). The methodology of LES, which was first introduced in atmospheric boundary layer research in the 1970s, is increasingly used in process studies of the ocean mixed later. However, unlike the LES model for ocean mixed

layer, in which both the subgrid turbulence and the surface wave dynamics are parameterized, the proposed LES-LWS model for simulating air-water interfacial turbulent flow resolves not only the energetic turbulent eddies but also the gravity-dominant surface waves. In contrast to the well developed LES for "wall" turbulent boundary layer, subgrid-scale (SGS) parameterization for turbulent flow underneath a deformable wavy surface is yet to be developed. In addition, parameterization models of wave dynamics of sub-surface-grid scales, including the interactions among the SGS wavelets, the interactions between the SGS wavelets and the resolved "large waves", and the interaction between the SGS wavelets and the turbulence underneath (e.g. Tsai and Hung 2010), also require further development.

2.4 Exchanged Quantities

2.4.1 Physical Quantities

Transfer across the air-sea interface involves of a number of properties, the most prominent is the exchange of momentum. Basically the exchange of momentum originates from friction at the surface extracting energy from the mean atmospheric flow. This is the major source of energy for turbulence in the atmosphere and the ocean, as well as for surface gravity waves. The transfer of momentum over the sea is different to that over land since the surface changes form as a response to the atmospheric forcing. The transfer of momentum can be expressed in terms of kinematic stress (τ) and can be partitioned into turbulent, wave induced and viscous components (Phillips 1977):

$$\tau = \tau_t + \tau_w + \tau_\nu \tag{2.19}$$

the turbulent part (τ_t) depends on the wind shear, wave induced part (τ_w) generated by the waves; the viscous part (τ_ν) is neglected from some millimetres above the surface. Since the contribution from the different components varies with height, it is possible that the vertical flux is not constant with height within the wave boundary layer (the layer directly influenced by the waves). This also means that the surface stress is highly wave dependent.

The kinematic stress τ is directly related to the friction velocity u_* by

$$u_* = \sqrt{\frac{\tau}{\rho}}, \tag{2.20}$$

where ρ is the density of the fluid. The friction velocity can be seen from the air-side (u_{*a}) or from the water-side (u_{*w}) and are related according to

$$u_{*a} = \sqrt{\frac{\rho_w}{\rho_a}} u_{*w}. \tag{2.21}$$

For near neutral conditions one can consider heat to act as a passive scalar, however, when the heat flux is larger it is dynamically active and influences the turbulence in the atmosphere and the ocean. An upward buoyancy flux influences the density of the lower atmosphere and acts to make the atmospheric stratification unstable, in contrast a buoyancy flux directed to the surface makes the atmospheric stratification stable. The turbulent heat flux has a sensible component (direct) and a latent component (indirect, linked to the energy being used/released during evaporation/condensation). For the water surface the buoyancy flux consists of turbulent heat fluxes (sensible, latent heat) as well as long wave radiation lowering the temperature of the surface water. Together with evaporation acting to make the surface more saline, this can act to make the water surface buoyantly stable or unstable.

The transfer of momentum close to the surface is caused by viscosity and pressure perturbations, but the transfer of heat is ultimately caused by diffusivity. Thus the transfer of momentum is more efficient and exhibits a stronger wind speed dependence than the transfer of heat. The latent heat flux is generally greater during warmer conditions (in the tropics) as the specific humidity at saturation (controlling the surface value) is strongly temperature dependent. Skin-temperature as well as sea spray have been shown to influence the sensible and latent heat (e.g. Fairall et al. 1996, 2003).

2.4.2 Gases

Similarly to heat, mass is a scalar quantity. However, different gases will be transported at significantly different rates. Review articles exists on the issue (Jähne and Haußecker 1998; Wanninkhof et al. 2009), hence only a brief overview is given here.

The transfer velocity k_w (defined in Sect. 2.1) will depend both on the Schmidt number (Sc) and the dimensionless solubility α. Both these quantities are

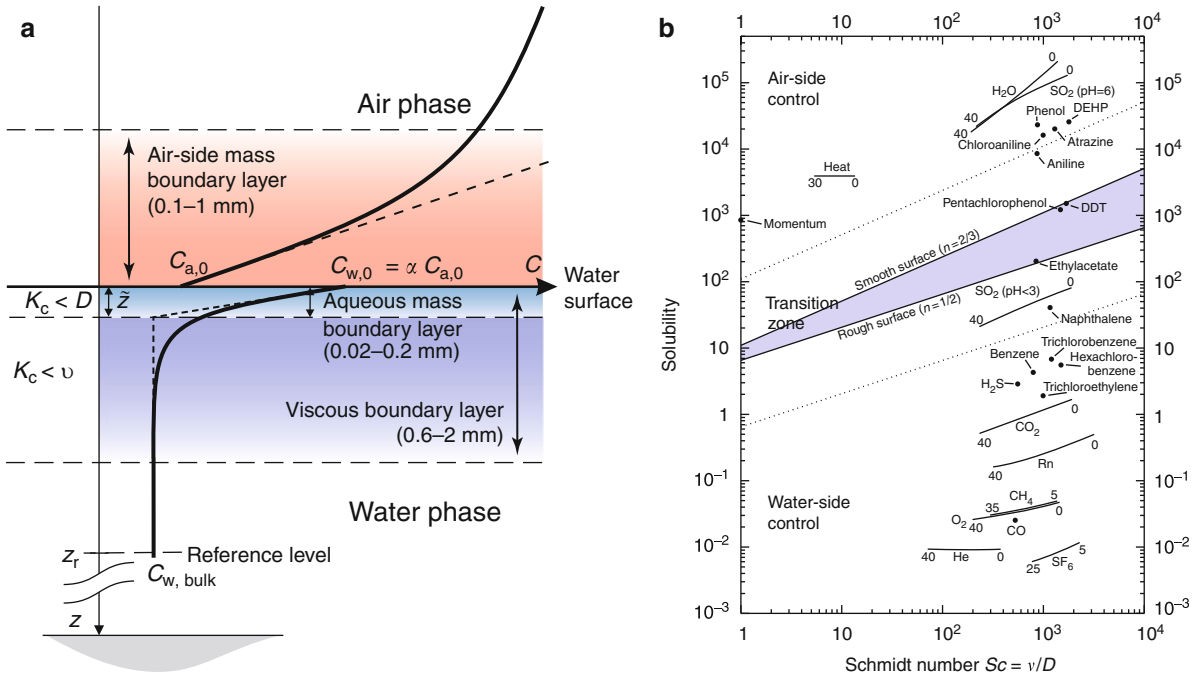

Fig. 2.7 (**a**) Schematic graph of the mass boundary layers at a gas-liquid interface for a tracer with a solubility $\alpha = 3$. (**b**) Schmidt number/solubility diagram including various volatile tracers, momentum, and heat for a temperature range (1 °C) as indicated. *Filled circles* refer to a temperature of 20 °C. The regions for air-side, mixed, and waterside control to the transfer process between gas and liquid phase are marked. At the *solid lines*, the transfer resistance is equal in both phases (Adapted from Jähne and Haußecker (1998))

material properties and depend on temperature and salinity (Johnson 2010). A Schmidt number/solubility diagram can be seen in Fig. 2.7. The solubility α is also termed a partition coefficient. It generally (i.e not when $\alpha = 1$) causes a concentration jump at the surface (c.f. Fig. 2.7). This is due to the thermodynamic solubility equilibrium that is established between the tracer concentration C_a in the gas phase and C_w in the liquid phase. Directly at the interface, this results in

$$C_{w,0} = \alpha \cdot C_{a,0}. \tag{2.22}$$

$C_{x,0}$ indicates the concentration in the phase x directly at the surface.

A mass boundary layer exists on both sides of the interface. This leads to a transfer resistance R, the inverse of the transfer velocity k. The total transfer resistance R_t is the sum of the transfer resistance R_w in the water and R_a in the air-phase. Due to the solubility, this transfer resistance will be different when viewed from the air-side or the water-side of the interface:

$$\begin{aligned} &\text{air-side}: \quad R_{ta} = R_a + R_w/\alpha, \\ &\frac{1}{k_{ta}} = \frac{1}{k_a} + \frac{1}{\alpha \cdot k_w} \end{aligned} \tag{2.23}$$

$$\begin{aligned} &\text{water-side}: \quad R_{tw} = \alpha \cdot R_a + R_w, \\ &\frac{1}{k_{tw}} = \frac{\alpha}{k_a} + \frac{1}{k_w} \end{aligned} \tag{2.24}$$

The ratio $\alpha k_w/k_a$ indicates which boundary layer controls the transfer process, i.e. on which side of the interface is the dominant transfer resistance. Figure 2.7 indicates which side of the interface dominates the transfer resistance for a range of relevant gases.

The transfer velocity is related to the friction velocity u_{*w} and the Schmidt number Sc by

$$k_w = u_{*w}\beta(s)Sc^{n(s)} \tag{2.25}$$

where both $\beta\,(s)$ and $n(s)$ depend on parameters describing the surface conditions. The Schmidt

number exponent $n(s)$ transitions from $n(s) = -2/3$ for a smooth interface to $n(s) = -1/2$ for wavy conditions. The exact functional form and details of the transition are still subject to research. Equation 2.25 allows the scaling between different gas species. Since the surface conditions will be the same for the two species, the quotient between the transfer velocities k_1 and k_2 of the species results in

$$\frac{k_1}{k_2} = \left(\frac{Sc_1}{Sc_2}\right)^{n(s)} \tag{2.26}$$

From the knowledge of the Schmidt numbers of two species Sc_1 and Sc_2 and the transfer velocity of one (k_1), the transfer velocity of the other (k_2) can easily be calculated. Generally, the transfer velocities are scaled to that of CO_2 at 20 °C in seawater with a Schmidt number of $Sc = 660$, while $Sc = 600$ for CO_2 in freshwater at 20 °C. In the remainder of this chapter, we will refer to $Sc = 660$. In most studies, the Schmidt number exponent is assumed to be $n(s) = -1/2$.

2.4.3 Particles

Particle fluxes are governed by a set of processes of different temporal and spatial scales. They are produced at the sea surface (primary aerosol), as condensates from gas molecules in the atmosphere (secondary aerosol), are advected from continents (c.f. de Leeuw et al. 2013), are removed by direct deposition at the sea surface as explained below and wet depostion when they are entrained in precipitation rain droplets. The particles are also changed due to cloud processing. Here we follow the historical approach dividing the intertwined processes into sources and sinks. The sources are covered in Chap. 4 while the sinks are the focus of this section.

The process of particle removal from the atmosphere by their collection on a solid or fluid surface is called deposition. The particles can be scavenged by precipitation (wet depostion) or be deposited directly on a surface (dry deposition). A measure of the efficiency of the deposition process is the deposition velocity v_d, defined as the ratio of particle flux F to the particle concentration. It has be noted that although deposition velocity has the unit of ms^{-1}, in general case it is not the velocity of any physical object, not even necessarily the average vertical speed of the particles. Especially, it should not be confused with the gravitational settling velocity v_g. The two parameters would have identical values only if gravitational settling was the only process leading to particle deposition. Deposition velocity is also influenced by air turbulence, Brownian motion of the particles and in the case of deposition on the sea surface by the movement of the surface itself ("water slip").

2.4.3.1 Dry Deposition

In the case of dry deposition of particles to the sea surface, the standard approach is the one proposed by Slinn and Slinn (1980). In this the atmosphere is divided into a constant flux layer dominated by turbulence and a thin "deposition layer" just above the water interface where wind speed is close to zero and air movement is dominated by diffusion and microphysical processes such as diffusiophoresis. The particles in the deposition layer are assumed to have their radius increased (a_w) due to high humidity, compared to dry particle radius a_d. The particle concentration at the sea surface is assumed to be zero (no resuspension). In such a case, assuming that both the turbulent and deposition layers have their respective transfer velocities (analogous to gas transfer), k'_C and k'_D which can be calculated separately, the deposition velocity v_d may be derived from

$$\frac{1}{v_d} = \frac{1}{k_C} + \frac{1}{k_D} - \frac{v_g(a_d)}{k_C k_D} \tag{2.27}$$

where $k_C = k'_C + v_g(a_d)$ and $k_D = k'_D + v_g(a_w)$.

The formula is analogous to the one for parallel resistance of electric current where the "overall transfer resistance", v_d^{-1}, is the sum of the transfer resistances for both layers reduced by gravitational settling. This approach, similar to one used for gas transfer velocity, allows for adding additional transfer resistances for other processes, as well as to adjust the two transfer velocity parameters. This explains its popularity; it has been cited almost 300 times according to the ISI Web of Science database.

However in the 32 years since Eq. 2.27 was created it has also been the target of criticism from the theoretical point of view. The electrical analogy was shown by Venkatram and Pleim (1999) to be incorrect if transport cannot be represented in terms of a concentration gradient, as in the case of particle settling. Equation 2.27 is not consistent with mass

conservation. A rigorous derivation based on mass conservation (which implies fluxes being constant with altitude) gives the following formula

$$v_d = \frac{v_g}{1 - \exp(r\, v_g)} \tag{2.28}$$

where r is total resistance to transport.

A special case of the general Eq. 2.28 occurs assuming the viscous deposition layer not being rate-determining has been independently derived by Carruthers and Choularton (1986) for conditions of neutral stability. It has been introduced to the marine aerosol research field by Smith et al. (1991). Its use in the gradient method of flux measurements by Petelski and Piskozub (2006) has been recently criticised by de Leeuw et al. (2011) on the ground that it does not include processes such as impaction, molecular diffusion, or growth of particles due to increased relative humidity (RH) near the sea surface, yielding dry deposition velocities that are considerably greater than those from most other formulations for particles with radii smaller than several micrometers.

Another point where the Slinn and Slinn (1980) description seems an oversimplification for most marine conditions is the assumption of zero particle concentration at the sea surface. Because the surface is not only a sink but also source of particles (see Chap. 4 and de de Leeuw et al. (2011) for a review), this condition is rarely true and particle fluxes are the net result of two processes: aerosol production at the sea surface and particle deposition (Nilsson et al. 2001). Hoppel et al. (2002) suggested that when the two processes are in equilibrium, deposition velocity at any fixed height equals the gravitational settling velocity, allowing turbulent mixing processes to be neglected. However, the time needed to achieve equilibrium for particles with radii smaller than about 5–10 μm is so long that other processes (such as wet deposition) will remove them before the two fluxes are in equilibrium. In a follow-up study, Hoppel et al. (2005) proposed that in the case of a surface source, both the source function and deposition velocity should be considered above the interfacial (deposition) layer. The logic behind this proposition is that measurements of the surface source function are made above the interface layer while the microscopic processes occurring in the interface layer are poorly characterised.

In situ direct measurements of deposition velocity from ships and other platforms are inherently difficult. Any such study would need to measure both particle concentrations and deposition fluxes. Direct measurements of fluxes (eddy correlation and similar techniques) measure net fluxes that are the difference between source and deposition fluxes. This method also needs correction for platform motion, a non-trivial problem on research ships, but which could be avoided by using spectral techniques (Sorensen and Larsen 2010). This lack of experimental verification of deposition velocity parameterisation (Andreas et al. 2010) is worrying, particularly considering that its theoretical values are used to estimate source fluxes using equilibrium methods (de Leeuw et al. 2011). These assume that the source and sink terms are in balance (an assumption unreliable for particles with radii smaller than 10 μm (Hoppel et al. 2002)).

2.4.3.2 Wet Deposition

A separate process of aerosol particle removal from the atmosphere is wet deposition, scavenging by water droplets both within clouds and by precipitation below them (see Zhang and Vet (2006) for a review). In-cloud scavenging consists of nucleation scavenging (where particles become condensation nuclei for cloud droplets) and impaction scavenging (particles are collected by cloud droplets, raindrops or snow crystals). The form of mathematical description of wet deposition is usually based on the concept of a scavenging ratio formulation (Iversen 1989), where the dimensionless parameter is the ratio of solution increase of the particles in the precipitation element over the effective scavenging height to its air concentration. This parameter is expected to have higher values inside the cloud than below it.

The details of the scavenging processes are still poorly constrained due to scarcity of in situ measurements from aircraft platforms. A climatology of wet deposition scavenging ratios for the continental USA (Hicks 2005) showed that the ratios for individual rain events are distributed over two orders of magnitude, with standard deviations for weekly averages being twice the mean value (for daily predictions, the factor increases to about five). Similarly, comparison of aerosol concentrations measured over the oceans with the results of aerosol transport models (Witek et al. 2007) shows that

model-measurements discrepancies increase with the amount of precipitation, showing that wet deposition is still the weakest link in aerosol transport models. However, at the same time this result suggests that presently used parametrisations of the aerosol production function and deposition velocity, with all the still existing uncertainties, are able to provide reasonably good agreement with shipboard measurements.

It has been recently proposed (Piskozub and Petelski 2009) that marine aerosol composed of water droplets is able to scavenge small particles in a similar manner to precipitation droplets. Because this (still unconstrained) process would be dependent on the surface (aerosol production function rather than precipitation) it should be included in deposition velocity formulations as it is expected to affect the flux by changing vertical concentration gradients.

2.5 Measurement Techniques

There exists a variety of measurement techniques to estimate the sea spray aerosol production (de Leeuw et al. 2011) and the gas transfer velocity. Here we mainly focus on the three most frequently used types of methods for gas transfer velocity, small-scale techniques, micrometeorological methods and mass-balance techniques. The focus is on the methodology, accuracy, advantages and disadvantages. In addition a section on pCO_2 near-surface profiles is included due to the importance when estimating the transfer velocity or calculating air-sea CO_2 fluxes. In the case of large near-surface gradients, measurement depth is an issue.

2.5.1 Small-Scale Measurements Techniques

2.5.1.1 Particle-Based Techniques

In particle-based flow-measurement techniques, the fluid is seeded with small (μm) particles for visualizing the flow. In standard Particle Imaging Velocimetry (PIV) techniques, the particles are illuminated with a 2D laser light sheet (Raffel et al. 2007). Existing particle-based flow-measurement techniques can be grouped as proposed by Adrian (1991) in three main categories:

Laser Speckle Velocimetry (LSV) which assesses flow-information by analysing random interference patterns caused by a high seeding density of tracer particles,

Particle Tracking Velocimetry (PTV) which uses lower seeding densities to enable tracking of single particles through a long exposure time or multiple images in a sequence, and

Particle Image Velocimetry (PIV) that extracts the flow information from a fluid with a medium seeding density where the displacement of small groups of particles within an interrogation window are analysed statistically.

Most proposed approaches in the third category use correlation based methods to find similar particle constellations within an interrogation window in consecutive image pairs. This mode is often referred to as 'standard PIV'. These PIV techniques have been widely used in laboratory measurements at the air-water interface, both on the water-side (Siddiqui and Loewen 2010; Siddiqui et al. 2004; Turney et al. 2005; Banner and Peirson 1998) or, more challengingly, on the air-side (Reul et al. 2008; Shaikh and Siddiqui 2010; Troitskaya et al. 2011). Particularly for anisotropic turbulent flow, 2D measurement of velocities is problematic as out of plane velocities are not captured (Adrian 2005). Therefore, a strong effort has been put into extending the measurement techniques to volumetric three-dimensional three-component (v3D3C). These approaches can also be distinguished according to the technique used to obtain 3D-velocity information and the methods used to measure volumetric datasets. The most popular method to access three-components (3C) of the velocity field is to measure the out-of-plane velocity using Stereoscopic methods (Prasad 2000), extended by a technique called multi-plane PIV by using multiple laser-sheets (Kähler and Kompenhans 2000; Müller et al. 2001; Liberzon et al. 2004; Cenedese and Paglialunga 1989; Brücker 1996) or intensity graded light sheets (Dinkelacker et al. 1992) for the reconstruction of the third velocity component. In the recent past many methods were proposed to access volumetric information from 3D flow fields. This was achieved using holographic measurements (Hinsch 2002; Sheng et al. 2008), by combining PIV with Doppler global velocimetry (PIV/DGV) (Wernet 2004), using tomography

(Elsinga et al. 2006; Schröder et al. 2008), defocussing-based approaches (Pereira et al. 2000, 2007; Willert and Gharib 1992), scanning-light-sheet methods (Burgmann et al. 2008; Hoyer et al. 2005; Brücker 1995) and absorption based methods (Jehle and Jähne 2008; Berthe et al. 2010; Voss et al. 2012).

For gaining a better understanding of transport processes at the air-water interface, flow structures relative to the location of the interface are of interest. Most techniques measure in a Eulerian reference frame. This makes an accurate extraction of the interface location necessary. Absorption based methods do not need this additional step, which may introduce further sources of errors. They encode the depth below the interface by light absorption in the dyed water body (Jehle and Jähne 2008; Berthe et al. 2010; Voss et al. 2012). Recently, an approach was presented for using one single plenoptic camera for assessing v3D3C flows (Garbe et al. 2012). A micro–lens array in front of the camera's sensor allows the extraction of depth and all-in-focus from computational photography.

While Steinbuck et al. (2010) have employed PIV techniques in an autonomous profiler at depth 10–60 m in the ocean, such measurements directly at the air-water interface are not practical.

2.5.1.2 Thermographic Techniques

Infrared measurements of the sea surface have been used to detect breaking waves (Jessup et al. 1997a), microscale breaking waves (Jessup et al. 1997b; Zappa et al. 2001), internal wave structures (Zappa and Jessup 2005), interfacial turbulence (Smith et al. 2007; Scott et al. 2008; Handler and Smith 2011; Schnieders et al. 2013), the momentum flux (Garbe et al. 2007; Garbe and Heinlein 2011) and also used to infer gas flux (Jähne and Haußecker 1998; Garbe et al. 2003, 2004; Schimpf et al. 2004; Asher et al. 2004).

In thermographic technique, an infrared camera is used for visualizing thermal patterns directly at the interface. Generally, midrange (sensitive spectral range: $\lambda = 3$–5 μm) or longrange (sensitive spectral range: $\lambda = 8$–10 μm) thermal imagers are used. In these spectral ranges, the penetration depth of the radiation is ≈ 20 μm. Thermographic techniques are distinguished as active or passive techniques. In passive techniques, visualized temperature fluctuations occur from a natural net heat flux at the interface. For active techniques, a heat source such as a laser is used for imposing an external heat flux.

One such active thermographic technique is the active controlled heat flux method proposed by Jähne (1989). Haußecker and Jähne (1995) used an IR-camera to track a small patch at the water surface heated up by a short pulse from a CO_2 laser. The temporal temperature decay of the patch was fitted based on solving the diffusive transport equation and utilising the surface renewal model (Higbie 1935; Danckwerts 1951) as a first-order process. The time constant of the decay was identified with the surface renewal time scale and the heat transfer rate calculated. A further method for the analysis of the decay curves was proposed by Atmane et al. (2004), in which the diffusive transport is combined with a Monte Carlo simulation of the renewal process based on the surface penetration model (Harriott 1962). Zappa et al. (2004) and Asher et al. (2004) measured a scaling factor of roughly 2.5 between the gas and heat transfer velocity when they applied the active controlled flux technique. Following Asher et al. (2004), the surface penetration theory provides a more accurate conceptual model for air-sea gas exchange. This is supported by the work of Jessup et al. (2009) who found evidence for complete and partial surface renewal at an air-water interface.

Passive techniques were used successfully to estimate the net heat flux, the temperature difference across the thermal skin layer and parameters of the surface renewal model by Garbe et al. (2003, 2004). Recently, Schnieders et al. (2013) extracted characteristics of interfacial turbulence from passive thermography.

2.5.2 Micrometeorological Techniques

Turbulence is an efficient transport mechanism for both physical quantities such as heat and momentum as well as mass transport i.e. gases and particles. If a gradient of some air constituent exists and a turbulent element, an eddy, moves in this gradient, the eddy mixing of the air will result in transport, a flux, of this air constituent from high concentration to low. Micrometeorological techniques are commonly used to measure the turbulent flux. In this section we will briefly present two of these techniques. The most direct technique is called the eddy-covariance (EC) method (also called eddy-correlation method). The turbulent flux can be directly obtained from the turbulent fluctuations of the wind speed components and the

air constituent in question. The turbulent fluctuations are extracted from the measurement signal by the use of Reynolds decomposition:

$$x = \bar{x} + x' \tag{2.29}$$

where x is a measurement signal, overbar represents a mean value and the prime deviation from the mean, a perturbation. The mean value represents the mean flow and the perturbation the turbulent fluctuations. Applying Reynolds averaging (see e.g. Stull 1988) to the product between the vertical wind, w, and the air constituent, c, yields the covariance term $\overline{w'c'}$ which represents the vertical turbulent flux.

In order to capture all relevant fluctuations contributing to the flux, the sampling needs to be fast, usually > 10 Hz is required. In addition the measurement period needs to be long enough to include all relevant scales but not too long since this risks including slower variations not related to the local turbulence, e.g. diurnal cycles and mesoscale variations. Typically periods between 10 and 60 min are used.

Alternatively, if a fast response analyzer is unavailable the EC method can be modified by using disjunct eddy sampling, originally presented by Haugen (1978). The air constituent is sampled discontinuously, e.g. every 10 s, allowing the instrumentation a longer time to analyse the sample. As long as the sampling period is sufficiently short, the covariance between the vertical wind and the air constituent will still represent the flux. This version of the EC method is called Disjunct Eddy Covariance (DEC) and has been verified experimentally with the EC method (e.g. Rinne et al. 2008).

The flux measured using eddy-covariance techniques is representative for some surface area upstream of the sensor, called the footprint. The spatial and intensity distribution of the footprint is described by the footprint function and is dependent on several variables such as sensor height, atmospheric stability, surface roughness length, wind speed and wind direction. Different approaches have been used to calculate the footprint: analytical, Lagrangian and backward trajectory models, see Vesala et al. (2008) for an overview. The footprint is important in regions where one would expect systematic variations of the signal source at the surface. Typically most important for coastal sites but also in experiments investigating effects of e.g. surfactants on fluxes, researchers must be aware of where the flux footprint is positioned.

Although the EC-method is straightforward in principle, some issues need to be dealt with in the processing of the signals such as: motion correction (if measuring on a moving platform), dilution effects (the so called Webb or WPL-correction (Webb et al. 1980)), salt contamination, correction for sensor separation, corrections for flow distortion (if measurements are made from a bulky platform) and possibly corrections related to flux losses in closed path systems (see below). Some of these issues will be presented here. The motion correction is needed to remove effect of platform motions from the measured wind speed. This can be done by measuring the platform motion, see e.g. Edson et al. (1998) or Anctil et al. (1994) and is a necessary requirement when using the EC-method on ships and buoys.

The dilution correction is applied when calculating fluxes from density measurements of some air constituent like CO_2. Density fluctuations may arise not only by concentration variation of the air constituent but also through variations in water vapour, temperature and pressure (Webb et al. 1980; Fairall et al. 2000). This correction can be applied in the post processing or directly on the measured time series (Sahlée et al. 2008).

Measuring over the open ocean will cause salt contamination on the sensors, and if not dealt with properly will cause poor quality measurements. The instrumentation must be washed regularly with fresh water to remove salt contamination. Salt build up on open path gas analysers may cause cross-talk between the water vapour measurements and the CO_2 measurements. A method to correct for this was suggested by Peter K. Taylor and is presented in Prytherch et al. (2010).

When two sensors are used to measure fluxes, problems arise since the instruments are separated by some distance and thus don't measure in the same air volume. This will cause an underestimation of the flux since decorrelation arises between the measured velocity and the measured scalar. This flux attenuation is a function of separation distance, atmospheric stability and measurement height (determining the scale of the turbulent eddies), see e.g. Nilsson et al. (2010) or Horst and Lenschow (2009) for more details on this issue.

If measurements are planned over areas where small fluxes are expected, i.e. in areas with a relatively small air-sea gradient, a gas analyser should be chosen accordingly. The resolution should be sufficient to resolve the expected fluctuations. Otherwise the measurements will be dominated by instrumental noise (Rowe et al. 2011). Data with a low signal-to-noise ratio should be excluded from the analysis.

For measurements of gas fluxes, two types of gas analysers are available, closed or open path sensors. Open path sensor measure directly in the ambient air, whereas closed path sensors measure in air that has been drawn through some distance of tubing before reaching the analyser. Both types have their merits and complications. The open path is a more direct measurement, but the sensor is exposed and thus has problems with salt contamination and may be unable to function during precipitation. The closed path sensor is protected and may function also during precipitation events. Also, if the tube is long enough heat loss in the tubing makes the WPL-correction independent of temperature (Rannik et al. 1997; Sahlée and Drennan 2009). However, flux loss related to signal damping in the tube might be significant and need to be corrected. The closed path system requires pumps which are energy consuming and thus these type of instrument might be unsuitable on buoys where power is limited.

When measuring gas fluxes for which no fast response sensor exists one can utilise the eddy accumulation method (or the DEC method mentioned above). The eddy accumulation method is based on conditional sampling where the upward and downward moving gases are collected in two separate containers and analysed later. The total flux is then the sum of the two covariances calculated separately for the two containers (Desjardins 1977). Difficulties arise since the two separate terms in the total covariance may be much larger than the total term i.e. they need to be measured with great accuracy. Also, the air flow to the containers needs to be proportional to the magnitude of the vertical wind, which makes this a difficult method to implement in practice. The relaxed eddy accumulation method, REA, (Businger and Oncley 1990) is based on the same principle but combines it with the flux-variance similarity, thus the flux can be written as:

$$\overline{w'c'} = b\sigma_w(c^+ - c^-) \tag{2.30}$$

where σ_w is the standard deviation of the vertical velocity, c is the mean concentration of the sampled gas and the sign denotes the direction of the vertical wind, b is a coefficient ≈ 0.6, with little stability dependence. Using Eq. 2.30 the air flow to the two containers can be set at a constant rate making the sampling easier and only dependent on the actual sign of the vertical wind.

Commercially-available gas analysers used with EC systems have typically been developed for use on fixed platforms on land. Some instruments have been found to introduce artificial signals when mounted on moving platforms. Such inaccuracy can be dealt with methodologically (e.g. Yelland et al. 2009) but there is also room for improvement by creating sturdier sensors. Recent development in methodology also allows for correcting water-vapour cross-talk on open-path sensors due to salt contamination Prytherch et al. (2010). It is very likely that this methodology will continue to develop. Future versions of current sensors will likely be more sensitive allowing the instrumentation to resolve smaller variations. This will reduce the flux uncertainty (particular for the smallest fluxes). Current efforts are ongoing to develop new gas analysers. For example, one such approach is based on photoacoustic spectroscopy with a target sensitivity of 20 ppb for CO_2.

2.5.3 Mass Balance

2.5.3.1 Techniques

On a global scale, inventories of radiocarbon (^{14}C) in the ocean (Broecker et al. 1985; Naegler et al. 2006; Peacock 2004) produced by spallation in the atmosphere due to cosmic rays (natural) or aboveground thermonuclear (bomb) testing have been used to determine the global mean gas transfer velocity for CO_2. Inventories are combined with wind data to predict how this transfer might vary with wind speed (Wanninkhof 1992). There has been some debate about the accuracy of the ^{14}C inventories and the relationships of CO_2 transfer with wind speed have since been re-evaluated (Sweeney et al. 2007).

On timescales of process studies, two main geochemical mass balance technique utilising natural and deliberately-injected tracers have been used in the ocean to determine gas transfer velocities.

The first technique, called the radon deficit method, assumes that ^{222}Rn and ^{226}Ra are in secular equilibrium in the mixed layer and below, and the observed deficit of radon in the surface ocean is due to evasion of ^{222}Rn out of the ocean (e.g. Bender et al. 2011; Peng et al. 1979; Roether and Kromer 1984).

The second technique involves the deliberate simultaneous injection of two volatile tracers with very different diffusion coefficients (^{3}He and SF_6) in the mixed layer of the ocean or into coastal seas, and the subsequent monitoring of their concentrations with time (e.g. Wanninkhof et al. 1993; Watson et al. 1991). Dilution will not alter the ^{3}He/SF_6 ratio, whereas the gas exchange of ^{3}He is faster than SF_6, and so the ^{3}He/SF_6 ratio will decrease with time, and allow the gas transfer velocity to be determined.

2.5.3.2 Scales (Spatial and Temporal)

The ^{222}Rn-deficit method has a time scale of about a week, as this is dictated by the ^{222}Rn half-life of 3.8 days, yielding a mean life of ca. 5.5 days, and has a spatial resolution 100s of km. The ^{3}He/SF_6 technique has a temporal resolution of at best 12–24 h, since there needs to be a detectable change in the ^{3}He/SF_6 ratio. The method typically has a spatial resolution of 10s of km.

2.5.3.3 Accuracy and Limitations

Besides the limitations imposed by the sampling methods and ability of analytical instruments to measure ^{222}Rn, ^{226}Ra, ^{3}He, and SF_6 accurately and precisely, both methods have other complications.

The dual tracer technique was originally developed for use in non-stratified coastal seas where the tracers would be well mixed to the seafloor (Watson et al. 1991). However, when used in the open ocean, both mass balance techniques depend on knowledge of the mixed layer depths, see Ho et al. (2011a) for a detailed discussion of mixed layer depth estimates derived using different methods. Because a profile of ^{222}Rn reflects processes taking place over days to weeks, a one-time estimate of the mixed layer depth may not reflect its variability over time. This has been overcome by repeated sampling over a period of time (Emerson et al. 1991). Also, with both methods, there is the possibility of entrainment of water from the pycnocline underlying the mixed layer either through convection or internal waves, which could alter the ^{222}Rn deficit or ^{3}He/SF_6 ratios.

In addition, the radon deficit method is confounded by many complications, as documented by Roether and Kromer (1984) and others. Among them:

1. The method relies on the assumption that ^{226}Ra concentrations throughout and below the mixed layer is constant, which is not always the case;
2. The relatively long half life of ^{222}Rn (3.8 days) compared to gas exchange means that both the wind history and the ^{222}Rn deficit history have to be known;
3. Because the ^{222}Rn deficit is not horizontally homogeneous, advection can perturb the "steady state" assumption.

A complication of the dual tracer technique is that it actually determines the difference in the transfer velocities of ^{3}He and SF_6. A knowledge of the Schmidt number dependence is required to obtain an estimate of the transfer velocity of either gas. Although lake experiments (Watson et al. 1991) and multiple tracer experiments in the North Sea. (Nightingale et al. 2000b) have shown that the value for n is close to 0.5 for the ^{3}He/SF_6 pair, this may not hold true under high wind conditions when significant populations of bubbles are expected to enhance air-sea gas transfer and might cause a deviation from $n = 0.5$ for ^{3}He/SF_6 (see Sect. 2.2.3 and Asher (2009)).

2.5.3.4 Current and Recent Field Studies

Most of the field studies with ^{222}Rn were conducted in the 1970s and 1980s (e.g. Kromer and Roether 1983; Peng et al. 1979; Smethie et al. 1985). The method has fallen into disuse because of the complications confounding its use as described above, and the difficulty in determining a relationship between wind speed and gas exchange. This is primarily due to the multi-day half life of ^{222}Rn, averaging significantly different sea-surface and wind conditions. This makes establishing a relationship with wind speed particularly difficult.

The ^{3}He/SF_6 dual tracer technique has emerged as the mass balance technique of choice in the ocean and in coastal seas. Experiments have been conducted in a variety of locations, the North Sea (Watson et al. 1991; Nightingale et al. 2000b), the Georges Bank (Asher and Wanninkhof 1998), the Florida Shelf (Wanninkhof et al. 1997), the Atlantic Ocean (McGillis et al. 2001; Salter et al. 2011), the equatorial Pacific (Nightingale et al. 2000a) and the Southern Ocean (Wanninkhof et al. 2004; Ho et al. 2006, 2011b).

2.5.4 Profiles of pCO_2 Near the Surface

To quantify the global exchange of CO_2 between the atmosphere and ocean with great accuracy requires the inclusion of factors which influence the air–sea flux, such as diurnal warming. This occurs at the sea surface when incoming shortwave radiation can cause stratification in the absence of wind-induced mixing. Temperature differences of up to 3 K can occur across this warm layer, which is ~ 10 m in depth (Ward 2006). This warm layer influences the air-sea flux of CO_2 because the partial pressure of CO_2 in seawater has an experimentally determined temperature dependence under isochemical conditions (Takahashi et al. 1993):

$$\Delta pCO_2^{WL} = pCO_2\left[1 + e^{0.0423\Delta T^{WL}}\right] \qquad (2.31)$$

The diurnal warm layer enhances the flux of CO_2 in regions where the ocean acts as a CO_2 source and therefore reduces the oceanic carbon uptake (Olsen et al. 2004).

An experiment was conducted off Martha's Vineyard in 2002 (McNeil et al. 2006) in which in situ profiles of temperature/salinity were acquired with a seabird microcat, and pCO_2 with water pumped from depth to an equilibrator, where a sample of the headspace was analysed with a LI-COR LI-7000 IRGA. The profile data and subsequent pCO_2/temperature relationship is shown in Fig. 2.8. There is a relatively strong diurnal warm layer, with a ΔT of about 0.6 °C over the upper 4.5 m. There is a corresponding pCO_2 gradient of about 12 µatm and the best fit provides $(\partial pCO_2/\partial T)/pCO_2 = 0.062\ °C^{-1}$, compared to the value from Takahashi et al. (1993) of 0.0423 $°C^{-1}$.

For a global net flux of CO_2 from the atmosphere to ocean, atmospheric pCO_2 levels are about 2 % (approximately 6 µatm) greater than the oceanic partial pressure for CO_2, making measurements susceptible to small biases in the determination of the correct partial pressure difference (McGillis and Wanninkhof 2006). Therefore the diurnal warm layer can mask the true air-sea fluxes when calculated with measurements of ΔpCO_2 when the water concentration is measured several meters below the sea surface.

Further work is required to understand the dependency of the ocean carbon system on temperature so that the most appropriate value for the change in seawater pCO_2 with temperature can be determined (McGillis and Wanninkhof 2006).

2.5.5 Method Evaluation

There are a large number of techniques to estimate gas transfer velocities from measurements, here we mainly discuss three different types, small-scale technique, micrometeorological technique (mainly Eddy-Covariance) and mass-balance technique (mainly Dual Tracer). The spatial and temporal scales resolved by each method are shown in Fig. 2.9.

Small scale techniques as outlined in Sect. 2.5.1 have significant advantages in laboratory conditions, making spatio-temporally resolved water-side concentration measurements at the frame rate of the camera used in the visualisation system feasible (up to 2,000 frames per second). Concentration gradients, flow dynamics and turbulence in the air and in the water can be resolved. This leads to a better understanding of processes, their relevance to the transport and their variability. To extract parameters from these techniques, inverse problems have to be solved, which introduces uncertainties. For field measurements, most small-scale techniques are not applicable, either because they are too delicate for the field, because the set up and the lighting conditions cannot be controlled, or because the water body cannot be seeded with the tracer. Thermographic techniques have been applied successfully in field campaigns. However, besides having to deal with artefacts in challenging conditions, they mainly measure the transport of heat with the transfer of gases being determined indirectly. Not all transfer mechanisms can be captured from thermography. The most dominant of these is bubble-mediated gas transfer, making thermographic techniques mainly applicable in low to medium wind speed ranges. However, when thermographic measurement techniques are applicable in the field, they make measuring natural variability or spatial homogeneity of fluxes possible. Not capturing bubble-mediated transfer can also be an advantage since its contribution to gas exchange can be assessed through comparison with complementary measurement techniques. Small-scale measurement techniques may therefore be very beneficial in combination with other techniques such as eddy-correlation, as the

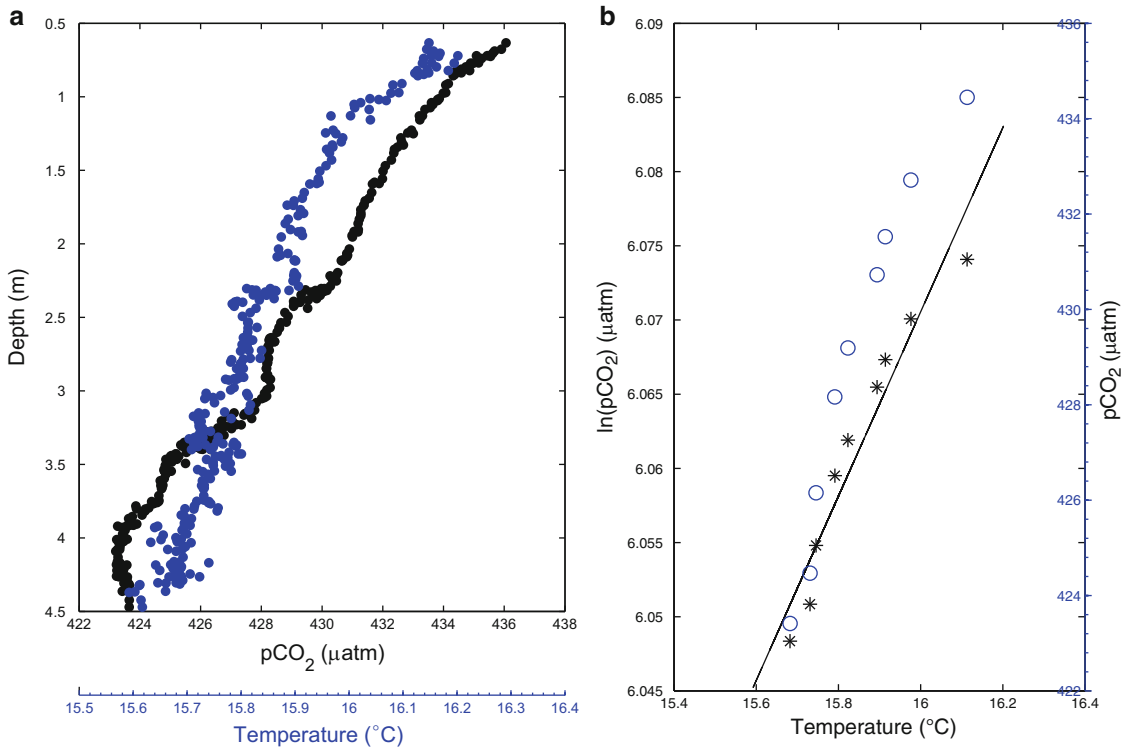

Fig. 2.8 *Left*: In situ profiles of temperature and pCO_2. *Right*: Relationship between temperature and pCO_2 for this profile. Although this relationship is non–linear, the best fit provides $(\partial pCO_2/\partial T)/pCO_2 = 0.062\ ^\circ C^{-1}$

assumptions underlying these techniques may be verified under the measurement conditions.

For dual tracer techniques, 2–3 stations are typically used and gas exchange on a time scale of 12–24 h can be resolved, in addition to integrated measurements over days to weeks. Eddy-Covariance measurements resolve fluxes on a 30 min–1 h time-scale. However, even during perfect conditions and no instrumental problems, a single flux estimate for a 30-min period using the covariance method would still be uncertain. This is due to the fact that turbulence is not sampled properly i.e. we cannot measure the ensemble mean, instead we are limited to time averages at a fixed point (i.e. tower and ship measurements) or spatial averages (aircraft measurements) which are bound to be limited. This means that we do not sample all possible realisations that a turbulent field can attain given the ambient atmospheric conditions. During conditions with large variability of surface conditions within the flux foot-print the variability of EC data is significantly larger.

All methods have methodological problems as well as instrumental uncertainties. For the dual tracer methods relevant instrumental accuracy is 0.2–0.5 % for ^3He and 2 % for SF_6, methodological difficulties relate to determination of mixed layer depth which typically adds 10 % uncertainty to the calculation of k_w.

Discussions of uncertainty in eddy-covariance flux measurements can be found in the literature, see e.g. Fairall et al. (2000) and Vickers et al. (2010) and references therein. Uncertainties arise from both instrumental problems and methodological issues. For CO_2 the relative instrumental uncertainty is estimated to be 17–20 % for tower-based fluxes (Rutgersson et al. 2008; Vickers et al. 2010). The uncertainty is higher for moving platforms (ship-based) in high-salinity environments. Better accuracy is, however, acquired with gases that can be measured with a larger signal-to-noise-ratio over sea, like DMS (Huebert et al. 2004).

Eddy-Covariance is the most direct method since the flux of interest is directly measured, it does not rely

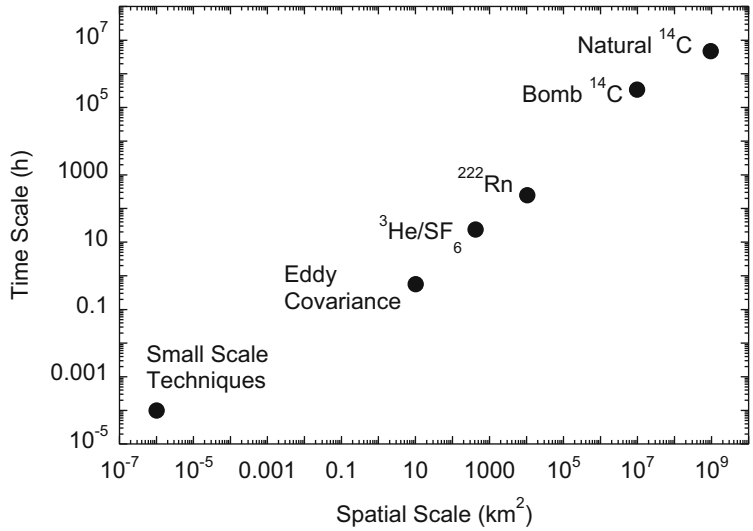

Fig. 2.9 Spatial and temporal scales of different measurement techniques frequently applied to gas exchange at the air-water interface

on assumptions about gas properties or approximations concerning the turbulent structure of the atmospheric boundary layer (Wanninkhof et al. 2009); the problem is presently the relatively high instrumental uncertainty in marine conditions, in particular for CO_2. Dual Tracer is an indirect method with the advantage of an integrated measurement of the gas transfer velocity with relatively high accuracy.

Wind stress at the ocean surface is responsible for kinetic energy input into the water, which generates turbulence. Several studies have shown a relationship with the transfer velocity and the dissipation of turbulence kinetic energy ε (Asher and Pankow 1986; Zappa et al. 2007). One can thus infer k_w by measuring dissipation in the water (see Sect. 2.6.4), although operational measurements of ε (e.g. remote sensing for assessing inventories), will be challenging.

2.6 Parameterization of Gas Exchange

Measuring transfer rates or transfer velocities of gas exchange directly is challenging. Therefore it is appealing to relate them to readily accessible parameters that dominate the transfer. These parameters might be the wind speed at a certain reference height or surface roughness. Such parameters can also be assessed globally from satellite remote sensing or are available in simulations. In this section, different parameterisations are examined. The most obvious ones are wind speed dependent $k_w - U$ relationships or sea state dependent ones through the surface roughness. The NOAA-COARE algorithm is a mixture of basic interfacial physics along with empirical additions such as bubbles and tuneable parameters. It requires more parameters than simple $k_w - U$ relationships but also probably results in more accurate estimates. Parameterising gas transfer with energy dissipation is appealing as it relates the transport directly to turbulence but this parameter is challenging to measure in itself.

2.6.1 Wind Speed Relationships

The processes mediating diffusive gas exchange across the air-sea interface are complex, with multiple physical controls (e.g. capillary waves, bubbles, small scale eddy turbulence etc., cf Sect. 2.2). In the ocean environment these processes are directly or indirectly related to wind via turbulent forcing and wave breaking and as such wind speed is found to correlate well with transfer velocity in observational data (Ho et al. 2011b). Wind is routinely measured and can be derived from remotely sensed data and ground-truthed by high precision instruments on ships (Wanninkhof et al. 2009; Bender et al. 2011; Ho et al. 2011b); hence

it is likely to remain the key variable used in empirical parameterisations of transfer velocities for the foreseeable future.

The first parameterisation of environmental air-water transfer velocity from wind speed (U) were theoretical or based on simple laboratory experiments (e.g. Liss and Slater (1974) and references therein, Deacon (1977)). For the water-side transfer velocity (k_w), these have since been validated to first order by wind tunnel experiments (e.g. Liss and Merlivat 1986) and field studies as outlined previously in this chapter.

All of these methods yield a net flux over some scale of area and time and thus enable calculation of transfer velocity from flux (F) and the magnitude of the concentration gradient between air and sea (ΔC), following Eqs. 2.12 and 2.13. There is a considerable range in the estimates of the $k_w - U$ relationship from these methods (c.f. Fig. 2.10) – approximately a factor of 2 at a typical average wind speed of 7 ms^{-1} (e.g. Yang et al. 2011; Ho et al. 2011b; Johnson et al. 2011). However, this might be considered rather good agreement considering the differing scales of space and time over which the various methods operate e.g. eddy covariance (10^2–10^3 m^2 and minutes) and global ^{14}C estimates (10^{15} m^2 and decades).

Generally, at least for mass balance techniques, the field is tending to converge around a smaller range of uncertainty in the $k_w - U$ relationship (for CO_2), bringing estimates from ^{14}C inventory (e.g. Sweeney et al. 2007), dual/multiple tracer experiments (e.g. Ho et al. 2011b) and ^{222}Rn distributions (e.g. Bender et al. 2011) into reasonable agreement, all broadly in line with the commonly used parametrisation of Nightingale et al. (2000b), at least to within the experimental uncertainty in mass balance techniques (Asher 2009; Johnson et al. 2011). The Nightingale et al. (2000b) parametrisation is largely based on the results of a multiple tracer study conducted in the coastal North Sea and as such is potentially subject to surfactant and limited fetch effects which might inhibit k_w. However, their parametrisation compares well with that presented for the equatorial Pacific (Nightingale et al. 2000a) and more recent measurements in the Southern Ocean (Ho et al. 2006, 2011b); suggesting that the $k_w - U$ relationship as quantified by mass balance techniques is remarkably robust to local and regional conditions.

One key uncertainty in the parameterisation of k_w with U is the functional form of the relationship i.e. linear, quadratic, cubic, polynomial. A simple quadratic function ($k_w \approx U^2$) has been observed in wind-wave tanks (e.g. Wanninkhof and Bliven 1991). Such relationships have been assumed in scaling global ^{14}C inventories (and inferred fluxes) to global average wind speed (Wanninkhof 1992; Sweeney et al. 2007). Simple and polynomial quadratic functions have been found to fit dual tracer and ^{222}Rn deficiency data well (e.g. Wanninkhof 1992; Nightingale et al. 2000b; Ho et al. 2011b).

The considerably greater transfer velocities observed at high wind speeds in direct flux measurements of CO_2 via the eddy covariance technique (see Sect. 2.5.2) have led to suggestions of a cubic relationship to wind speed as a best fit to the data (e.g. McGillis et al. 2001; Prytherch et al. 2010), although given the large uncertainties in the measurements, a quadratic could also be fitted in most cases. This has been explained by the proposed cubic relationship between windspeed and whitecapping (e.g. Monahan and Spillane 1984) and the importance of whitecaps on bubble-mediated gas exchange (e.g. Woolf 1997) at high winds plus a reduction in gas transfer at low winds due to the supposed presence of surfactants (see Sect. 2.2.7). The cubic relationship is not supported by water-side eddy covariance measurements of O_2 and N_2 exchange by D'Asaro and McNeil (2007) using autonomous floats deployed in hurricane-force winds. They show a relationship that demonstrates much lower k_w at hurricane-force winds than predicted by the cubic parameterisations of Wanninkhof and McGillis (1999) and McGillis et al. (2001), although with k_w scaling to approximately the 6th power of windspeed (McNeil and D'Asaro 2007). McNeil and D'Asaro (2007) suggest that this is due to the much greater bubble-mediated transfer for O_2 and N_2, which are considerably more insoluble than CO_2. Other studies of oxygen (Kihm and Körtzinger 2010) and oxygen and nitrogen (Vagle, McNeil and Steiner, 2010) suggest considerably stronger bubble effects.

Evidence that CO_2 exchange may be considerably enhanced by bubbles comes from comparison with the eddy covariance measurements of DMS fluxes at high winds (see Fig. 2.3). This is summarised in Yang et al. (2011), where a near-linear relationship with wind speed is seen, and is quantitatively close to the linear relationship predicted for the non-bubble mediated component of the transfer velocity in the

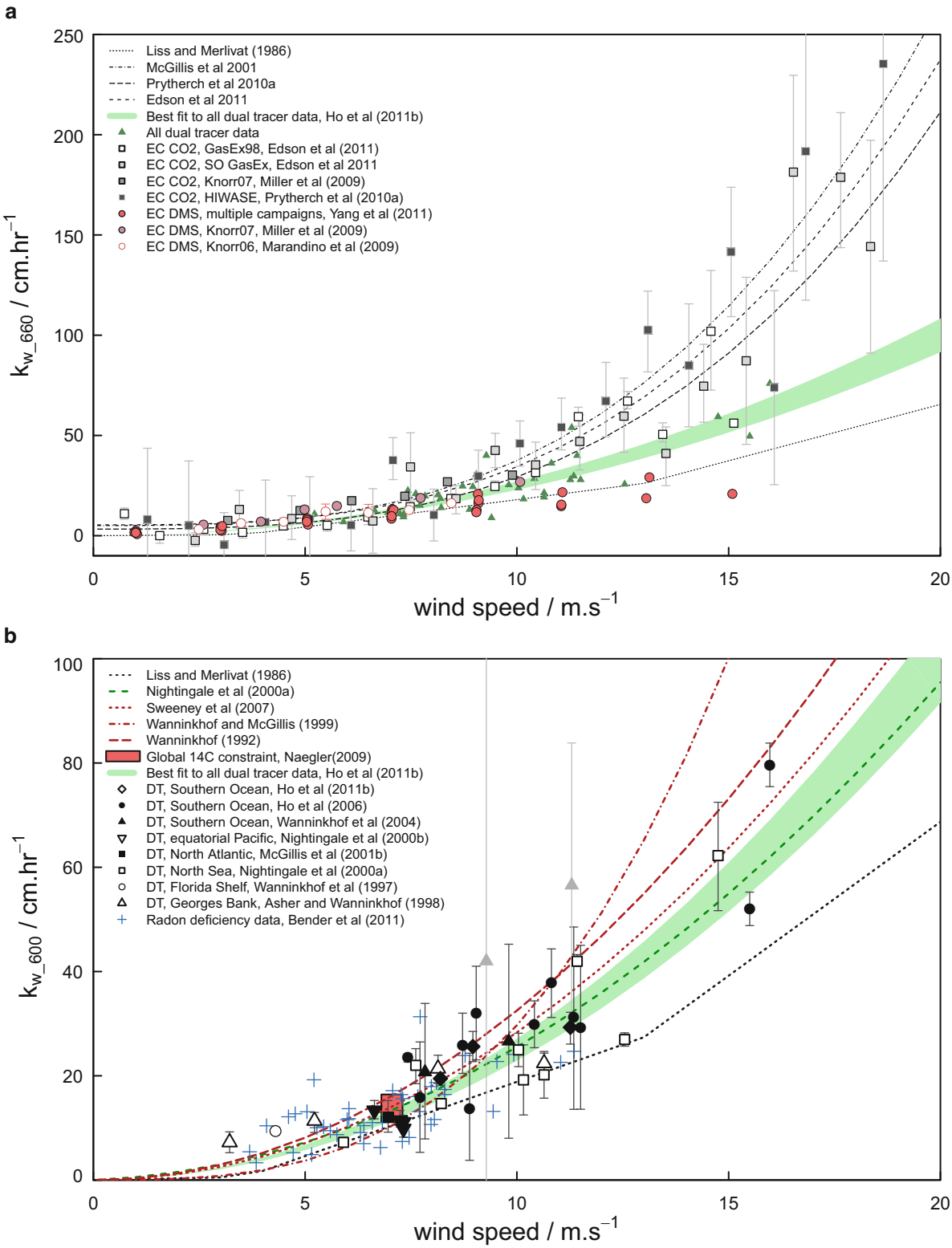

Fig. 2.10 A comparison of different windspeed relationships of the water side transfer velocity, k_w. Measurements from eddy covariance techniques are presented in (**a**), those from mass balance techniques are shown in (**b**) (Figures by M.T. Johnson, shared under creative commons license at http://dx.doi.org/10.6084/m9.figshare.92419)

physically-based bubble model of Woolf (1997), suggesting that DMS is sufficiently soluble to be unaffected by the bubble effect (Sect. 2.2.3), whilst CO_2 is not. This also suggests that, for gases of intermediate solubility such as DMS, non-linear parameterisations such as Nightingale et al. (2000b) may lead to substantial overestimates of fluxes at higher wind speeds.

For gases more soluble than DMS, where the air-side transfer velocity becomes limiting, the relationship of interest is that between wind speed and the air-side transfer velocity (k_a). This is less well constrained than k_w, with very little field validation of the empirical models, particularly for gases other than water vapour (e.g. Johnson 2010). Typically, however, $k_a - U$ parameterisations are close to linear (e.g. Johnson 2010; Sect. 2.6.3) and physically-based model predictions (e.g. Duce and Tindale 1991; Jeffery et al. 2010) tend to agree reasonably with wind-tunnel observations for trace gases by Mackay and Yeun (1983).

2.6.2 Surface Roughness, Slope

Frew et al. (2004) have shown from field measurements in coastal and offshore waters that the gas transfer velocity better correlates with mean square slope computed for the wave number range of 40–800 rad m^{-1} than with the classically used wind speed. This is consistent with laboratory observations and the use of mean square slope (mss) was shown to be of particular interest in case of surface films. This study was performed from low to moderate wind speed and the observed relationship between gas transfer velocity and mean square slope was linear.

Dual frequency measurements of altimeter like TOPEX and JASON in Ku-band and C-band, provide a mean of retrieving the mss contribution of small scale waves between 40 and 100 rad m^{-1}, as derived by a geometric optics model. Frew et al. (2007), after calibrating satellite mss with field mss, derived k-mss relationships and global k_w maps. The main difficulty is to calibrate satellite mss relationships and k-mss relationships, due to few existing field measurements of k_w and mss and to even fewer collocations between altimeter mss with these field measurements. Other difficulties arise from the fact that at high wind speed the effect of bubbles is not implicitly included in such algorithms so that these algorithms underestimate k_w at high wind speed (Wanninkhof et al. 2009). k_w fields derived from altimeters are very undersampled compared to k_w-fields deduced from satellite wind speeds due to the poor spatial coverage of altimeter measurements compared to scatterometer and microwave radiometer wind speeds.

2.6.3 NOAA-COARE

Details of the original development of the COARE algorithm for meteorological fluxes (sensible heat, latent heat, momentum) can be found in Fairall et al. (1996, 2000), and the subsequent development of the algorithm to include gas transfer is shown in Hare et al. (2004) and Fairall et al. (2011).

Advancements in sensor technologies led to the application of the micrometeorological direct covariance method to estimate air-sea fluxes at hourly time scales on the atmospheric side of the interface. This method was first successfully applied in the GasEx field programmes beginning in 1998 (McGillis et al. 2001; Fairall et al. 2000).

The short time scale of the covariance estimates enables observational investigations of the relationship of k to physical/chemical forcing beyond wind speed – examples include wind stress, buoyancy flux, surfactants, or surface gravity wave properties. Physically-based parameterisations (Hare et al. 2004; Soloviev 2007; Vlahos and Monahan 2009) are now available that incorporate these additional forcing factors and may lead to quite different transfer properties for different gases. For example, the dependence of bubble-mediated exchange on gas solubility implies the Wanninkhof (1992) formula may not be appropriate for the fairly soluble biogenic gas dimethylsulfide (DMS) (Woolf 1993; Blomquist et al. 2006). Thus, application of a single wind-speed formula for all gases is inconsistent with current understanding of gas transfer physics (Fig. 2.11).

In the COARE gas transfer algorithm (COAREG), the flux of a trace gas on the atmospheric side of the interface is estimated as

$$F_c = \alpha k_a (C_w/\alpha - C_a) = \alpha k_a \Delta C = \frac{\alpha k_a}{u_{*a}} u_{*a} \Delta C \tag{2.32}$$

where k_a is the transfer velocity on the air-side, α is dimensionless solubility, C_w and C_a the mean concentration of the gas in the water and air at reference depth

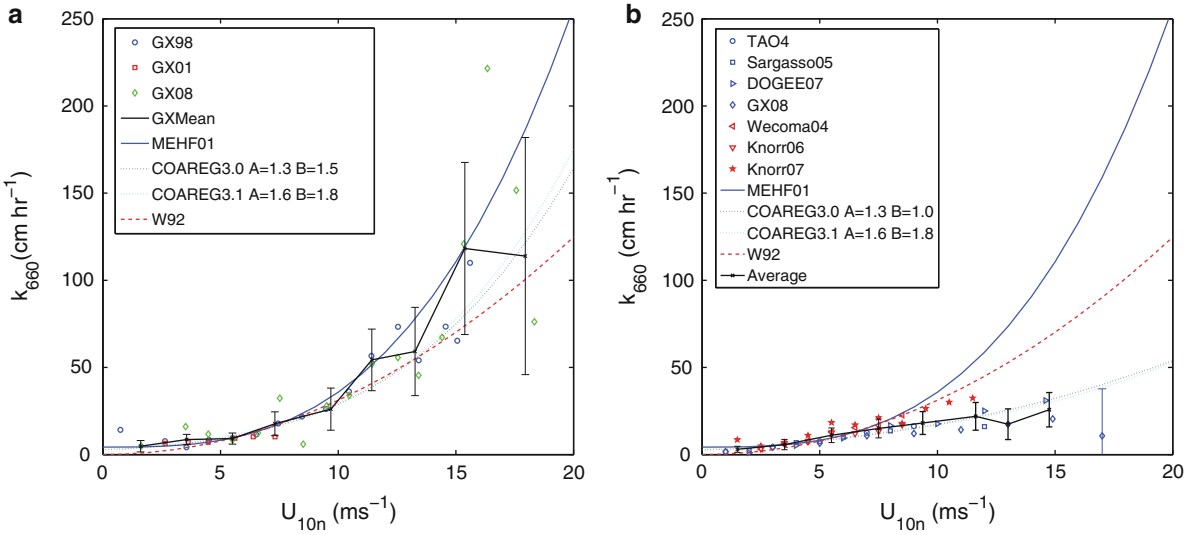

Fig. 2.11 (**a**) Gas transfer velocity for CO_2 as a function of 10-m neutral wind speed U_{10n} from direct surface-based observations. The *black line* is the mean of the data sets; the *error bars* are statistical estimates of the uncertainty in the mean computed. Symbols are: ○ – GASEX98, * – GASEX01, ◊ – SOGASEX08. The parameterisations shown are: *blue solid line* – McGillis et al. (2001); *black dotted line* – COAREG3.0 CO_2; *cyan dotted line* – COAREG3.1 CO_2 using tangential u_*; *red dashed line* – W92 (Wanninkhof 1992). (**b**) DMS gas transfer coefficient as a function of 10-m neutral wind speed U_{10n} from direct surface-based observations. The *black line* is the mean of the data sets; the *error bars* are statistical estimates of the uncertainty in the mean computed. Symbols are: ○ – TAO04 (Equatorial Pacific); □ – Sargasso Sea 05, ▷ – DOGEE07, ◊ – SOGASEX08, ◁ – Wecoma04, ▽ – Knorr06, * – Knorr07. The parameterisations shown are: *blue solid line* – McGillis et al. (2001), *black dotted line* – COAREG3.0 DMS; *cyan dotted line* – COAREG3.1 DMS using tangential u_*; *red dashed line* – W92

and height. The COAREG algorithm (current public version is COAREG3.0) gives a simple form for the transfer velocity (see Hare et al. 2004),

$$k_a = \frac{u_{*a}}{r_w + \alpha r_a} \quad \text{where} \qquad r_w = \left(r_{wt}^{-1} + k_b/u_{*a}\right)^{-1}. \tag{2.33}$$

Here u_{*a}/r_{wt} represents molecular-turbulent transfer which has a basis in air-sea physics and k_b represents bubble transfer based on empirical formulation. On the atmospheric side we neglect spray-mediated gas transfer, so there is only molecular-turbulent transfer $r_a = r_{at}$.

In the COAREG model the individual terms are represented as

$$r_{wt} = \sqrt{\frac{\rho_w}{\rho_a}}\left(h_w Sc_w^{1/2} + \kappa^{-1}\ln\left(\frac{z_w}{\delta_w}\right)\right), \tag{2.34}$$

where z_w is the water depth of the reference measurements, δ_w the molecular sublayer thickness, Sc_w the Schmidt number of water, ρ_w the density of water, and $h_w = 13.3/(A\varphi)$.

In this expression, A is an empirical constant and φ accounts for surface buoyancy flux enhancement of the transfer. A similar expression is used for r_{at}, but the molecular sublayer thickness is explicitly approximated by incorporating the velocity drag coefficient, C_d, which is a function of the atmospheric measurement height, z_a,

$$r_{at} = \left(h_a Sc_a^{1/2} + C_d^{-1/2}(z_a) - 5 + \ln(Sc_a)/(2\kappa)\right) \tag{2.35}$$

where $h_a = 13.3$. The bubble-driven part of the transfer is taken from Woolf (1997) as

$$k_b = BV_0 f_{wh}\alpha^{-1}\left[1 + \left(e\alpha Sc_w^{-1/2}\right)^{-1/n}\right]^{-n} \tag{2.36}$$

where B is a second adjustable constant, $V_o = 2{,}450$ cm h^{-1}, f_{wh} is the whitecap fraction, $e = 14$, and

$n = 1.2$ for CO_2. The parameters A and B have been adjusted to fit observations with values between 1 and 2. Note there is no capability at present to describe the presence of surface films.

Recently COAREG was extended to include the case of an atmospheric gas (such as ozone) that reacts strongly in the ocean (Fairall et al. 2007). Using the notation from Fairall et al. (2000), the budget equation for the oceanic concentration of a chemical, C_w, is

$$\frac{\partial C_w}{\partial t} + U\nabla C_w = \frac{\partial[-(D_c + K)\partial C_w/\partial z]}{\partial z} - aC_w \tag{2.37}$$

where z is the vertical coordinate (depth for the ocean), D_c is the molecular diffusivity of C_w in water, K the turbulent eddy diffusivity, and the last term is the loss rate of C_w due to reactions with chemical Y. Thus, $a = R_{cy}Y$, where Y is the concentration of the reacting chemical, and R_{cy} the reaction rate constant. Assuming that the concentration of Y is much larger than C_w so that is remains effectively constant and that a is sufficiently large that C_w is completely removed within the molecular sublayer, Garland et al. (1980) showed that the water-side resistance is

$$\frac{u_{*a}}{r_w} = \sqrt{aD_c} \tag{2.38}$$

Fairall et al. (2007) relaxed the requirement that the reaction was confined to the molecular sublayer and obtained a solution that allowed the ozone deposition velocity to depend on the oceanic turbulence

$$\frac{u_{*w}}{r_w} = \sqrt{aD_c}\frac{K_1(\xi_0)}{K_0(\xi_0)} \tag{2.39}$$

Here K_0 and K_1 are modified Bessel functions of order 0 and 1 and

$$\xi_0 = \frac{2}{k_w u_{*w}}\sqrt{aD_c}. \tag{2.40}$$

COARE3.0 is a good fit to mean observed momentum and heat transfer coefficients over a considerable range of wind speeds (more observations are above 18 ms^{-1}). However, at any specific wind speed bin there is considerable scatter – more than can be explained by atmospheric sampling variability alone. It is also clear that over the open ocean there is, on average, a systematic change in the influence of waves on air-sea turbulent exchange with increasing wind speed. Attempts to find simple scaling expressions that explain variations in surface roughness length (or drag coefficient) due to variations in surface wave properties have been of limited success (Drennan et al. 2005).

The most recent results from application of the algorithm to CO_2 and DMS transfer for SO GasEx can be found in Edson et al. (2011), while an analysis of the implementation of COAREG for ozone is outlined in Bariteau et al. (2010) and Helmig et al. (2011). Current application of COAREG includes input of satellite fields of sea surface temperature, near surface humidity and temperature, and wind speed to obtain global estimates of air-sea gas transfer (Jackson et al. 2011).

One major technical problem is the poor performance of fast CO_2 sensors at sea, which limit field work to regions with very large air-sea differences in CO_2 concentration. Some clarity in scientific issues could also come from high-quality eddy covariance measurements of gases more soluble than DMS and less soluble than CO_2. There is considerable room for progress on bubble-mediated transfer through field, laboratory, and numerical modeling studies.

COAREG is publicly available from the authors of (Fairall et al. 2011). The latest version of the code (COAREG3.1) includes a scheme to partition the wind stress into tangential and wave-induced components (see Fairall et al. (2011) for more details).

2.6.4 Energy Dissipation

The flux of slightly soluble, non-reactive gases (i.e. water side-controlled) between the ocean and atmosphere is determined from knowledge of the concentration difference across the diffusive layer as well as the gas transfer velocity k_w (see Eq. 2.14).

The ease of availability of wind speed U (m s^{-1}) measurements has resulted in many attempts to develop parameterisations between k_w and U (see Sect. 2.6.1). However, the primary mechanism for controlling k_w is shear-produced turbulence at the air-sea interface (Salter et al. 2011; Asher 1997; Wanninkhof et al. 2009), whose generation mechanism is wind stress

acting on the ocean surface (Asher 1997; Kitaigorodskii and Donelan 1984).

There has been much effort to describe k_w in terms of molecular diffusivity D ($m^2\ s^{-1}$), kinematic viscosity ν ($m^2\ s^{-1}$), and a function based on a velocity Q ($m\ s^{-1}$) and length L (m) (Danckwerts 1951; Fortescue and Pearson 1967; Lamont and Scott 1970; Deacon 1977; Ledwell 1984; Jähne et al. 1987; Brumley and Jirka 1988; Soloviev and Schlüssel 1994; Fairall et al. 2000):

$$k_w = \beta Sc^n f(Q, L) \tag{2.41}$$

where β is an experimentally determined constant and $Sc = \nu/D$ is the Schmidt number. The Schmidt number exponent has been shown to vary between $n = -2/3$ for conditions of low winds (e.g. Deacon 1977; Davies 1972) or where surfactants are present at the water surface (Asher and Pankow 1986), to $n = -1/2$ at winds greater than 5 ms^{-1} (Jähne et al. 1987). Lamont and Scott (1970) used an eddy cell model to describe $f(Q, L)$ which resulted in a scaling relation:

$$k_w = 0.4 Sc^{-1/2} (\varepsilon \nu)^{1/4} \tag{2.42}$$

where ε ($m^3\ s^{-2}$) is the dissipation rate of kinetic energy, a parameter that can be measured in the field.

Zappa et al. (2007) provided the first field investigations that supported the mechanistic model in Eq. 2.42 based on surface water turbulence that predicts gas exchange for a range of aquatic and marine processes. Their findings indicated that the gas transfer rate varies linearly with the turbulent dissipation rate to the ¼ power in a range of systems with different types of forcing – in the coastal ocean, in a macro-tidal river estuary, in a large tidal freshwater river, and in a model ocean.

An underlying assumption in Eq. 2.42 is that ε is measured directly at the water surface. Since the profile of turbulence near the air-water interface may be complicated by the interplay between wind, waves, current shear and other processes, measurements at depth will not be representative of ε at the surface because the profile changes nonlinearly with environmental forcing. Zappa et al. (2009) implement the Craig-Banner turbulence model, modified for rain instead of breaking-wave turbulence, to successfully predict the near-surface dissipation profile that varies by two orders of magnitude over the top 50 cm at the onset of the rain event before stratification plays a dominant role. This result is important for predictive modeling of k_w as it allows inferring the surface value of ε fundamental to gas transfer.

Lorke and Peeters (2006) took the approach of using law of the wall scaling to describe ε (z) as a function of depth z (m):

$$\varepsilon = \frac{u_{*w}^3}{\kappa z} \tag{2.43}$$

where $\kappa \sim 0.41$ is the von Kármán constant and $u_{*w} = \sqrt{\tau/\rho_w}$ is the friction velocity, τ is the wind stress acting on the ocean surface which is parameterised with knowledge of the drag coefficient C_D and ρ_w is the water density. Although this provides a mechanism to derive the parameters to parameterise k_w according to Eq. 2.42, it is unlikely that law of the wall scaling will adequately describe ε at the ocean surface (e.g. Agrawal et al. 1992; Terray et al. 1996; Babanin and Haus 2009).

Compared to wind speed, dissipation in the ocean is much more challenging to measure as it requires sophisticated instumentation and an ability to provide data close to the air-sea interface for the application of air-sea transfer parameterisation. Future progress requires a new generation of experiments which combine turbulence data with estimates of gas transfer velocities (Lorke and Peeters 2006).

2.6.5 Evaluating and Selecting Transfer Velocity Parameterisations

The above sections demonstrate that various different turbulent forcing terms can be used to parameterise k_w. Wind speed, which is the most commonly used predictor for k_w is only indirectly related to the key forcing terms and hence a great deal of variability is expected (and observed) in $k_w - U$ relationships. The choice of most appropriate parameterisation depends on both the forcing data available and the application to which k_w is to be used (e.g. spatial and temporal scale, gas of interest).

For example, when considering fluxes of CO_2 at the global scale there is a constraint on the transfer velocity given the bomb ^{14}C inventory of the ocean (e.g. Sweeney et al. 2007). Thus, notwithstanding

uncertainties in both the inventory (Wanninkhof 1992; Naegler et al. 2006) and the global average wind speed, which may be as much as 1.3 m s^{-1} between different datasets (Naegler et al. 2006), there is a 'known point' on the $k_w - U$ curve for global CO_2 fluxes. Note that whilst parameterisations derived from this value have tended to apply a quadratic relationship, as described in Sect. 2.6.1, there is no evidence from this global approach to support any particular form for the $k_w - U$ relationship. Furthermore, whilst this is a valuable constraint on long timescale global fluxes, it is not necessarily a constraint for regional or local fluxes or over shorter timescales, due to variable and non-wind speed dependent forcings (e.g. fetch/wave slope, thermal stability, etc.) or the effects of other processes such as chemical or biological enhancement, rainfall etc.

Where wind speed is the only available forcing term for a particular study on smaller-than-global scale (as is commonly the case), an empirical $k_w - U$ parameterisation must be employed to quantify the flux of a gas given wind speeds averaged over an appropriate timescale. Data on k_w over a range of wind speeds in the natural environment come primarily from the dual tracer and eddy covariance approaches. As noted above, significant variability due to processes not directly related to wind speed is to be expected in observations of such relationships, but even accounting for this there are apparent inconsistencies which must be addressed. First and foremost is the apparently greater transfer velocities observed by CO_2 eddy covariance measurements than by the dual tracer technique, particularly at higher wind speeds (Sect. 2.6.1). It is possible that these two methods are measuring empirically different properties – it has been suggested by Ho et al. (2011b) that, whilst on the timescale of eddy covariance measurements (minutes-hours) the apparent transfer velocity varies with the cube of the wind speed, over the timescale of a tracer study (days) the vertical mixing of the bulk water becomes limiting to the total tracer mass balance and thus the higher-order dependence is not apparent. Alternatively, Asher (2009) suggests that the increasing importance of bubbles and thus increasingly turbulence dominated transfer at higher winds means that the scaling of k_w to $Sc^{-0.5}$ might break down, which would lead to errors in the relationship calculated by the dual tracer method.

The dual tracer method also fails to account for the effect of the solubility dependence of bubble-mediated transfer. Bubble fluxes are predicted to be lower for more soluble gases, and this is supported by laboratory experiment (e.g. Rhee et al. 2007; Woolf et al. 2007) and circumstantially by the lower and more linear transfer velocities of DMS (compared to CO_2) observed in the field by various studies (Sects. 2.6.1 and 2.6.3, Figs. 2.3 and 2.10). Such effects, however, should mean that the dual tracer method (based on the exchange of ^3He and SF_6, which are considerably less soluble than CO_2) should predict greater fluxes than those directly observed for CO_2, which is the opposite of what is observed. It has been suggested that such inconsistencies may be reconciled by the application of an improved representation of the bubble flux such as that outlined by Woolf et al. (2007), which accounts for the high void fraction in dense bubble plumes. This may lead to 'suffocation' of the bubble flux (i.e. the flux of gas into the bubbles starts to be limited by the decreasing concentration in the water around the bubble plumes). This effect will be largest for the most diffusive gases and as such there is likely to be a differential in the effect between the highly diffusive ^3He and rather less diffusive SF_6. The result of this effect when calculating k_w from dual tracer data would be an underestimation of k_w (Woolf et al. 2007).

Such explanations may be able to reconcile all the available data and may also satisfy the ^{14}C and ^{222}Rn derived values for k_w where appropriate, given that they are subject to significant uncertainty themselves. Given the current uncertainties associated with eddy covariance and dual tracer methods and the magnitude of the effect of bubbles on CO_2 fluxes in the ocean environment, it is impossible to determine which of the above explanations for observed discrepancies between methods is correct. It is possible that under different regimes of thermal stability, wave field, fetch and other forcings, the observed range of $k_w - U$ relationships may all be valid in particular situations. With forthcoming advances in CO_2 sensors for eddy covariance measurements, progress may be made towards better understanding and resolution of the above discrepancies.

With sufficient environmental forcing data, probably the best estimates of transfer velocity can be achieved by using physically-based models of boundary layer interactions such as NOAA-COARE. The latest

incarnation, COARE G 3.0 (Fairall et al. (2011), including a generalised scheme to enable application to any gas following Johnson (2010)) might be considered the 'state of the art' in quantifying k_w. Nonetheless it still contains some physical parameterisations which are not state of the art. For instance it applies the 'classic' bubble model of Woolf (1997) rather than the dense bubble plume model mentioned above, and relies on rather uncertain empirical parameterisations such as the empirical windspeed-whitecapping relationship of Monahan and O'Muircheartaigh (1980) which is subject to significant uncertainty (Johnson et al. 2011) although recent developments are leading to considerable constraint of said uncertainty (Goddijn-Murphy et al. 2011). Recent measurements of whitecap fraction were discussed in de Leeuw et al. (2011) as outlined in Sect. 2.2.3.

Selection of an appropriate transfer velocity must be based on the requirements of the particular study. It is important to recognise that parameterisations are not necessarily universally applicable to gases of differing solubilites, or to differing environmental situations. However, it must also be acknowledged that in the context of the wide range of other uncertainties associated with quantifying air-sea gas fluxes (summarised by Johnson et al. 2011), not least the uncertainty in concentrations and selection of appropriate wind speed averaging, the uncertainty in k_w parameterisations is often relatively small.

2.7 Sea Ice

Sea ice affects air-sea exchanges of greenhouse gases in ice covered waters in several ways. The first effect is that sea ice prevents air-sea exchange of gases. First studies of the vertical distribution of anthropogenic CO_2 in the Weddell Sea showed limited air-sea exchange of CO_2 in the winter surface water when it is subducted and mixed with other water masses to form Weddell Bottom Water (Weiss 1987; Poisson and Chen 1987). This suggested that sea ice was acting as an inert and impermeable barrier for gas exchange so that most carbon cycle research has not considered the possibility of either direct air-sea CO_2 exchange in the presence of sea ice or indirect air-ice-sea CO_2 exchange related to sea ice melting (Bates and Mathis 2009; Tison et al. 2002). However, it is well established that sea ice is a permeable medium, depending of its brine volume fraction (Golden 2003; Golden et al. 1998). Golden et al. (1998) showed that sea ice is permeable to brine transport when brine volume fraction is above 5 %, corresponding to a temperature of −5 °C and sea ice salinity of 5 – the so-called "law of fives"-. Gas transport within sea ice is therefore possible as observed by (Gosink et al. 1976) who reported CO_2 and SF_6 diffusion in sea ice at −7 °C. More recently, Loose et al. (2011b) measured accurately diffusion of SF_6 and O_2 through columnar sea-ice and reported diffusion coefficient values within permeable artificial columnar ice of $1.3 \cdot 10^{-4}$ cm^2 s^{-1} and $3.9 \cdot 10^{-5}$ cm^2 s^{-1} for SF_6 and O_2, respectively. These values are rather low compared to air-sea transfers in open water. However, it must be borne in mind that sea ice covers about 7 % of the Earth surface at its maximal seasonal extent and represents one of the largest biomes on Earth. Even though fluxes through sea ice are modest, integrated over the global sea ice cover can potentially be significant (Delille et al. 2006).

Several studies reported measurements of direct air-ice CO_2 exchanges. Most studies reported air-ice CO_2 fluxes in spring and summer (Delille et al. 2006; Semiletov et al. 2004; Zemmelink et al. 2006; Nomura et al. 2010a, b; Papakyriakou and Miller 2011). Strikingly, some studies reported air-ice CO_2 exchange during the winter season when the air-ice interface is supposed to be impermeable to gas exchanges (Heinesch et al. 2009; Miller et al. 2011). Indeed, despite the fact that sea ice can be seen as an ideal environment for micro-meteorological measurement of CO_2 fluxes (Loose et al. 2011a) since the surface is relatively smooth and levelled, air-ice CO_2 fluxes measurements are still in their infancy. Different methods are used, without inter-comparison, and temporal and spatial coverage is scarce. In addition, the early studies of Semiletov et al. (2004) and Zemmelink et al. (2006) should be considered cautiously as they do not take into account bias of open path sensor CO_2 analysers in cold environments, as pointed out by Burba et al. (2008). For the time being, sea ice heterogeneity, gaps in understanding of sea ice biogeochemistry, poor understanding of the role of snow in controlling air-ice gas fluxes and poor temporal and spatial coverage prevent robust integration of air-ice gas fluxes at large scale. Further studies are required to provide such assessments.

Whatever the magnitude of air-ice gases fluxes, the role of sea ice in gas exchange is not limited to the ability to transfer gases from the ocean to the atmosphere. O_2, CO_2 and DMS observations within sea ice show clearly that gas dynamics within sea ice are different to that in the underlying layer. Several peculiar processes e.g. temperature change, brine concentration/dilution, brine transport, primary production and respiration by sympagic[1] microbial communities and others biogeochemical processes affect gases dynamics within sea ice (Delille et al. 2006, 2007; Tison et al. 2010; Trevena and Jones 2006; Trevena et al. 2000, 2003; Glud et al. 2002; Rysgaard and Glud 2004; Rysgaard et al. 2008), so that sea ice cannot be seen as a simple open/closed pathway between ocean and the atmosphere. Peculiar gas dynamics within sea ice determine gas contents of sea ice and subsequently air-ice partial pressure gradients of each gas. Therefore, the way and potential magnitude of air-ice gas fluxes are controlled by gas dynamics within sea ice rather than the gas content of the underlying water.

Rysgaard et al. (2011) recently reviewed the significance of sea ice related processes in terms of air-sea CO_2 exchange and pointed out the role of rejection of CO_2-rich brines in the underlying layer during sea ice growth. Sea ice expels about 80 % of solutes, including gases, out of the ice matrix, mainly into the underlying water. In the Southern Ocean, this brine rejection is one of the main drivers of Antarctic Deep Water formation. Gases transported together with brines can therefor potentially sink towards deep layers, providing an efficient path-way for CO_2 sequestration (Rysgaard et al. 2011). In addition, Loose et al. (2009) observed in artificial ice experiments that rejection of gases (SF_6 and O_2) is enhanced compared to salts.

$CaCO_3$ precipitation within sea ice as ikaite (Papadimitriou et al. 2004; Dieckmann et al. 2008, 2010) has also been suggested as an efficient pathway for atmospheric CO_2 sequestration (Rysgaard et al. 2007) depending on the conditions where precipitation takes place (Delille et al. 2006). In certain sea ice permeability conditions, assuming that $CaCO_3$ precipitates in the early sea ice growth phase (Assur 1958; Marion et al. 2009), CO_2 produced by $CaCO_3$ precipitation is rejected with brine to the underlying layer, while $CaCO_3$ crystals remain trapped within the ice matrix. In summer, $CaCO_3$ dissolution and related CO_2 consumption within the ice or release of alkalinity depleted meltwater into the underlying water promote atmospheric CO_2 uptake by the ice and underlying water, respectively (Delille et al. 2006; Rysgaard et al. 2007). In parallel to CO_2-rich brine rejection, this precipitation acts as an effective pathway for atmospheric CO_2 sequestration (Rysgaard et al. 2007, 2011; Delille et al. 2006).

The impact of sea ice transfer estimates can be very important regionally. This is less the case at the global scale, assuming impermeability of ice to be appropriate for many applications. Rysgaard et al. (2011) recently provided a first tentative budget of the global significance of sea ice related processes for atmospheric CO_2 uptake. They assessed that sea-ice related atmospheric CO_2 uptake is about 45 TgC y^{-1} and 71 TgC y^{-1} in the Arctic and Southern Ocean, respectively. Oceanic CO_2 up-take during the seasonal cycle of sea ice growth and decay in ice-covered oceanic regions therefore equals almost half of the net atmospheric CO_2 uptake in ice-free polar seas. Finally, remobilisation of CH_4 held in East Siberian Arctic Shelf sediments has been assessed to be a major contributor to the oceanic CH_4 flux to the atmosphere (Shakhova et al. 2010a, b). Shakhova et al. (2010b) reported large bubbles of methane entrapped in fast sea ice probably originating from ebullition from sediments. Either the ice acts as a simple inert transient buffer for the ebullition CH_4 flux or as more complex pathway has still to be determined.

2.8 Applications of Air-Sea Gas Transfer

There exist a wide range of applications in which air-sea transport are important. In this section we focus on applications in global models, large-scale measurements from satellite remote sensing and computations of global inventories. These applications are not exclusive but are the dominant topics from air-sea gas exchange studies to global environmental research.

[1] A sympagic environment is one where water exists mostly as solid ice.

2.8.1 Models

Nearly all numerical models employed to date to simulate the cycling of carbon in the ocean are using the parameterisation of Wanninkhof (1992) to estimate the gas-transfer velocity, k_w, i.e. a parameterisation that suggests a quadratic dependence of k_w on the windspeed (see Sect. 2.6.1). Different coefficients have been used with the quadratic dependence, but we are not aware of any ocean model that uses a linear (Krakauer et al. 2006), a cubic (Wanninkhof and McGillis 1999), or piecewise linear function (Liss and Merlivat 1986) for k_w. The very small diversity of parameterisations used today is a legacy of the Ocean Carbon-cycle Model Intercomparison Project (OCMIP-2), where it was decided to use the same parameterisations for all models (Najjar and Orr 1998). In this particular study, k_w was proposed to be parameterised as follows:

$$k_w = (1 - f_{ice})[a \cdot (U^2 + v)](Sc/660)^{-1/2} \quad (2.44)$$

Where f_{ice} is the sea-ice fraction, U^2 the square of the windspeed at 10 m, v is the variance of the windspeed, added to reflect the non-linear nature of the relationship, and Sc the Schmidt number. For OCMIP, the instantaneous windspeed was first averaged to form a monthly climatology of U, and then squared. v was similarly computed from the instantaneous windspeed. The coefficient a was then chosen such that the global mean k_w matched the global bomb radiocarbon-derived estimate of Broecker et al. (1986). This gave a coefficient a of 0.336 cm h^{-1} s^2 m^{-2}, which is slightly larger than the value of 0.31 cm h^{-1} s^2 m^{-2} proposed by Wanninkhof (1992) due to the use of different winds.

This parameterisation has been carried forward into nearly all ocean carbon cycle models since then, with the only major development being the suggestion that the coefficient a needs to be downscaled substantially to about 0.24 cm h^{-1} s^2 m^{-2} in order to take into consideration that Broecker et al. (1986) bomb radiocarbon inventory estimate was too large (Peacock 2004; Naegler et al. 2006; Sweeney et al. 2007; Müller et al. 2008; Nägler 2009). This gives a global mean transfer velocity k_w for CO_2 of about 15 cm h^{-1} instead of Broecker's mean value of 19 cm h^{-1}.

Very few sensitivity studies have been performed to investigate the influence of different gas exchange parameterisations on the exchange of trace gases. This is likely a consequence of the influential paper by Sarmiento et al. (1992) where the authors demonstrated little sensitivity of the uptake of anthropogenic CO_2 with respect to different formulations of the gas transfer velocity. This is because the rate limiting step for the uptake of this transient tracer is its transport from the near surface ocean into the ocean's interior. But this lack of sensitivity does not apply to the exchange of natural CO_2, where a higher transfer velocity generally leads to stronger fluxes (Fig. 2.12). However, the modelled flux changes are less than proportional to the change in the gas transfer velocity, since the surface ocean concentration of CO_2 adjusts to the change in the "resistance" across the air-sea interface by generally decreasing the air-sea gradient when k_w is increased (Fig. 2.12c). Due to lateral transport and mixing, the altered CO_2 concentration also affects regions away from regions of strong air-sea gradients, even leading to a change in the sign of the gradient.

An even larger sensitivity to the choice of k_w exists for the air-sea transfer of the isotopes of CO_2, i.e., $^{14}CO_2$ and $^{13}CO_2$, since the characteristic exchange time-scale for these isotopes is about ten times longer than that for CO_2 itself (Broecker and Peng 1974). This is a consequence of the fact that isotopic equilibrium across the air-sea interface needs to be established by equilibrating all carbonate species in the surface ocean, while for CO_2, the shortcut reaction involving HCO_3^- and CO_3^{-2} establish a faster equilibrium. Few numerical simulations have been performed to investigate this sensitivity explicitly, but Broecker and Maier-Reimer (1992) demonstrated that a doubling of the gas transfer velocity resulted in a substantial change in the surface ocean distribution of the $^{13}C/^{12}C$ ratio with a near doubling of the range.

For DMS and N_2O, virtually all models have used the gas transfer formulation of Wanninkhof (1992) to represent the air-sea flux of these gases (Le Clainche et al. 2010; Jin and Gruber 2003; Suntharalingam et al. 2012). In contrast, for less soluble gases, such as argon and neon, a broader set of parameterisations have been employed, particularly to reflect the importance of bubble mediated transfer. For the latter, most modellers follow the suggestion of Asher and

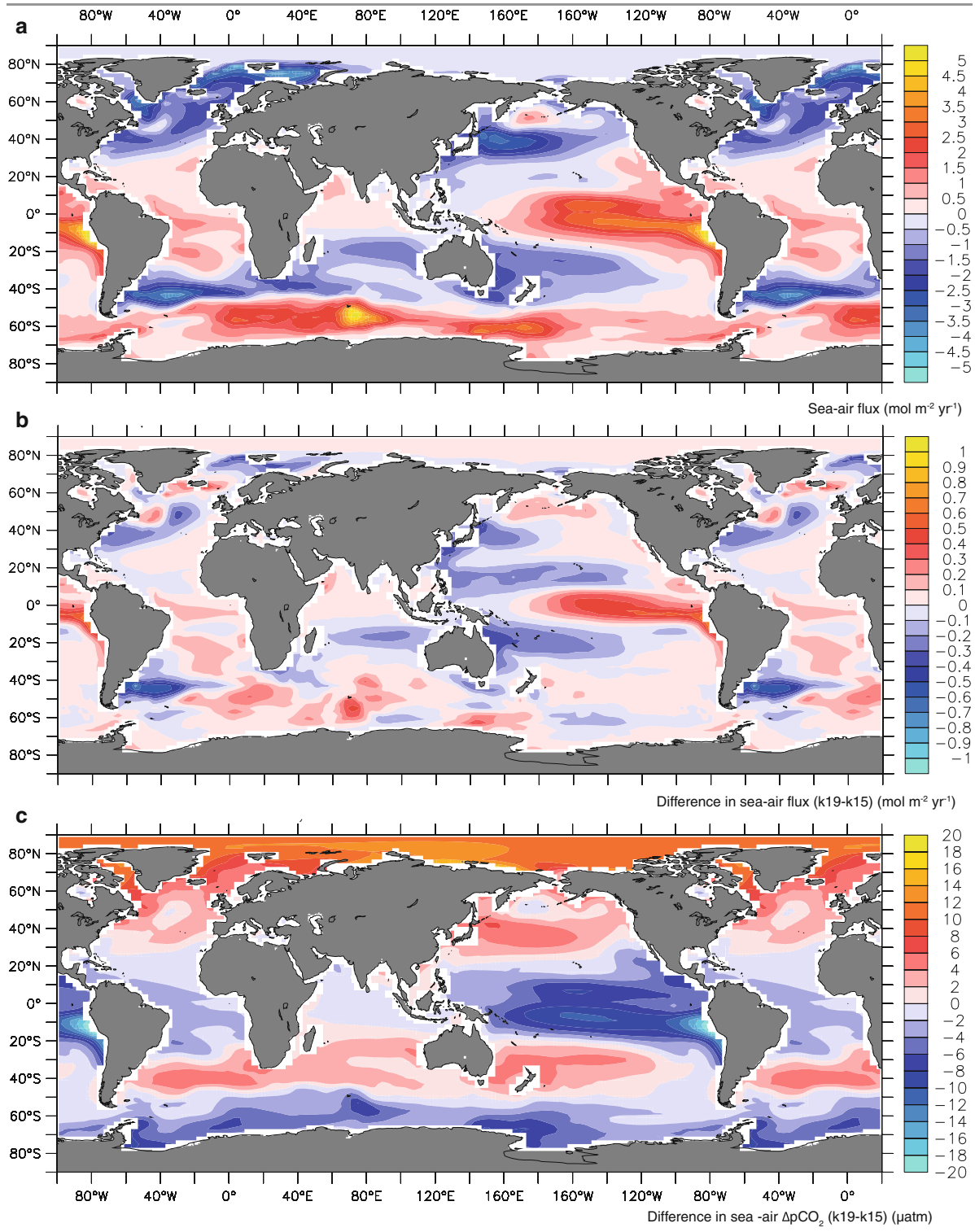

Fig. 2.12 Impact of the gas transfer velocity parameterisation on the model simulated air-sea flux of CO_2. (**a**) Annual mean sea-to-air flux of CO_2 in pre-industrial times simulated using a global mean gas transfer velocity of 15 cm h^{-1}. (**b**) Difference in the annual mean sea-to-air flux of CO_2 in pre-industrial times between a simulation using a global mean gas transfer velocity of 19 cm h^{-1} and the standard one with 15 cm h^{-1}. (**c**) Difference in the annual mean sea-air partial pressure difference in preindustrial times between the 19 cm h^{-1} and 15 cm h^{-1} cases. Based on model simulations executed with the global NCAR CCSM model (Graven et al. 2012)

Wanninkhof (1998) to scale the bubble-mediated flux with the cubic power of the wind speed (Hamme and Severinghaus 2007; Ito et al. 2011), but also other powers have been used (Spitzer and Jenkins 1989).

In the last decade, global and regional modellers have paid relatively little attention to the parameterisations used for the modelling the transfer of gases across the air-sea interface. This is likely to change in the coming years. On the one hand, the increasing computational power permits modellers to increase the spatial and temporal resolutions of their models, pushing them to the level where some of the assumptions underlying the classical parameterisations may no longer be fulfilled. For example, when employing the Wanninkhof (1992) parameterisation, most (global) models use the parameters for long-term average winds, while models are now being run with winds that change every 6 h, requiring the parameters for short-term winds. This change has not been undertaken in most models, yet. But the need for a reconsideration of the appropriateness of the chosen parameterisations needs to go further. Processes such as diurnal heating and cooling, eddies and fronts, and organic slicks that were considered of secondary importance at basin to global scales, may be important at local to regional scales, thus requiring renewed attention.

Furthermore, models are now increasingly being used to assimilate ocean observations, including pCO_2. Given the substantial sensitivity of surface ocean pCO_2 to the value of k_w (Fig. 2.12), it will be necessary to better handle gas transfer in order to exploit also the usefulness of pCO_2 to determine the rate of net community production, for example. With the possible advent of large-scale observations of dissolved oxygen by floats (Johnson et al. 2009), this need will increase even further, as the interpretation of the biologically generated O_2 signal requires accurate estimates of the amount of O_2 that is exchanged with the atmosphere.

2.8.2 Remote Sensing

Gas transfer velocity has been retrieved at global scale from satellite measurements using mainly two approaches:

1. The use of satellite wind speed and $k_w - U$ relationships (see Boutin et al. (2009) for a review).
2. Or using mean square slope (mss) derived from dual frequency altimeters (Glover et al. 2007).

Whatever the approach used, the big advantage of the satellite measurements is that they provide a better description of the spatio-temporal variability than meteorological models or at-sea measurements. In particular, a correct determination of k_w following point (1) requires a good knowledge of the statistical moments of the wind speed (at least its average and variance (see Wanninkhof et al. (2009))).

The main advantages of point (1) are related to the excellent spatial and temporal coverage of the wind speed owing to the large swaths of scatterometers and microwave radiometers, and to the mature algorithms for retrieving wind speed from satellite measurements (the rms difference of satellite wind speed with respect to buoy neutral wind speeds being on the order of 1 m s^{-1} (Bourassa et al. 2010)), while field measurements almost always provide k_w and U simultaneously, but not always surface stress. Although satellite wind speeds are expressed as neutral wind speeds to facilitate the comparison with in situ measurements, a scatterometer measures a backscatter coefficient that is related to resonant Bragg scattering by centimetric waves. Hence it is expected that scatterometer measurements would better correlate with k_w than wind speed at 10 m height. But this is almost impossible to demonstrate with field measurements due to the spatio-temporal variability of U (scatterometer measurements are integrated over typically 25 km while k_w is obtained from point measurements) and temporal undersampling of satellite measurements (at best two measurements per day while measurements of k_w by dual tracer techniques are integrated over several days). It is remarkable that the use of $k_w - U$ relationship derived from dual tracer experiments (Ho et al. 2006; Nightingale et al. 2000b) and scatterometer wind speeds give global k_w average within the new ^{14}C constraints without a-posteriori adjustments (Boutin et al. 2009) as shown in Fig. 2.13. Nevertheless, given the 30 % uncertainty in the global k_w average deduced from the ^{14}C inventory (Sweeney et al. 2007), the remaining uncertainty on the functional form of the $k_w - U$ relationship (quadratic, cubic, or hybrid, see Wanninkhof et al. (2009) for a review) and the remaining uncertainty

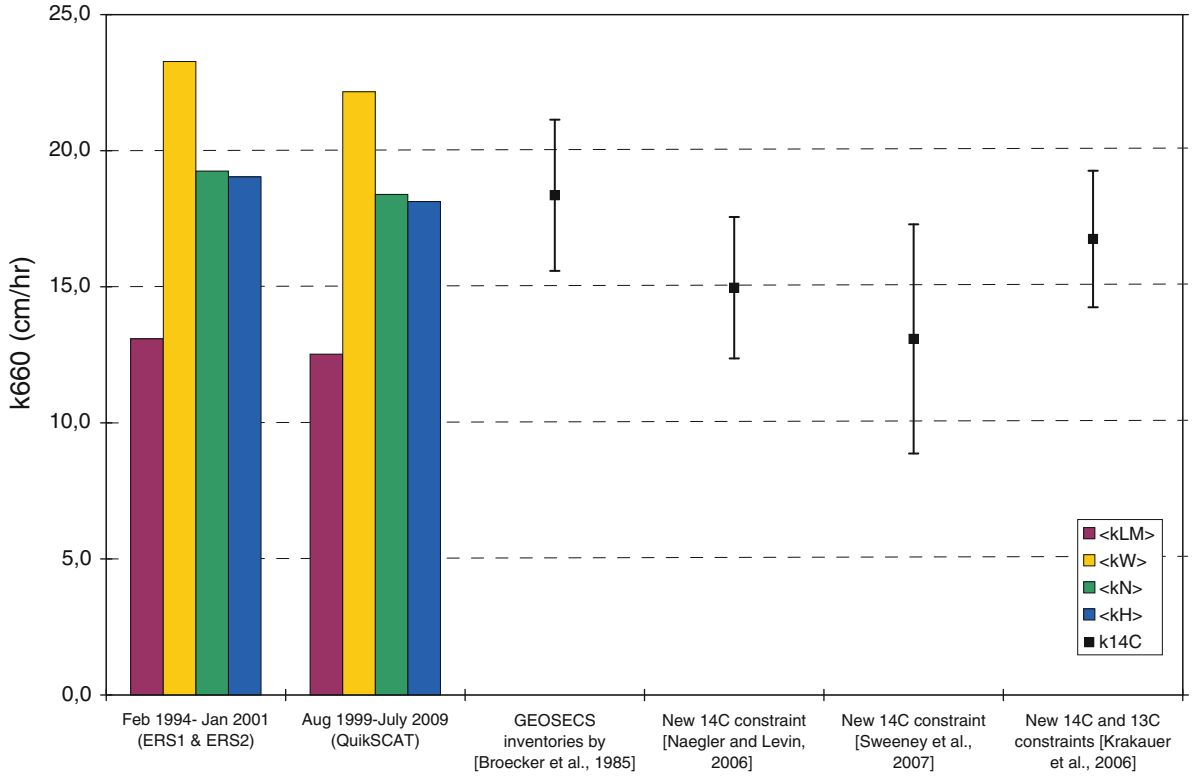

Fig. 2.13 Global averages of k_w (in cm h^{-1}) deduced from long time series of satellite wind speeds and $k_w - U$ relationships (*bar charts*) (*maroon bars* indicate k_{LM} (Liss and Merlivat 1986), *yellow bars* indicate k_W (Wanninkhof 1992), *green bars* indicate k_N (Nightingale et al. 2000a), and *blue bars* indicate k_H (Ho et al. 2006)) and deduced from ^{14}C global inventories (*black squares*). Methodology to derive k_w from satellite wind speed is described in Boutin et al. (2009); K_W fields are available at http://cersat.ifremer.fr/Data/Discovery/By-product-type/Gridded-products/

on the wind speed, the new ^{14}C estimates are not sufficient to fully constrain a $k_w - U$ relationship.

Method (2) has been developed because of experimental evidences that k_w is better correlated to small scale mss than to wind speed or wind stress (as reviewed in Frew et al. (2007)). Nevertheless, it has some limitations described in Sect. 2.6.2. Future large swath altimeters will improve the spatial coverage but in situ measurements of both mss and k_w in various regions of the globe are critical to definitely assess the utility of this method with respect to the $k_w - U$ method.

2.8.3 Inventories, Climatologies Using In Situ Data

Until now, long time series of k_w or of CO_2 exchange coefficients, K_W, (K_W is usually preferred when building maps as it minimises the temperature dependence due to the CO_2 Schmidt number and to the CO_2 solubility in the air-sea CO_2 flux computation) have mostly been built from a single satellite instrument. K_W derived from ERS1, ERS2 and QuickSCAT wind speeds between 1994 and 2009 are available at http://cersat.ifremer.fr/Data/Discovery/By-product-type/Gridded-products/K-CO2-QuikSCAT. Global averages of k_w derived from these scatterometer wind speeds are presented on Fig. 2.13.

Using k_w-mss relationships and after a thorough cross-validation of Jason-1 and TOPEX, Glover et al. (2007) have produced global k_w fields from 1993 to 2005. Because of the quadratic or cubic dependency of k_w with U, the accuracy of the wind speed fields used to build k_w fields is a big issue and the merging of several satellite wind speeds requires a thorough cross-validation (e.g. Fangohr et al. 2008). Not only the average wind speed must be well known but also at

least the second moment of the wind speed. On the other hand, biases of a few tenths of meter per second remain between the various types of satellite wind speeds because of the difficulty of validating satellite wind speeds integrated over typically 25 km with point measurements of wind speeds in the field and because the various satellite instruments are not sensitive to the same surface state. For instance, a microwave radiometer or an altimeter will better sense high wind speeds than a scatterometer; a Ku-band scatterometer will be closer to friction velocity than a C-band scatterometer but will be more affected by rain.

Recently, the numerous satellite wind speeds available since 1987, and the existence of biases between various satellite wind products have motivated the development of cross-calibrated multiplatform surface wind products (CCMP) (e.g. Atlas et al. 2011). Such merged products are necessary to ensure long term continuity of wind speed records (in particular scatterometer measurements are not continuous), and are very useful for monitoring K_W using existing $k_w - U$ relationships and for computing the air-sea CO_2 flux from CO_2 partial pressure. Mean k_w deduced with a quadratic $k_w - U$ relationship and CCMP wind speeds between 2000 and 2009 and between 50 °S and 50 °N agrees to within 2.5 % with mean k_w deduced from QuickSCAT products available at Ifremer.[2]

2.9 Summary

Transfer across the air-sea interface is traditionally described by a wind-speed dependent function, where different studies indicate different functional forms and scaling dependencies. Measurements from mass-balance techniques seem to converge at a quadratic wind speed dependence (e.g. Nightingale et al. 2000b), agreeing with estimates from ^{14}C inventories. Eddy covariance techniques tend to give higher values, in particularly at higher winds, partly explained by the enhancement due to bubble mediated transfer (not fully captured by mass-balance techniques). It is generally agreed that wind is not the only forcing factor of importance. For better understanding additional processes need to be taken into account (micro breaking waves, small- and large scale turbulence, waves, bubbles and sea spray, surface films, chemical and biological enhancement, rain and atmospheric processes etc.). This is particularly important when more detailed information is required in time and space. Further understanding of the transfer can be obtained by measurements, where it is necessary to consider the strengths/weaknesses of the various methods and the scale being resolved by each method. High-resolution numerical simulation is an alternative approach for studying transfer mechanisms with the potential of giving detailed information on the action/interaction of various mechanisms.

Global transfer velocities are often derived from remote sensing or various inventories and use wind speed estimates from satellites or surface wind speed products and $k_w - U$ based relationships, although mean squares slopes from altimeter data are sometimes used. Here the accuracy of the satellite products and resolution in time and space are important factors to consider when used for flux calculations. Air-sea transfer velocities are frequently used in models. Fluxes derived from models or modelled marine biogeochemical processes have shown relatively small sensitivity to the formulation of transfer velocity, partly due to feed-back mechanisms in the models (the air-sea gradient is slightly adjusted) but the modelling community have not focused much on the issue. Global gas flux estimates calculated using air-sea gradients estimated from global inventories (from in situ data or remote sensing) are more sensitive to the formulation of transfer velocity than modelled estimates.

To be able to derive more accurate regional and global methods of determining the transfer velocity it is necessary to increase our understanding of the dependence of various processes and their relative importance. The variation in time and space can then be better explained and described. To achieve this, it is suggested to combine different measurement techniques and use gases of different solubility.

[2] http://cersat.ifremer.fr/data/discovery/by_product_type/gridded_products/k_co2_quikscat

References

Adrian R (1991) Particle-imaging techniques for experimental fluid mechanics. Annu Rev Fluid Mech 23:261–304

Adrian R (2005) Twenty years of particle image velocimetry. Exp Fluids 39(2):159–169. doi:10.1007/s00348-005-0991-7

Agrawal Y, Terray E, Donelan M, Hwang P, Williams AJ III, Drennan W, Kahma K, Kitaigorodskii S (1992) High dissipation beneath surface waves due to breaking. Nature 359:219–220. doi:10.1038/359219a0

Anctil F, Donelan M, Drennan W, Graber H (1994) Eddy-correlation measurements of air-sea fluxes from a discus buoy. J Atmos Ocean Technol 11:1144–1150

Andreas E (1992) Sea spray and the turbulent air–sea heat fluxes. J Geophys Res 97:11429–11441

Andreas EL, Jones KF, Fairall CW (2010) Production velocity of sea spray droplets. J Geophys Res 115(C12):C12065. doi:10.1029/2010JC006458

Anis A, Moum J (1995) Surface wave-turbulence interactions: scaling $\varepsilon(z)$ near the sea surface. J Phys Oceanogr 25:2025–2045

Asher W (1997) The sea-surface microlayer and its effect on global air-sea gas transfer. In: Liss PS, Duce RA (eds) The sea surface and global change. Cambridge University Press, Cambridge, pp 251–285

Asher WE (2009) The effects of experimental uncertainty in parameterizing air-sea gas exchange using tracer experiment data. Atmos Chem Phys 9(1):131–139

Asher WE, Pankow JF (1986) The interaction of mechanically generated turbulence and interfacial films with a liquid phase controlled gas/liquid transport process. Tellus 38B:305–318

Asher W, Wanninkhof R (1998) The effect of bubble-mediated gas transfer on purposeful dual-gaseous tracer experiments. J Geophys Res 103. doi:10.1029/98JC00245

Asher W, Karle L, Higgins B, Farley P (1996) The influence of bubble plumes on air-seawater gas transfer velocities. J Geophys Res 101:12027–12041

Asher WE, Jessup AT, Atmane MA (2004) On the use of the active controlled flux technique for in situ measurement oh the air–sea transfer velocity of heat and gas. J Geophys Res 109:C08S14. doi:10.1029/2003JC001805

Assur A (1958) Composition of sea ice and its tensile strength. In: Arctic sea ice, vol 598, Publication. National Academy of Sciences-National Research Council, Washington, DC, pp 106–138

Atlas R, Hoffman R, Ardizzone J, Leidner S, Jusem J, Smith D, Gombos D (2011) A cross-calibrated, multiplatform ocean surface wind velocity product for meteorological and oceanographic applications. Bull Am Meteorol Soc 92:157–174. doi:10.1175/2010BAMS2946.1

Atmane MA, Asher W, Jessup AT (2004) On the use of the active infrared technique to infer heat and gas transfer velocities at the air-water interface. J Geophys Res 109:C08S14

Babanin A (2006) On a wave-induced turbulence and a wave-mixed upper ocean layer. Geophys Res Lett 33:L20605. doi:10.1029/2006GL027308

Babanin AV, Haus BK (2009) On the existence of water turbulence induced by nonbreaking surface waves. J Phys Oceanogr 39(10):2675–2679

Babanin AV, Ganopolski A, Phillips WR (2009) Wave-induced upper-ocean mixing in a climate model of intermediate complexity. Ocean Model 29(3):189–197. doi:10.1016/j.ocemod.2009.04.003

Banks RB, Herrera FF (1977) Effect of wind and rain on surface reaeration. J Environ Eng 103:489–504

Banks RB, Wickramanayake GB, Lohani BN (1984) Effect of rain on surface reaeration. J Environ Eng 110:1–14

Banner ML (1990) The influence of wave breaking on the surface pressure distribution in wind-wave interactions. J Fluid Mech 211:463–495

Banner M, Peirson W (1998) Tangential stress beneath wind-driven air-water interfaces. J Fluid Mech 364:115–145

Banner ML, Phillips OM (1974) On the incipient breaking of small-scale waves. J Fluid Mech 65:647–656

Banner ML, Jones ISF, Trinder JC (1989) Wavenumber spectra of short gravity waves. J Fluid Mech 198:321–344

Bariteau L, Hueber J, Lang K, Helmig D, Fairall CW, Hare JE (2010) Ozone deposition velocity by ship-based eddy correlation flux measurements. Atmos Meas Tech 3:441–455. doi:10.5194/amt-3-441-2010

Bates N, Mathis J (2009) The arctic ocean marine carbon cycle: evaluation of air-sea co2 exchanges, ocean acidification impacts and potential feedbacks. Biogeosciences 6:2433–2459

Belanger TV, Korzun EA (1990) Rainfall-reaeration effects. J Irrig Drain 116:582–587. doi:10.1061/(asce)0733-9437(1990)116:4(582)

Belanger TV, Korzun EA (1991) Rainfall-reaeration effects. In: Wilhelms SC, Gulliver JS (eds) Air-water mass transfer. ASCE, New York, pp 388–399

Belcher SE, Grant ALM, Hanley KE, Fox-Kemper B, Van Roekel L, Sullivan PP, Large WG, Brown A, Hines A, Calvert D, Rutgersson A, Pettersson H, Bidlot J-R, Janssen PAEM, Polton JA (2012) A global perspective on Langmuir turbulence in the ocean surface boundary layer. Geophys Res Lett 39(18):L18605. doi:10.1029/2012GL052932

Beljaars ACM (1995) The parameterization of surface fluxes in large-scale models under free convection. Q J R Meteorl Soc 121:255–270

Bender ML, Kinter S, Cassar N, Wanninkhof R (2011) Evaluating gas transfer velocity parameterizations using upper ocean radon distributions. J Geophys Res 116(C2):C02010. doi:10.1029/2009JC005805

Berthe A, Kondermann D, Christensen C, Goubergrits L, Garbe C, Affeld K, Kertzscher U (2010) Three-dimensional, three-component wall-PIV. Exp Fluids 48(6):983–997. doi:10.1007/s00348-009-0777-4

Blanchard D (1963) The electrification of the atmosphere by particles from bubbles in the sea. Prog Oceanogr 1:71–202

Blomquist BW, Fairall CW, Huebert B, Kleiber DJ (2006) Dms sea-air transfer velocity: direct measurements by eddy covariance and parameterization based on the NOAA/COARE gas transfer model. Geophys Res Lett 33(7):L07601. doi:10.1029/2006GL025735

Bock EJ, Hara T, Frew NM, McGillis WR (1999) Relationship between air-sea gas transfer and short wind waves. J Geophys Res Ocean 104(C11):25821–25831, j NOV 15

Bortkovskii R, Novak V (1993) Statistical dependencies of sea state characteristics on water temperature and wind-wave age. J Mar Syst 4:161–169

Bourassa M, Stoffelen A, Bonekamp H, Chang P, Chelton D, Courtney J, Edson R, Figa J, He Y, Hersbach H, Hilburn K, Jelenak Z, Kelly K, Knabb R, Lee T, Lindstrom E, Liu W, Long D, Perrie W, Portabella M, Powell M, Rodriguez E, Smith D, Swail V, Wentz F (2010) Remotely sensed winds and wind stresses for marine forecasting and ocean modeling. In: Hall J, Harrison D, Stammer D (eds) Proceedings of OceanObs'09: sustained ocean observations and information for society, vol 2. ESA Publication WPP-306, Venice, 21–25 Sept 2009. doi:10.5270/OceanObs09.cwp.08

Boutin J, Etcheto J (1995) Estimating the chemical enhancement effect on the air-sea CO_2 exchange using the ERS1 scatterometer wind speeds. In: Monahan EC (ed) Air-water gas transfer. AEON Verlag & Studio, Hanau, pp 827–841

Boutin J, Quilfen Y, Merlivat L, Piolle J (2009) Global average of air-sea CO_2 transfer velocity from QuikSCAT scatterometer wind speeds. J Geophys Res 114:C04007. doi:10.1029/2007JC004168

Broecker W, Maier-Reimer E (1992) The influence of air and sea exchange on the carbon isotope distribution in the sea. Global Biogeochem Cycles 6:315–320. doi:10.1029/92GB01672

Broecker WS, Peng TH (1974) Gas exchange rates between air and sea. Tellus 26:21–35. doi:10.1111/j.2153-3490.1974.tb01948.x

Broecker HC, Petermann J, Siems W (1978) The influence of wind on co_2 exchange in a wind wave tunnel, including the effects of monolayers. J Mar Res 36:595–610

Broecker WS, Peng T-H, Ostlund G, Stuiver M (1985) The distribution of bomb radiocarbon in the ocean. J Geophys Res 90:6953–6970. doi:10.1029/JC090iC04p06953

Broecker WS, Ledwell JR, Takahashi T, Weiss R, Merlivat L, Memery L, Jähne B, Münnich KO (1986) Isotopic versus micrometeorologic ocean CO_2 fluxes: a serious conflict. J Geophys Res 91(C9):10517–10528. doi:10.1029/JC091iC09p10517

Brücker C (1995) Digital-particle-image-velocimetry (dpiv) in a scanning light-sheet: 3D starting flow around a short cylinder. Exp Fluids 19:255–263

Brücker C (1996) 3D PIV via spatial correlation in a color-coded light-sheet. Exp Fluids 21:312–314

Brumley BH, Jirka GH (1988) Air-water transfer of slightly soluble gases: turbulence, interfacial processes and conceptual models. Physicochem Hydrodyn 10:295–319

Budzianowski W, Koziol A (2005) Stripping of ammonia from aqueous solutions in the presence of carbon dioxide: effect of negative enhancement of mass transfer. Trans ICHemE Part A Chem Eng Res Des 83:196–204. doi:10.1205/cherd.03289

Burba G, McDermitt D, Grelle A, Anderson D, Xu L (2008) Addressing the influence of instrument surface heat exchange on the measurements of co2 flux from open-path gas analyzers. Glob Chang Biol 14:1854–1876

Burgmann S, Dannemann J, Schröder W (2008) Time-resolved and volumetric piv measurements of a transitional separation bubble on an sd7003 airfoil. Exp Fluids 44:609–622. doi:10.1007/s00348-007-0421-0

Businger J, Oncley S (1990) Flux measurement with conditional sampling. J Atmos Ocean Technol 7:349–352

Callaghan A, White M (2009) Automated processing of sea surface images for the determination of whitecap coverage. J Atmos Ocean Technol 26:384–394

Carlsson B, Rutgersson A, Smedman A (2009) Impact of swell on simulations using a regional atmospheric climate model. Tellus 61A:527–538

Carruthers DJ, Choularton TW (1986) The microstructure of hill cap clouds. Q J R Meteorol Soc 112:113–129

Cenedese A, Paglialunga A (1989) A new technique for the determination of the third velocity component with piv. Exp Fluids 8:228–230. doi:10.1007/BF00195799

Charnock H (1955) Wind stress on a water surface. Q J R Meteorol Soc 81:639–640

Chernyshenko SI, Baig MF (2005) The mechanism of streak formation in near-wall turbulence. J Fluid Mech 544:99–131. doi:10.1017/S0022112005006506

Coantic M (1986) A model of gas transfer across air–water interfaces with capillary waves. J Geophys Res 91:3925–3943. doi:10.1029/JC091iC03p03925

Csanady GT (1990) The role of breaking wavelets in air-sea gas transfer. J Geophys Res 95(C1):749–759

Csanady G (1997) The "slip law" of the free surface. J Oceanogr 53:67–80

Cunliffe M, Whitely A, Schafer H, Newbold L (2009) Comparison of bacterioneuston and bacterioplankton dynamics during a phytoplankton bloom in the a fjord microcosm. Appl Environ Microbiol 75:7173–7181

D'Asaro E, McNeil C (2007) Air–sea gas exchange at extreme wind speeds measured by autonomous oceanographic floats. J Mar Syst 66(1–4):92–109. doi:10.1016/j.jmarsys.2006.06.007

Danckwerts PV (1951) Significance of a liquid-film coefficients in gas absorption. Ind Eng Chem 43:1460–1467. doi:10.1021/ie50498a055

Davies JT (1972) Turbulence phenomena. An introduction to the eddy transfer of momentum, mass, and heat, particularly at interfaces. Academic, New York

de Leeuw G, Andreas EL, Anguelova MD, Fairall CW, Lewis ER, O'Dowd C, Schulz M, Schwartz SE (2011) Production flux of sea spray aerosol. Rev Geophys 49:RG2001. doi:10.1029/2010RG000349

de Leeuw G, Guieu C, Arneth A, Bellouin N, Bopp L, Boyd P, Denier van de Gon HAC, Desboeufs K, Dulac F, Facchini C, Gantt B, Langmann B, Mahowald N, Maranon E, O'Dowd C, Olgun N, Pulido-Villena E, Rinaldi M, Stephanou E, Wagener T (2013) Ocean–atmosphere interactions of particles. In: Liss P, Johnson M (eds) Ocean–atmosphere interactions of gases and particles. Springer, this volume

Deacon EL (1977) Gas transfer to and across an air-water interface. Tellus 29:363–374. doi:10.1111/j.2153-3490.1977.tb00746.x

Deardorff JW (1970) Convective velocity and temperature scales for the unstable planetary boundary layer and for rayleigh convection. J Atmos Sci 27(8):1211–1213. doi:10.1175/1520-0469(1970)027<1211:CVATSF>2.0.CO;2

Delille B, Tilbrook B, Lannuzel D, Schoemann V, Borges A, Lancelot C, Chou L, Dieckmann G, Tison J (2006) Air – sea ice exchange of carbon dioxide: the end of a long-lived paradigm? Science Submitted

Delille B, Jourdain B, Borges A, Tison J, Delille D (2007) Biogas (CO_2, O_2, dimethylsulfide) dynamics in spring Antarctic fast ice. Limnol Oceanogr 52:1367–1379

Department of Scientific and Industrial Research (1964) Effects of polluting discharges on the thames estuary: the reports of the Thames Survey Committee and of the Water Pollution, Research Laboratory. Her Majesty's Stationery Office, London, p 609

Desjardins R (1977) Description and evaluation of a sensible heat flux detector. Bound-Lay Meteorol 11:147–154

Dieckmann G, Nehrke G, Papadimitriou S, Göttlicher J, Steininger R, Kennedy H, Wolf-Gladrow D, Thomas D (2008) Calcium carbonate as ikaite crystals in Antarctic sea ice. Geophys Res Lett 35:L08501

Dieckmann G, Nehrke G, Uhlig C, Göttlicher J, Gerland S, Granskog M, Thomas D (2010) Ikaite (CaCO3*6H2O) discovered in Arctic sea ice. Cryosphere Discuss 4:153–161

Dinkelacker F, Schäfer M, Ketterle W, Wolfrum J, Stolz W, Köhler J (1992) Determination of the third velocity component with PTA using an intensity graded light sheet. Exp Fluids 13:357–359. doi:10.1007/BF00209511

Donelan MA (2001) A nonlinear dissipation function due to wave breaking. In: ECMWF workshop on ocean wave forecasting, The European Centre for Medium-Range Weather Forecasts, pp 87–94

Donelan M, Drennan W, Katsaros K (1997) The air-sea momentum flux in conditions of wind sea and swell. J Phys Oceanogr 27:2087–2099

Drennan W, Donelan M, Terray E, Katsaros K (1996) Oceanic turbulence dissipation measurements in SWADE. J Phys Oceanogr 26:808–815. doi:10.1175/1520-0485(1996)026<0808:OTDMIS>2.0.CO;2

Drennan W, Kahma K, Donelan M (1999) On momentum flux and velocity spectra over waves. Bound Lay Meteorol 92:489–515

Drennan W, Graber H, Hauser D, Quentin C (2003) On the wave age dependence of wind stress over pure wind seas. J Geophys Res 108. doi:10.1029/2000JC000715

Drennan W, Taylor P, Yelland M (2005) Parameterizing the sea surface roughness. J Phys Oceanogr 35:835–848

Duce RA, Tindale NW (1991) Atmospheric transport of iron and its deposition in the ocean. Limnol Oceanogr 36:1715–1726

Edson J, Hinton A, Prada K, Hare J, Fairall C (1998) Direct covari-ance measurements from mobile platforms at sea. J Atmos Ocean Technol 15:547–562

Edson J, Zappa C, Ware J, McGillis W, Hare J (2004) Scalar flux profile relationships over the open ocean. J Geophys Res 109:C08S09. doi:10.1029/2003JC001960

Edson J, Fairall C, Bariteau L, Helmig D, Zappa C, Cifuentes-Lorenzen A, McGillis W, Pezoa S, Hare J (2011) Direct covariance measurement of CO_2 gas transfer velocity during the 2008 Southern Ocean Gas Exchange Experiment: wind speed dependency. J Geophys Res. doi:10.1029/2011JC007022 (in press)

Elsinga GE, Scarano F, Wieneke B (2006) Tomographic particle image velocimetry. Exp Fluids 41:933–947

Emerson S, Quay P, Stump C, Wilbur D, Knox M (1991) O_2, ar, n_2, and ^{222}rn in surface waters of the subarctic Ocean: net biological o_2 production. Global Biogeochem Cycles 5(1):49–69. doi:10.1029/90GB02656

Eugster W, Kling G, Jonas T, McFadden J, Wuest A, MacIntyre S, Chapin F (2003) CO_2 exchange between air and water in an Arctic Alaskan and midlatitude Swiss lake: importance of convective mixing. J Geophys Res 108(D12):4362. doi:10.1029/2002JD002653

Fairall C, Bradley E, Rogers D, Edson J, Young G (1996) Bulk parameterization of air-sea fluxes for TOGA COARE. J Geophys Res 101:3747–3764

Fairall C, Hare J, Edson J, McGillis W (2000) Parameterization and micrometeorological measurements of air-sea gas transfer. Bound-Lay Meteorol 96:63–105. doi:10.1023/A:1002662826020

Fairall C, Bradley E, Hare J, Grachev A, Edson J (2003) Bulk parameterization of air-sea fluxes: updates and verification for the coare algorithm. J Climate 16:571–591

Fairall CW, Hare JE, Helmig D, Ganzveld L (2007) Water-side turbulence enhancement of ozone deposition to the ocean. Atmos Chem Phys 7:443–451. doi:10.5194/acp-7-443-2007

Fairall C, Yang M, Bariteau L, Edson J, Helmig D, McGillis W, Pezoa S, Hare J, Huebert B, Blomquist B (2011) Implementation of the coupled ocean–atmosphere response experiment flux algorithm with CO_2, dimethyl sulfide, and O_3. J Geophys Res 116:C00F09. doi:10.1029/2010JC006884

Fangohr S, Woolf D, Jeffery C, Robinson I (2008) Calculating long-term global air-sea flux of carbon dioxide using scatterometer, passive microwave, and model reanalysis wind data. J Geophys Res 113:C09032. doi:10.1029/2005JC003376

Fortescue GE, Pearson JRA (1967) On gas absorption into a turbulent liquid. Chem Eng Sci 22:1163–1176

Frew N (1997) The role of organic films in air-sea gas exchange. In: Liss PS, Duce RA (eds) The sea surface and global change. Cambridge University Press, Cambridge, pp 121–172

Frew N, Goldman J, Dennett M, Johnson A (1990) Impact of phytoplankton-generated surfactants on airsea gas-exchange. J Geophys Res 95:3337–3352

Frew N, Bock E, Schimpf U, Hara T, Haussecker H, Edson J, McGillis W, Nelson R, McKenna S, Uz B, Jähne B (2004) Air-sea gas transfer: its dependence on wind stress, small-scale roughness, and surface films. J Geophys Res Ocean C08S17:17. doi:10.1029/2003JC002131

Frew N, Glover D, Bock E, McCue S (2007) A new approach to estimation of global air-sea gas transfer velocity fields using dual-frequency altimeter backscatter. J Geophys Res 112:C11003. doi:10.1029/2006JC003819

Fulgosi M, Lakehal D, Banerjee S, Angelis VD (2003) Direct numerical simulation of turbulence in a sheared air–water flow with a deformable interface. J Fluid Mech 482:319–345

Garabetian F (1991) 14 c-glucose uptake and 14 C-CO_2 production in surface microlayer and surface water samples: influence of uv and visible radiation. Mar Ecol Prog Ser 77:21–26

Garbe C, Heinlein A (2011) Friction velocity from active thermography and shape analysis. In: Komori S, McGillis W, Kurose R (eds) Gas transfer at water surfaces 2010. Kyoto University Press, Kyoto, pp 535–543

Garbe C, Spies H, Jähne B (2003) Estimation of surface flow and net heat flux from infrared image sequences. J Math Imaging Vis 19(3):159–174. doi:10.1023/A:1026233919766

Garbe CS, Schimpf U, Jähne B (2004) A surface renewal model to analyze infrared image sequences of the ocean surface for

the study of air-sea heat and gas exchange. J Geophys Res 109:C08S15. doi:10.1029/2003JC001802
Garbe C, Degreif K, Jähne B (2007) Estimating the viscous shear stress at the water surface from active thermography. In: Garbe C, Handler RA, Jähne B (eds) Transport at the air sea interface – measurements, models and parametrizations. Springer, Berlin, pp 223–239. doi:10.1007/978-3-540-36906-6_16
Garbe C, Voss B, Stapf J (2012) Plenoptic particle streak velocimetry (ppsv): 3d3c fluid flow measurement from light fields with a single plenoptic camera. In: 16th international symposium on applications of laser techniques to fluid mechanics, Instituto Superior Técnico, Lisbon, pp 1–12
Gargett AE, Wells JR (2007) Langmuir turbulence in shallow water. Part 1. Observations. J Fluid Mech 576:27–61
Garland JA, Etzerman AW, Penkett SA (1980) The mechanism for dry deposition of ozone to seawater surfaces. J Geophys Res 85:7488–7492
Garratt JR (1992) The atmospheric boundary layer. Cambridge University Press, Cambridge
Glover D, Frew N, McCue S (2007) Air-sea gas transfer velocity estimates from the Jason-1 and TOPEX altimeters: prospects for a long-term global time series. J Mar Syst 66:173–181
Glud R, Rysgaard S, Kuhl M (2002) A laboratory study on o-2 dynamics and photosynthesis in ice algal communities: quantification by microsensors, o-2 exchange rates, c-14 incubations and a pam fluorometer. Aquat Microb Ecol 27:301–311
Goddijn-Murphy L, Woolf D, Callaghan A (2011) Parameterizations and algorithms for oceanic whitecap coverage. J Phys Oceanogr 41:742–756. doi:10.1175/2010JPO4533.1
Godfrey J, Beljaars A (1991) On the turbulent fluxes of buoyancy, heat and moisture at the air-sea interface at low wind speeds. J Geophys Res 96:22043–22048
Golden K (2003) Critical behavior of transport in sea ice. Phys B Condens Matter 338:274–283
Golden K, Ackley S, Lytle V (1998) The percolation phase transition in sea ice. Science 282:2238–2241
Goldman J, Dennett M, Frew N (1988) Surfactant effects on air sea gas-exchange under turbulent conditions. Deep-Sea Res 35:1953–1970
Gosink T, Pearson J, Kelley J (1976) Gas movement through sea ice. Nature 263:41–42
Grassl H (1976) The dependence of the measured cool skin of the ocean on wind stress and total heat flux. Bound-Lay Meteorol 10:465–474
Graven H, Gruber N, Key RF, Khatiwala S (2012) Changing controls on oceanic radiocarbon: new insights on shallow-to-deep ocean exchange and anthropogenic CO_2 uptake. J Geophys Res 117:C10005
Guo LX, Smedman A-S, Högström U (2004) Air-sea exchange of sensible heat over the baltic sea. Q J R Meteorol Soc 130:519–539
Hamme RC, Severinghaus JP (2007) Trace gas disequilibria during deep-water formation. Deep Sea Res Part I 54:939–950. doi:10.1016/j.dsr.2007.03.008
Handler RA, Smith GB (2011) Statistics of the temperature and its derivatives at the surface of a wind-driven air-water interface. J Geophys Res 116(C6):C06021. doi:10.1029/2010JC006496
Handler RA, Smith GB, Leighton RI (2001) The thermal structure of an air–water interface at low wind speeds. Tellus 53(A):233–244
Hara T, VanInwegen E, Wendelbo J, Garbe CS, Schimpf U, Jähne B, Frew N (2007) Estimation of air-sea gas and heat fluxes from infrared imagery based on near surface turbulence models. In: Garbe CS, Handler RA, Jähne B (eds) Transport at the air sea interface – measurements, models and parameterizations. Springer, Berlin. doi:10.1007/978-3-540-36906-6_17
Hare J, Fairall C, McGillis W, Edson J, Ward B, Wanninkhof R (2004) Evaluation of the NOAA/COARE air-sea gas transfer parameterization using GasEx data. J Geophys Res 109:C08S02. doi:10.1029/2003/C002256
Harriott P (1962) A random eddy modification of the penetration theory. Chem Eng Sci 17:149–154
Harrison EL, Veron F, Ho DT, Reid MC, Eggleston SS, Orton P, McGillis WR (2012) Nonlinear interaction between rain and wind induced air-water gas exchange. J Geophys Res 117:C03034
Hasse L, Liss P (1980) Gas exchange across the air-sea interface. Tellus 32:470–481. doi:10.1111/j.2153-3490.1980.tb00974.x
Haugen D (1978) Effects of sampling rates and averaging periods on me-teorlogical measurements. In: Fourth Symp Meteorol Observ Instr, Am Meteorol Soc, pp 15–18
Haußecker H, Jähne B (1995) In situ measurements of the air-sea gas transfer rate during the MBL/CoOP west coast experiment. In: Jähne B, Monahan EC (eds) Air-water gas transfer – selected papers from the third international symposium on air-water gas transfer. AEON Verlag & Studio, Hanau/Heidelberg, pp 775–784
Heinesch B, Yernaux M, Aubinet M, Geilfus N, Papakyriakou T, Carnat G, Eicken H, Tison J, Delille B (2009) Measuring air-ice CO_2 fluxes in the Arctic. FluxLetter Newsl FLUXNET 2:9–10
Helmig D, Lang E, Bariteau L, Ganzeveld L, Fairall C, Hare J, Boylan P, Hueber J (2011) Atmosphere-ocean ozone fluxes during the TexAQS 2006, STRATUS 2006, GOMECC 2007, GasEX 2008, and AMMA 2008 cruises. J Geophys Res 117:D04305
Hicks B (2005) A climatology of wet deposition scavenging ratios for the united states. Atmos Environ 39 (9):1585–1596. doi:10.1016/j.atmosenv.2004.10.039
Higbie R (1935) The rate of absorption of a pure gas into a still liquid during short periods of exposure. Trans Am Inst Chem Eng 31:365–389
Hinsch KD (2002) Holographic particle image velocimetry. Meas Sci Technol 13:R61–R72
Ho DT, Bliven LF, Wanninkhof R, Schlosser P (1997) The effect of rain on air-water gas exchange. Tellus 49:149–158
Ho DT, Asher WE, Bliven LF, Schlosser P, Gordan EL (2000) On mechanisms of rain-induced air-water gas exchange. J Geophys Res 105:24045–24057
Ho DT, Zappa CJ, McGillis WR, Bliven LF, Ward B, Dacey JWH, Schlosser P, Hendricks MB (2004) Influence of rain on air-sea gas exchange: lessons from a model ocean. J Geophys Res 109:C08S18. doi:10.1029/2003JC001806
Ho DT, Law CS, Smith MJ, Schlosser P, Harville M, Hill P (2006) Measurements of air-sea gas exchange at high wind speeds in the southern ocean: implications for global

parameterizations. Geophys Res Lett 33:16611–16616. doi:10.1029/2006GL026817

Ho DT, Veron F, Harrison E, Bliven LF, Scott N, McGillis WR (2007) The combined effect of rain and wind on air-water gas exchange: a feasibility study. J Mar Syst 66:150–160. doi:10.1016/j.jmarsys.2006.02.012

Ho DT, Sabine CL, Hebert D, Ullman DS, Wanninkhof R, Hamme RC, Strutton PG, Hales B, Edson JB, Hargreaves BR (2011a) Southern ocean gas exchange experiment: setting the stage. J Geophys Res 116:C00F08. doi:10.1029/2010JC006852

Ho DT, Wanninkhof R, Schlosser P, Ullman DS, Hebert D, Sullivan KF (2011b) Toward a universal relationship between wind speed and gas exchange: gas transfer velocities measured with $^{3}He/SF_6$ during the Southern Ocean Gas Exchange Experiment. J Geophys Res 116:C00F04. doi:10.1029/2010JC006854

Högström U (1996) Review of some basic characteristics of the atmospheric surface layer. Bound-Lay Meteorol 78:215–246

Högström U, Sahlée E, Drennan WM, Kahma KK, Smedman A-S, Johansson C, Pettersson H, Rutgersson A, Tuomi L, Zhang F, Johansson M (2008) Momentum fluxes and wind gradients in the marine boundary layer – a multi platform study. Boreal Environ Res 13:475–502

Holtslag A, De Bruin H (1988) Applied modeling of the nighttime surface energy balance over land. J Appl Meteorol 27:689–704

Hoover TE, Berkshire DC (1969) Effects of hydration on carbon dioxide exchange across an air-water interface. J Geophys Res 74(2):456–464

Hoppel WA, Frick GM, Fitzgerald JW (2002) Surface source function for sea-salt aerosol and aerosol dry deposition to the ocean surface. J Geophys Res 107:4382. doi:10.1029/2001JD002014

Hoppel WA, Caffrey PF, Frick GM (2005) Particle deposition on water: surface source versus upwind source. J Geophys Res 110:D10206. doi:10.1029/2004JD005148

Horst T, Lenschow D (2009) Attenuation of scalar fluxes measured with spatially displaced sensors. Bound-Lay Meteorol 130:275–300. doi:10.1007/s10546-008-9348-0

Hoyer K, Holzner M, Lüthi B, Guala M, Liberzon A, Kinzelbach W (2005) 3D scanning particle tracking velocimetry. Exp Fluids 39:923–934. doi:10.1007/s00348-005-0031-7

Huebert B, Blomquist B, Hare JE, Fairall CW, Johnson J, Bates T (2004) Measurements of the sea-air DMS flux and transfer velocity using eddy correlation. J Geophys Res Lett 31: L23113. doi:10.1029/2004GL021567

Hung L-P, Garbe CS, Tsai W-T (2011) Validation of eddy-renewal model by numerical simulation. In: Komori S, McGillis W, Krose R (eds) Gas transfer at water surfaces 2010. Kyoto University Press, Kyoto, pp 165–176

Hunt J, Belcher S, Stretch D, Sajjadi S, Clegg J (2011) Turbulence and wave dynamics across gas-liquid interfaces. In: Komori S, McGillis W, Kurose R (eds) Gas transfer at water surfaces 2010. Kyoto University Press, Kyoto

Ito T, Hamme RC, Emerson S (2011) Temporal and spatial variability of noble gas tracers in the north pacific. J Geophys Res 116:C08039. doi:10.1029/2010JC006828

Iversen T (1989) Numerical modelling of the long range atmospheric transport of sulphur dioxide and particulate sulphate to the arctic. Atmos Environ 23(11):2571–2595. doi:10.1016/0004-6981(89)90267-9

Jackson D, Wick G, Hare J (2011) A comparison of satellite-derived carbon dioxide transfer velocities from a physically-based model with GasEx cruise observations. J Geophys Res. doi:10.1029/2011JC007329 (in press)

Jähne B (1989) Energy balance in small-scale waves: an experimental approach using optical slope measuring technique and image processing. In: Komen GJ, Oost WA (eds) Radar scattering from modulated wind waves. Kluwer, Dordrecht, pp 105–120

Jähne B, Haußecker H (1998) Air-water gas exchange. Annu Rev Fluid Mech 30:443–468. doi:10.1146/annurev.fluid.30.1.443

Jähne B, Riemer KS (1990) Two-dimensional wave number spectra of small-scale water surface waves. J Geophys Res 95:11531–11546

Jähne B, Münnich KO, Siegenthaler U (1979) Measurements of gas exchange and momentum transfer in a circular wind-water tunnel. Tellus 31:321–329

Jähne B, Munnich K, Bosinger R, Dutzi A, Huber W, Libner P (1987) On the parameters influencing air-water gas exchange. J Geophys Res 92:1937–1949

Janssen PAEM (2004) The interaction of ocean waves and wind. Cambridge University Press, Cambridge

Jeffery CD, Woolf DK, Robinson IS, Donlon CJ (2007) One-dimensional modelling of convective CO_2 exchange in the Tropical Atlantic. Ocean Model 19:161–182. doi:10.1016/j.ocemod.2007.07.003

Jeffery C, Robinson I, Woolf D (2010) Tuning a physically-based model of the air-sea gas transfer velocity. Ocean Model 31:28–35. doi:10.1016/j.ocemod.2009.09.001

Jehle M, Jähne B (2008) A novel method for three-dimensional three-component analysis of flow close to free water surfaces. Exp Fluids 44:469–480. doi:10.1007/s00348-007-0453-5

Jessup AT, Zappa C, Loewen MR, Hesany V (1997a) Infrared remote sensing of breaking waves. Nature 385(6611):52–55. doi:10.1038/385052a0

Jessup AT, Zappa CJ, Yeh HH (1997b) Defining and quantifying microscale wave breaking with infrared imagery. J Geophys Res 102(C10):23145–23153

Jessup AT, Asher WE, Atmane M, Phadnis K, Zappa CJ, Loewen MR (2009) Evidence for complete and partial surface renewal at an air-water interface. Geophys Res Lett 36:1–5. doi:10.1029/2009GL038986

Jin X, Gruber N (2003) Offsetting the radiative benefit of ocean iron fertilization by enhancing N_2O emissions. Geophys Res Lett 30:2249. doi:10.1029/2003GL018458

Johnson M (2010) A numerical scheme to calculate temperature and salinity dependent air-water transfer velocities for any gas. Ocean Sci 6:913–932. doi:10.5194/os-6-913-2010

Johnson KS, Berelson WM, Boss ES, Chase Z, Claustre H, Emerson SR, Gruber N, Körtzinger A, Perry MJ, Riser SC (2009) Observing biogeochemical cycles at global scales with profiling floats and gliders: prospects for a global array. Oceanography 22:216–225

Johnson M, Hughes C, Bell T, Liss P (2011) A rumsfeldian analysis of uncertainty in air-sea gas exchange. In: Gas transfer at water surface 2010. Kyoto University Press, Kyoto, pp 464–484

Kähler C, Kompenhans J (2000) Fundamentals of multiple plane stereo particle image velocimetry. Exp Fluids 29:70–77

Keeling R (1993) On the role of large bubbles in air-sea gas exchange and supersaturation in the ocean. J Mar Res 51:237–271

Keller K (1994) Chemical enhancement of carbon dioxide transfer across the air-sea interface. Ph.D. thesis, Massachusetts Institute of Technology. http://dspace.mit.edu/bitstream/handle/1721.1/35997/32162323.% pdf?sequence=1

Kihm C, Körtzinger A (2010) Air-sea gas transfer velocity for oxygen derived from float data. J Geophys Res 115:C12003. doi:10.1029/2009JC006077

Kitaigorodskii S (1984) On the fluid dynamical theory of turbulent gas transfer across an air-sea interface in the presence of breaking wind waves. J Phys Oceanogr 14:960–972. doi:10.1175/1520-0485(1984)014<0960:OTFDTO>2.0.CO;2

Kitaigorodskii S (2011) The calculation of the gas transfer between the ocean and atmosphere. In: Komori S, McGillis W, Kurose R (eds) Gas transfer at water surfaces 2011. Kyoto University Press, Kyoto, pp 13–28

Kitaigorodskii S, Donelan MA (1984) Wind–wave effects on gas transfer. In: Brutsært W, Jirka GH (eds) Gas transfer at water surfaces. Reidel, Dordrecht, pp 147–170

Kline SJ, Reynolds WC, Schraub FA, Runstadler PW (1967) The structure of turbulent boundary layers. J Fluid Mech 30 (04):741–773. doi:10.1017/S0022112067001740

Komori S, Takagaki N, Saiki R, Suzuki N, Tanno K (2007) The effect of raindrops on interfacial turbulence and air-water gas transfer. In: Handler RA, Garbe C, Jähne B (eds) Transport at the air-sea interface. Springer, Berlin/Heidelberg, pp 169–179

Krakauer NY, Randerson JT, Primeau FW, Gruber N, Menemenlis D (2006) Carbon isotope evidence for the latitudinal distribution and wind speed dependence of the air-sea gas transfer velocity. Tellus B 58(5):390–417

Kromer B, Roether W (1983) Field measurements of air-sea gas exchange by the radon deficit method during jasin 1978 and fgge 1979. In: Meteor Forschungsergebnisse, Reihe A/B Allgemeines, Physik und Chemie des Meeres, Gebrüder Bornträger, vol A/B24, Deutsche Forschungsgemeinschaft, Berlin/Stuttgart, pp 55–76

Lakehal D, Fulgosi M, Yadigaroglu G, Banerjee S (2003) Direct numerical simulation of turbulent heat transfer across a mobile, sheared gas-liquid interface. J Heat Transf 15:1129–1139

Lamont JC, Scott DS (1970) An eddy cell model of mass transfer into the surface of a turbulent liquid. AIChE J 16:512–519. doi:10.1002/aic.690160403

Langmuir I (1938) Surface motion of water induced by wind. Science 87(2250):119–123. doi:10.1126/science.87.2250.119

Le Clainche Y, Vézina A, Levasseur M, Cropp RA, Gunson JR, Vallina SM, Vogt M, Lancelot C, Allen JI, Archer SD, Bopp L, Deal C, Elliott S, Jin M, Malin G, Schoemann V, Simo R, Six KD, Stefels J (2010) A first appraisal of prognostic ocean DMS models and prospects for their use in climate models. Global Biogeochem Cycles 24(3):GB3021. doi:10.1029/2009GB003721

Le Quéré C, Saltzman ES (eds) (2009) Surface ocean-lower atmosphere processes, vol 187, Geophysical monograph series. AGU, Washington, DC

Ledwell J (1984) The variation of the gas transfer coefficient with molecular diffusivity. In: Brutsært W, Jirka GH (eds) Gas transfer at water surfaces. Reidel, Dordrecht, pp 293–303

Lewis ER, Schwartz SE (2004) Sea salt aerosol production: mechanisms, methods, measurements, and models. American Geophysical Union, Washington, DC

Li M, Garrett C (1995) Is langmuir circulation driven by surface waves or surface cooling? J Phys Oceanogr 25(1):64–76. doi:10.1175/1520-0485(1995)025<0064:ILCDBS>2.0.CO;2

Li M, Garrett C, Skyllingstad E (2005) A regime diagram for classifying turbulent large eddies in the upper ocean. Deep-Sea Res 52(2):259–278. doi:10.1016/j.dsr.2004.09.004

Liberzon A, Gurka R, Hetsroni G (2004) XPIV-multi-plane stereoscopic particle image velocimetry. Exp Fluids 36:355–362

Liss PS (1971) Exchange of SO_2 between the atmosphere and natural waters. Nature 233(5318):327–329. doi:10.1038/233327a0

Liss P (1975) Chemistry of the sea surface microlayer. In: Riley J, Skirrow G (eds) Chemical oceanography, vol 2. Academic, London, pp 192–244

Liss P (1983) Gas transfer: experiments and geochemical implications. In: Liss P, Slinn W (eds) Air-sea exchange of gases and particles. Springer, Dordrecht, pp 241–298

Liss P, Martinelli F (1978) The effect of oil films on the transfer of oxygen and water vapour across an air-water interface. Thalass Jugosl 14:215–220

Liss PS, Merlivat L (1986) Air-sea gas exchange rates: introduction and synthesis. In: Buat-Menard P (ed) The role of air-sea exchange in geochemical cycling. Reidel, Boston, pp 113–129

Liss PS, Slater PG (1974) Flux of gases across the air-sea interface. Nature 247:181–184

Liss P, Watson A, Bock E, Jähne B, Asher W, Frew N, Hasse L, Korenowski G, Merlivat L, Phillips L, Schlüssel P, Woolf D (1997) Report group 1 – physical processes in the microlayer and the air-sea exchange of trace gases. In: Liss P, Duce R (eds) The sea surface and global change. Cambridge University Press, Cambridge, pp 1–33

Long MS, Keene WC, Kieber DJ, Erickson DJ, Maring H (2011) A sea-state based source function for size- and composition-resolved marine aerosol production. Atmos Chem Phys 11:1203–1216. doi:10.5194/acp-11-1203-2011

Longuet-Higgins MS, Cleaver RP, Fox MJH (1994) Crest instabilities of gravity waves. Part 2. Matching and asymptotic analysis. J Fluid Mech 259:333–344

Loose B, McGillis W, Schlosser P, Perovich D, Takahashi T (2009) Effects of freezing, growth, and ice cover on gas transport processes in laboratory seawater experiments. Geophys Res Lett 36. doi:10.1029/2008gl036318

Loose B, Miller L, Elliott S, Papakyriakou T (2011a) Sea ice biogeochemistry and material transport across the frozen interface. Oceanography 24:202–218. doi:10.5670/oceanog.2011.72

Loose B, Schlosser P, Perovich D, Ringelberg D, Ho D, Takahashi T, Reynolds C, McGillis W, Tison J (2011b) Gas diffusion through columnar laboratory sea ice: implications for mixed-layer ventilation of CO_2 in the seasonal ice zone. Tellus B 63. doi:10.1111/j.1600-0889.2010.00506.x

Lorke A, Peeters F (2006) Toward a unified scaling relation for interfacial fluxes. J Phys Oceanogr 36(5):955–961

MacIntyre S, Eugster W, Kling GW (2002) The critical importance of buoyancy flux for gas flux across the air-water interface. In: Donelan MA, Drennan WM, Saltzman ES, Wanninkhof R (eds) Gas transfer at water surfaces, vol 127, Geophysical monograph. American Geophysical Union, Washington, DC, pp 13–28

Mackay D, Yeun ATK (1983) Mass transfer coefficient correlations for volatilization of organic solutes from water. Environ Sci Technol 17:211–217

Manasseh R, Babanin AV, Forbes C, Richards K, Bobevski I, Ooi A (2006) Passive acoustic determination of wave-breaking events and their severity across the spectrum. J Atmos Ocean Technol 23:599–618

Marion G, Millero F, Feistel R (2009) Precipitation of solid phase calcium carbonates and their effect on application of seawater SA-T -P models. Ocean Sci 5:285–291

Matthews B (1999) The rate of air-sea CO_2 exchange: chemical enhancement and catalysis by marine microalgae. Ph.D. thesis, University of East Anglia, Norwich

McGillis WR, Wanninkhof R (2006) Aqueous CO_2 gradients for air-sea flux estimates. Mar Chem 98:100–108

McGillis W, Edson J, Hare J, Fairall C (2001) Direct covariance air-sea CO_2 fluxes. J Geophys Res 106:16729–16745

McGillis W, Edson J, Zappa C, Ware J, McKenna S, Terray E, Hare J, Fairall C, Drennan W, Donelan M, DeGrandpre M, Wanninkhof R, Feely R (2004a) Air-sea CO_2 exchange in the equatorial Pacific. J Geophys Res 109:C08S02. doi:10.1029/2003JC002256

McGillis WR, Asher WE, Wanninkhof R, Jessup AT, Feely RA (2004b) Air-sea CO_2 exchange in the equatorial pacific. J Geophys Res 109:C08S01

McKenna SP, McGillis WR (2004) The role of free-surface turbulence and surfactants in air-water gas transfer. Int J Heat Mass Transf 47:539–553. doi:10.1016/j.ijheatmasstransfer.2003.06.001

McNeil C, D'Asaro E (2007) Parameterization of air sea gas fluxes at extreme wind speeds. J Mar Syst 66:110–121. doi:10.1016/j.jmarsys.2006.05.013

McNeil CL, Ward B, McGillis WR, DeGrandpre MD, Marcinowski L (2006) Fluxes of N_2, O_2, and CO_2 in near-shore waters off Martha's Vineyard. Cont Shelf Res 26:1281–1294

McWilliams J, Sullivan P, Moeng C (1997) Langmuir turbulence in the ocean. J Fluid Mech 334:1–30

Melville WK (1996) The role of surface-wave breaking in air-sea interaction. Annu Rev Fluid Mech 28:279

Miller L, Papakyriakou T, Collins R, Deming J, Ehn J, Macdonald R, Mucci A, Owens O, Raudsepp M, Sutherland N (2011) Carbon dynamics in sea ice: a winter flux time series. J Geophys Res 116:C02028. doi:10.1029/2009jc006058

Monahan E, O'Muircheartaigh I (1980) Optimal power-law description of oceanic whitecap coverage dependence on wind speed. J Phys Oceanogr 10:2094–2099

Monahan EC, Spillane MC (1984) The role of whitecaps in air-sea gas exchange. In: Brutsaert W, Jirka GH (eds) Gas transfer at water surfaces. Reidel, Hingham, pp 495–503

Monahan E, Fairall C, Davidson K, Jones-Boyle P (1983) Observed interrelations between 10 m winds, ocean whitecaps and marine aerosols. Q J R Meteorol Soc 109:379–392

Müller D, Müller B, Renz U (2001) Three-dimensional particle-streak tracking (PST) velocity measurements of a heat exchanger inlet flow. Exp Fluids 30(6):645–656. doi:10.1007/s003480000242

Müller SA, Joos F, Plattner GK, Edwards NR, Stocker TF (2008) Modeled natural and excess radiocarbon: sensitivities to the gas exchange formulation and ocean transport strength. Global Biogeochem Cycles 22(3):GB3011. doi:10.1029/2007GB003065

Naegler T, Ciais P, Rodgers K, Levin I (2006) Excess radiocarbon constraints on air-sea gas exchange and the uptake of CO_2 by the oceans. Geophys Res Lett 33(11):L11802. doi:10.1029/2005GL025408

Nägler T (2009) Reconciliation of excess ^{14}C-constrained global CO_2 piston velocity estimates. Tellus B 61(2):372–384. doi:10.1111/j.1600-0889.2008.00408.x

Najjar R, Orr J (1998) Design of OCMIP-2 simulations of chlorofluorocarbons, the solubility pump and common biogeochemistry, http://www.cgd.ucar.edu/oce/klindsay/OCMIP/design.pdf

Nakagawa H, Nezu I (1981) Structure of space-time correlation of bursting phenomena in an open-channel flow. J Fluid Mech 104:1–43. doi:10.1017/S0022112081002796

Nightingale PD, Liss PS, Schlosser P (2000a) Measurements of air-sea gas transfer during an open ocean algal bloom. Geophys Res Lett 27(14):2117–2120. doi:10.1029/2000GL011541

Nightingale PD, Malin G, Law CS, Watson AJ, Liss PS, Liddicoat MI, Boutin J, Upstill-Goddard RC (2000b) In situ evaluation of air-sea gas exchange parameterizations using novel conservative and volatile tracers. Global Biogeochem Cycles 14(1):373–387. doi:10.1029/1999GB900091

Nilsson ED, Rannik U, Swietlicki E, Leek C, Aalto PP, Zhou J, Norman M (2001) Turbulent aerosol fluxes over the Arctic Ocean. 2. wind driven sources from the sea. J Geophys Rev 106:32129–32154. doi:10.1029/2000JD900747

Nilsson E, Rutgersson A, Sullivan P (2010) Flux attenuation due to sensor separation over sea. J Atmos Ocean Technol 27:856–868. doi:10.1175/2010JTECHA1388.1

Nomura D, Eicken H, Gradinger R, Shirasawa K (2010a) Rapid physically driven invesrion of the air-sea ice CO_2 flux in the seasonal landfast ice off Barrow, Alaska after onset of surface melt. Cont Shelf Res 30:1998–2004

Nomura D, Yoshikawa-Inoue H, Toyota T, Shirasawa K (2010b) Effects of snow, snowmelting and refreezing processes on air-sea-ice CO_2 flux. J Glaciol 56:262–270

Oh S-H, Mizutani N, Suh K-D (2008) Laboratory observation of coherent structures beneath microscale and large-scale breaking waves under wind action. Exp Therm Fluid Sci 32:1232–1247

Okuda K (1982) The internal structure of short wind waves. Part I: on the internal vorticity structure. J Oceanogr Soc Jpn 38:28–42

Olsen A, Omar AM, Stuart-Menteth AC, Triñanes JA (2004) Diurnal variations of surface ocean pCO_2 and sea–air CO_2 flux evaluated using remotely sensed data. Geophys Res Lett 31:L20304. doi:10.1029/2004GL020583

Osborne T, Farmer D, Vagle S, Thorpe S, Cure M (1992) Measurements of bubble plumes and turbulence from a submarine. Atmos Ocean 30:419–440. doi:10.1080/07055900.1992.9649447

Panofsky H, Dutton J (1984) Atmospheric turbulence, models and methods for engineering applications. Wiley, New York

Papadimitriou S, Kennedy H, Kattner G, Dieckmann G, Thomas D (2004) Experimental evidence for carbonate precipitation and CO_2 degassing during sea ice formation. Geochim Cosmochim Acta 68:1749–1761. doi:10.1016/j.gca.2003.07.004

Papakyriakou T, Miller L (2011) Springtime CO_2 exchange over seasonal sea ice in the Canadian Arctic Archipelago. Ann Glaciol 52:215–224

Peacock S (2004) Debate over the ocean bomb radiocarbon sink: closing the gap. Global Biogeochem Cycles 18(2):GB2022. doi:10.1029/2003GB002211

Peirson WL, Banner ML (2003) Aqueous surface layer flows induced by microscale breaking wind waves. J Fluid Mech 479:1–38. doi:10.1017/S0022112002003336

Peng TH, Broecker WS, Mathieu GG, Li Y-H, Bainbridge A (1979) Radon evasion rates in the Atlantic and Pacific oceans as determined during the geosecs program. J Geophys Res 84(C5):2471–2487

Pereira F, Gharib M, Dabiri D, Modarress M (2000) Defocusing PIV: a three component 3D DPIV measurement technique. Application to bubbly flows. Exp Fluids 29:S78–S84

Pereira F, Lu J, Castaño GE, Gharib M (2007) Microscale 3D flow mapping with μDDPIV. Exp Fluids 42:589–599. doi:10.1007/s00348-007-0267-5

Petelski T, Piskozub J (2006) Vertical coarse aerosol fluxes in the atmospheric surface layer over the north polar waters of the atlantic. J Geophys Res 111:C06039. doi:10.1029/2005JC003295

Pettersson H, Kahma K, Tuomi L (2010) Wave directions in a narrow bay. J Phys Oceanogr 40:155–169. doi:10.1175/2009JPO4220.1

Pettersson H, Kahma K, Rutgersson A, Perttilä M (2011) Air-sea carbon dioxide exchange during upwelling. In: Komori S, McGillis W, Kurose R (eds) Gas transfer at water surfaces 2011. Kyoto University Press, Kyoto, pp 420–429

Phillips O (1977) The dynamics of the upper ocean, 2nd edn. Cambridge University Press, Cambridge

Phillips O, Posner F, Hansen J (2001) High range resolution radar measurements of the speed distribution of breaking events in wind-generated ocean waves: surface impulse and wave energy dissipation rates. J Phys Oceanogr 31:450–460. doi:10.1175/1520-0485(2001)031<0450:HRRRMO>2.0.CO;2

Piskozub J, Petelski T (2009) Scavenging by marine aerosol. In: SOLAS open science conference, Barcelona

Poisson A, Chen C (1987) Why is there little anthropogenic CO_2 in the Antarctic bottom water? Deep-Sea Res Part A 34:1255–1275

Prasad AK (2000) Stereoscopic particle image velocimetry. Exp Fluids 29:103–116

Prytherch J, Yelland M, Pascal R, Moat B, Skjelvan I, Neill C (2010) Direct measurements of the co2 flux over the ocean: development of a novel method. Geophys Res Lett 37:L03607. doi:10.1029/2009GL041482

Raffel M, Willert CE, Wereley ST, Kompenhans J (2007) Particle image velocimetry: a practical guide. Springer, Heidelberg

Rannik U, Vesala T, Keskinen R (1997) On the damping of temperature fluctuations in a circular tube relevant to the eddy covariance technique. J Geophys Res 102:12789–12794. doi:10.1029/97JD00362

Rashidi M, Banerjee S (1990) The effect of boundary conditions and shear rate on streak formation and breakdown in turbulent channel flows. Phys Fluids 2:1827–1838. doi:10.1063/1.857656

Reul N, Branger H, Giovanangeli J-P (2008) Air flow structure over short-gravity breaking water waves. Bound-Lay Meteorol 126(3):477–505

Rhee T, Nightingale P, Woolf D, Caulliez G, Bowyer P, Andreae M (2007) Influence of energetic wind and waves on gas transfer in a large wind-wave tunnel facility. J Geophys Res (Ocean) 112:5027. doi:10.1029/2005JC003358

Rinne J, Douffet T, Prigent Y, Durand P (2008) Field comparison of disjunct and conventional eddy covariance techniques for trace gas flux measurements. Environ Pollut 152:630–635. doi:10.1016/j.envpol.2007.06.063

Roether W, Kromer B (1984) Optimum application of the radon deficit method to obtain air–sea gas exchange rates. In: Brutsaert W, Jirka GH (eds) Gas transfer at water surfaces. Reidel, Hingham, pp 447–457

Rowe M, Fairall C, Perlinger J (2011) Chemical sensor resolution requirements for near-surface measurements of turbulent fluxes. Atmos Chem Phys 11:5263–5275. doi:10.5194/acp-11-5263-2011

Rutgersson A, Smedman A (2010) Enhanced air–sea CO_2 transfer due to water-side convection. J Mar Syst 80 (1–2):125–134. doi:10.1016/j.jmarsys.2009.11.004

Rutgersson A, Norman M, Schneider B, Pettersson H, Sahlée E (2008) The annual cycle of carbon-dioxide and parameters influencing the air-sea carbon exchange in the Baltic Proper. J Mar Syst 74:381–394. doi:10.1016/j.jmarsys.2008.02.005

Rutgersson A, Smedman A, Sahlée E (2011) Oceanic convective mixing and the impact on air-sea gas transfer velocity. Geophys Res Lett 38:L02602. doi:10.1029/2010GL045581

Rysgaard S, Glud R (2004) Anaerobic n-2 production in arctic sea ice. Limnol Oceanogr 49:86–94

Rysgaard S, Glud R, Sejr M, Bendtsen J, Christensen P (2007) Inorganic carbon transport during sea ice growth and decay: a carbon pump in polar seas. J Geophys Res 112:C03016. doi:10.1029/2006jc003572

Rysgaard S, Glud R, Sejr M, Blicher M, Stahl H (2008) Denitrification activity and oxygen dynamics in arctic sea ice. Polar Biol 31:527–537. doi:10.1007/s00300-007-0384-x

Rysgaard S, Bendtsen J, Delille B, Dieckmann G, Glud R, Kennedy H, Mortensen J, Papadimitriou S, Thomas D, Tison J-L (2011) Sea ice contribution to the air–sea CO_2 exchange in the Arctic and Southern Oceans. Tellus B 63(5). doi:10.1111/j.1600-0889.2011.00571.x

Sahlée E, Drennan W (2009) Measurements of damping of temperature fluctuations in a tube. Bound-Lay Meteorol 132:339–348. doi:10.1007/s10546-009-9396-0

Sahlée E, Smedman A, Rutgersson A, Högström U (2008) Spectra of CO_2 and water vapour in the marine atmospheric surface layer. Bound-Lay Meteorol 126:279–295. doi:10.1007/s10546-007-9230-5

Salter M, Upstill-Goddard R, Nightingale P, Archer S, Blomquist B, Ho D, Huebert B, Schlosser P, Yang M (2011) Impact of an artificial surfactant release on air-sea

gas fluxes during Deep Ocean Gas Exchange Experiment II. J Geophys Res 116:C11016. doi:10.1029/2011JC007023

Sarmiento J, Orr J, Siegenthaler U (1992) A perturbation simulation of CO_2 uptake in an ocean general circulation model. J Geophys Res 97(C3):3621–3645. doi:10.1029/91JC02849

Saylor JR, Handler RA (1997) Gas transport across an air/water interface populated with capillary waves. Phys Fluids 9:2529–2541

Schimpf U, Garbe C, Jähne B (2004) Investigation of transport processes across the sea surface microlayer by infrared imagery. J Geophys Res-Ocean 109(C8):C08S13. doi:10.1029/2003JC001803

Schnieders J, Garbe C, Peirson W, Smith G, Zappa C (2013) Analyzing the footprints of near surface aqueous turbulence – an image processing based approach. J Geophys Res 118(3):1272–1286. doi:10.1002/jgrc.20102

Schröder A, Geisler R, Elsinga G, Scarano F, Dierksheide U (2008) Investigation of a turbulent spot and a tripped turbulent boundary layer flow using time-resolved tomographic piv. Exp Fluids 44:305–316. doi:10.1007/s00348-007-0403-2

Scott NV, Handler RA, Smith GB (2008) Wavelet analysis of the surface temperature field at an air–water interface subject to moderate wind stress. Int J Heat Fluid Flow 29(4):1103–1112. doi:10.1016/j.ijheatfluidflow.2007.11.002

Semiletov I, Makshtas A, Akasofu S, Andreas E (2004) Atmospheric co2 balance: the role of arctic sea ice. Geophys Res Lett 31:L05121. doi:10.1029/02003GL017996

Shaikh N, Siddiqui K (2010) An experimental investigation of the near surface flow over air-water and air-solid interfaces. Phys Fluids 22(2):025103

Shakhova N, Semiletov I, Leifer I, Salyuk A, Rekant P, Kosmach D (2010a) Geochemical and geophysical evidence of methane release over the east siberian arctic shelf. J Geophys Res C08007. doi:10.1029/2009jc005602

Shakhova N, Semiletov I, Salyuk A, Yusupov V, Kosmach D, Gustafsson O (2010b) Extensive methane venting to the atmosphere from sediments of the east siberian arctic shelf. Science 327. doi:10.1126/science.1182221

Sheng J, Malkiel E, Katz J (2008) Using digital holographic microscopy for simultaneous measurements of 3d near wall velocity and wall shear stress in a turbulent boundary layer. Exp Fluids 45:1023–1035. doi:10.1007/s00348-008-0524-2

Siddiqui MHK, Loewen MR (2007) Characteristics of the wind drift layer and microscale breaking waves. J Fluid Mech 573:417–456. doi:10.1017/S0022112006003892

Siddiqui K, Loewen M (2010) Phase-Averaged flow properties beneath microscale breaking waves. Bound-Lay Meteorol 134(3):499–523. doi:10.1007/s10546-009-9447-6

Siddiqui M, Loewen M, Jessup A, Asher W (2001) Infrared remote sensing of microscale breaking waves andnear-surface flow fields. In: Geoscience and Remote Sensing Symposium, 2001. IGARSS 01, vol 2. IEEE 2001 International, pp 969–971. doi:10.1109/IGARSS.2001.976697

Siddiqui M, Loewen MR, Asher WE, Jessup AT (2004) Coherent structures beneath wind waves and their influence on air-water gas transfer. J Geophys Res 109:C03024

Slinn SA, Slinn VGN (1980) Predictions for particle deposition on natural waters. Atmos Environ 14:1013–1016

Smedman A-S, Tjernström M, Högström U (1994) The near-neutral marine atmospheric boundary layer with no surface shearing stress: a case study. J Atmos Sci 51:3399–3411

Smethie WM Jr, Takahashi T, Chipman DW, Ledwell JR (1985) Gas exchange and co_2 flux in the tropical atlantic ocean determined from ^{222}rn and pco_2 measurements. J Geophys Res 90(C4):7005–7022. doi:10.1029/JC090iC04p07005

Smith J (1998) Evolution of Langmuir circulation during a storm. J Geophys Res-Ocean 103:12649–12668. doi:10.1029/97JC03611

Smith CR, Paxson RD (1983) A technique for evaluation of three-dimensional behavior in turbulent boundary layers using computer augmented hydrogen bubble-wire flow visualization. Exp Fluids 1:43–49

Smith MH, Park PM, Consterdine IE (1991) North-atlantic aerosol remote concentrations measured at a hebridean coastal site. Atmos Environ 25A:547–555

Smith GB, Handler RA, Scott N (2007) Observations of the structure of the surface temperature field at an air-water interface for stable and unstable cases. In: Garbe CS, Handler RA, Jähne BH (eds) Transport at the air sea interface. Springer, Berlin, pp 205–222

Soloviev A (2007) Coupled renewal model of ocean viscous sublayer, thermal skin effect and interfacial gas transfer velocity. J Mar Syst 66:19–27. doi:10.1016/j.jmarsys.2006.03.024

Soloviev AV, Schlüssel P (1994) Parameterization of the cool skin of the ocean and of the air–ocean gas transfer on the basis of modelling surface renewal. J Phys Oceanogr 24:1339–1346

Soloviev A, Donelan M, Graber H, Haus B, Schlüssel P (2007) An approach to estimation of near-surface turbulence and co_2 transfer velocity from remote sensing data. J Mar Syst 66:182–194. doi:10.1016/j.jmarsys.2006.03.023

Sorensen LL, Larsen SE (2010) Atmosphere-surface fluxes of CO_2 using spectral techniques. Bound-Lay Meteorol 136:59–81

Spiel D (1998) On the births of film drops from bubbles bursting on seawater surfaces. J Geophys Res 103:24907–24918

Spitzer WS, Jenkins WJ (1989) Rates of vertical mixing, gas exchange and new production: estimates from seasonal gas cycles in the upper ocean near bermuda. J Mar Res 47(1):169–196. doi:10.1357/002224089785076370

Springer T, Pigford R (1970) Influence of surface turbulence and surfactants on gas transport through liquid interfaces. Ind Eng Chem Fundam 9:458–465

Steinbuck JV, Roberts PLD, Troy CD, Horner-Devine AR, Simonet F, Uhlman AH, Jaffe JS, Monismith SG, Franks PJS (2010) An autonomous open-ocean stereoscopic piv profiler. J Atmos Oceanic Tech 27(8):1362–1380. doi:10.1175/2010JTECHO694.1

Stull R (1988) An introduction to boundary layer meteorology. Kluwer, Dordrecht

Sullivan PP, McWilliams JC (2010) Dynamics of winds and currents coupled to surface waves. Annu Rev Fluid Mech 42:19–42. doi:10.1146/annurev-fluid-121108-145541

Sutherland G, Christensen KH, Ward B (2013) Wave-turbulence scaling in the ocean mixed layer. Ocean Sci 9:597–608. doi:10.5194/os-9-597-2013

Suntharalingam P, Buitenhuis ET, Quere CL, Dentener F, Nevison CD, Butler JH, Bange H, Forster GL (2012)

Quantifying the impact of anthropogenic nitrogen deposition on oceanic nitrous oxide. Geophys Res Lett. doi:10.1029/2011GL050778 (in press)

Sweeney C, Gloor E, Jacobson A, Key R, McKinley G, Sarmiento J, Wanninkhof R (2007) Constraining global air-sea gas exchange for CO_2 with recent bomb ^{14}C measurements. Global Biogeochem Cycles 21:GB2015. doi:10.1029/2006GB002784

Szeri AJ (1997) Capillary waves and air-sea transfer. J Fluid Mech 332:341–358

Takagaki N, Komori S (2007) Effects of rainfall on mass transfer across the air-water interface. J Geophys Res 112: C06006. doi:10.1029/2006jc003752

Takahashi T, Olafsson J, Goddard J, Chipman D, Sutherland S (1993) Seasonal variations of CO_2 and nutrients in the high–latitude surface oceans: a comparative study. Global Biogeochem Cycles 7:843–878

Terray E, Donelan M, Agrawal Y, Drennan W, Kahma K, Hwang P, Kitaigorodskii S (1996) Estimates of kinetic energy dissipation under breaking waves. J Phys Oceanogr 26:792–807. doi:10.1175/1520-0485(1996)026<0792:EOKEDU>2.0.CO;2

Thorpe S (2004) Langmuir circulation. Annu Rev Fluid Mech 36:55–79. doi:10.1146/annurev.fluid.36.052203.071431

Tison J, Haas C, Gowing M, Sleewaegen S, Bernard A (2002) Tank study of physico-chemical controls on gas content and composition during growth of young sea ice. J Glaciol 48:177–191

Tison J-L, Brabant F, Dumont I, Stefels J (2010) High resolution DMS and DMSP time series profiles in decaying summer first-year sea ice at ISPOL (Western Weddell Sea, Antarctica). J Geophys Res Submitted

Trevena A, Jones G (2006) Dimethylsulphide and dimethylsulphoniopropionate in Antarctic sea ice and their release during sea ice melting. Mar Chem 98:210–222

Trevena A, Jones G, Wright SW, van den Enden R (2000) Profiles of DMSP, algal pigments, nutrients and salinity in pack ice from eastern Antarctica. J Sea Res 43:265–273

Trevena A, Jones G, Wright S, van den Enden R (2003) Profiles of dimethylsulphoniopropionate (DMSP), algal pigments, nutrients, and salinity in the fast ice of Prydz Bay, Antarctica. J Geophys Res 108:3145

Troitskaya Y, Sergeev D, Ermakova O, Balandina G (2011) Statistical parameters of the air turbulent boundary layer over steep water waves measured by the PIV technique. J Phys Oceanogr 41:1421–1454. doi:10.1175/2011JPO4392.1

Tsai W-T, Hung L-P (2007) Three-dimensional modeling of small-scale processes in the upper boundary layer bounded by a dynamic ocean surface. J Geophys Res 112. doi:10.1029/2006JC003686

Tsai W-T, Hung L-P (2010) Enhanced energy dissipation by parasitic capillaries on short gravity–capillary waves. J Phys Oceanogr 40:2435–2450

Tsai W, Liu K (2003) An assessment of the effect of sea-surface surfactant onglobal atmosphere-ocean CO_2 flux. J Geophys Res 108:3127. doi:10.1029/2000JC000740

Tsai W-T, Chen S-M, Moeng C-H (2005) A numerical study on the evolution and structure of a stress-driven, free-surface turbulent shear flow. J Fluid Mech 545:163–192

Tsai W-T, Chen S-M, Lu G-H, Garbe C (2013) Characteristics of interfacial signatures on a wind-driven gravity-capillary wave. J Geophys Res 118. doi:10.1002/jgrc.20145

Tulin MP, Landrini M (2001) Breaking waves in the ocean and around ships. In: Proceedings of the 23rd symposium of naval hydrodynamics, The National Academies Press, pp 713–745

Turk D, Zappa CJ, Meinen CS, Christian JR, Ho DT, Dickson AG, McGillis WR (2010) Rain impacts on co2 exchange in the western equatorial pacific ocean. Geophys Res Lett 37: L23610. doi:10.1029/2010gl045520

Turney D, Smith W, Banerjee S (2005) A measure of near-surface fluid motions that predicts air-water gas transfer in a wide range of conditions. Geophys Res Lett 32(4): L04607

Upstill-Goddard R, Frost T, Henry G, Franklin M, Murrell J, Owens N (2003) Bacterioneuston control of air-water methane exchange determined with a laboratory gas exchange tank. Global Biogeochem Cycles 17(4):1108. doi:10.1029/2003GB002043

Vagle S, McNeil C, Steiner N (2010) Upper ocean bubble measurements from the NE Pacific and estimates of their role in air-sea gas transfer of the weakly soluble gases nitrogen and oxygen. J Geophys Res 115:C12054. doi:10.1029/2009JC005990

Venkatram A, Pleim J (1999) The electrical analogy does not apply to modeling dry deposition of particles. Atmos Environ 33:3075–3076

Veron F, Melville W, Lenain L (2008) Wave-coherent air-sea heat flux. J Phys Oceanogr 38:788–802. doi:10.1175/2007JPO3682.1

Veron F, Melville WK, Lenain L (2011) The effects of small-scale turbulence on air-sea heat flux. J Phys Oceanogr 41 (1):205–220. doi:10.1175/2010JPO4491.1

Vesala T, Kljun N, Rannik U, Rinne J, Sogachev A, Markkanen T, Sabel-feld K, Foken T, Leclerc M (2008) Flux and concentration footprint model-ling: state of the art. Environ Pollut 152:653–666. doi:10.1016/j.envpol.2007.06.070

Vickers D, Göckede M, Law B (2010) Uncertainty estimates for 1-h averaged turbulence fluxes of carbon diocide, latent heat and sensible heat. Tellus 62B:87–99. doi:10.1111/j.1600-0889.2009.00449.x

Vlahos P, Monahan EC (2009) A generalized model for the air-sea transfer of dimethylsulfide at high wind speeds. Geophys Res Lett 36:L21605. doi:10.1029/2009GL040695

Voss B, Stapf J, Berthe A, Garbe C (2012) Bichromatic particle streak velocimetry bpsv – interfacial, v3c3d velocimetry using a single camera. Exp Fluids 53:1405–1420. doi:10.1007/s00348-012-1355-8

Wanninkhof R (1992) Relationship between gas exchange and wind speed over the ocean. J Geophys Res 97 (C5):7373–7382. doi:10.1029/92JC00188

Wanninkhof RH, Bliven LF (1991) Relationship between gas exchange, wind speed and radar backscatter in a large wind wave tank. J Geophys Res 96(C2):2785–2796

Wanninkhof R, Knox M (1996) Chemical enhancement of CO_2 exchange in natural waters. Limnol Oceanogr 41 (4):689–697

Wanninkhof R, McGillis WR (1999) A cubic relationship between gas transfer and wind speed. Geophys Res Lett 26:1889–1892

Wanninkhof R, Asher WE, Wepperning R, Hua C, Schlosser P, Langdon C, Sambrotto R (1993) Gas transfer experiment on

georges bank using two volatile deliberate tracers. J Geophys Res 98(C11):20237–20248
Wanninkhof R, Hitchcock G, Wiseman WJ et al (1997) Exchange, dispersion, and biological productivity on the west florida shelf: results from a lagrangian tracer study. Geophys Res Lett 24(14):1767–1770
Wanninkhof R, Sullivan KF, Top Z (2004) Air-sea gas transfer in the southern ocean. J Geophys Res 109:C08S19. doi:10.1029/2003JC001767
Wanninkhof R, Asher WE, Ho DT, Sweeney C, McGillis WR (2009) Advances in quantifying air-sea gas exchange and environmental forcing. Annu Rev Mar Sci 1:213–244. doi:10.1146/annurev.marine.010908.163742
Ward B (2006) Near–surface ocean temperature. J Geophys Res 111:C02005. doi:10.1029/2004JC002689
Watson AJ, Upstill-Goddard RC, Liss PS (1991) Air-sea exchange in rough and stormy seas measured by a dual tracer technique. Nature 349(6305):145–147
Webb E, Pearman G, Leuning R (1980) Correction of the flux measure-ments for density effects due to hear and water vapour transfer. Q J R Meteorol Soc 106:85–100
Weiss R (1987) Winter weddell sea project 1986: trace gas studies during legs ant v/2 and ant v/3 of polarstern. Antarct J US 22:99–100
Wells AJ, Cenedese C, Farrar JT, Zappa CJ (2009) Variations in ocean surface temperature due to near surface flow: straining the cool skin layer. J Phys Oceanogr 39:2685–2710
Wernet MP (2004) Planar particle imaging doppler velocimetry: a hybrid piv/dgv technique for three-component velocity measurements. Meas Sci Technol 15(10):2011
Whitman WG (1923) The two-film theory of absorption. Chem Met Eng 29:147
Willert CE, Gharib M (1992) Three-dimensional particle imaging with a single camera. Exp Fluids 12:353–358
Witek ML, Flatau PJ, Quinn PK, Westphal DL (2007) Global sea-salt modeling: results and validation against multicampaign shipboard measurements. J Geophys Res 112:D08215. doi:10.1029/2006JD007779
Witting J (1971) Effects of plane progressive irrotational waves on thermal boundary layers. J Fluid Mech 50:321–334
Woolf D (1993) Bubbles and the air-sea transfer velocity of gases. Atmos-Ocean 31:517–540
Woolf D (1997) Bubbles and their role in air-sea gas exchange. In: Liss P, Duce R (eds) The sea surface and global change. Cambridge University Press, Cambridge, pp 173–205
Woolf D, Thorpe S (1991) Bubbles and the air-sea exchange of gases in near-saturation conditions. J Mar Res 49:435–466
Woolf D, Bowyer P, Monahan E (1987) Discriminating between the film drops and jet drops produced by a simulated whitecap. J Geophys Res 92:5142–5150
Woolf D, Leifer I, Nightingale P, Rhee T, Bowyer P, Caulliez G, de Leeuw G, Larsen S, Liddicoat M, Baker J, Andreae MO (2007) Modelling of bubble-mediated gas transfer; fundamental principles and a laboratory test. J Mar Syst 66:71–91
Wurl O, Wurl E, Miller L, Johnson L, Vagle S (2011) Formation and global distribution of sea-surface microlayers. Biogeosciences 8:121–135
Yang M, Blomquist B, Fairall C, Archer S, Huebert B (2011) Effects of sea surface temperature and gas solubility on air-sea exchange of Dimethylsulfide (DMS). J Geophys Res 116:C00F05. doi:10.1029/2010JC006526
Yelland M, Pascal R, Taylor P, Moat B (2009) Autoflux: an autonomous system for the direct measurement of the air-sea fluxes of co_2, heat and momentum. J Op Oceanogr 2:15–23
Young IR, Babanin AV (2006) Spectral distribution of energy dissipation of Wind-Generated waves due to dominant wave breaking. J Phys Oceanogr 36(3):376–394. doi:10.1175/JPO2859.1
Zappa C, Jessup AT (2005) High-resolution airborne infrared measurements of ocean skin temperature. IEEE Geosci Remote Sens Lett 2(2):146–150. doi:10.1109/LGRS.2004.841629
Zappa CJ, Asher WE, Jessup AT (2001) Microscale wave breaking and air-water gas transfer. J Geophys Res-Ocean 106(C5):9385–9391
Zappa CJ, Asher WE, Jessup AT, Klinke J, Long SR (2004) Microbreaking and the enhancement of air-water transfer velocity. J Geophys Res 109:C08S16. doi:10.1029/2003JC001897
Zappa CJ, McGillis WR, Raymond PA, Edson JB, Hintsa EJ, Zemmelink HJ, Dacey JWH, Ho DT (2007) Environmental turbulent mixing controls on the air-water gas exchange in marine and aquatic systems. Geophys Res Lett 34:L10601. doi:10.1029/2006GL028790
Zappa CJ, Ho DT, McGillis WR, Banner ML, Dacey JWH, Bliven LF, Ma B, Nystuen J (2009) Rain-induced turbulence and air-sea gas transfer. J Geophys Res 114:C07009. doi:10.1029/2008JC005008
Zemmelink H, Delille B, Tison J, Hintsa E, Houghton L, Dacey J (2006) CO_2 deposition over the multi-year ice of the western weddell sea. Geophys Res Lett 33:L13606. doi:10.1029/2006gl026320
Zhang L, Vet R (2006) A review of current knowledge concerning size-dependent aerosol removal. China Particuology 4:272–282
Zhao D, Toba Y (2001) Dependence of whitecap coverage on wind and wave properties. J Oceanogr 57:603–616
Zilitinkevich S (1994) A generalized scaling for convective shear flows. Bound-Lay Meteorol 70:51–78. doi:10.1007/BF00712523